Science
AAAS

Supplementary Materials for

Fly Cell Atlas: A single-nucleus transcriptomic atlas of the adult fruit fly

Authors: Hongjie Li†, Jasper Janssens†, Maxime De Waegeneer, Sai Saroja Kolluru, Kristofer Davie, Vincent Gardeux, Wouter Saelens, Fabrice P.A. David, Maria Brbić, Katina Spanier, Jure Leskovec, Colleen N. McLaughlin, Qijing Xie, Robert C. Jones, Katja Brueckner, Jiwon Shim, Sudhir Gopal Tattikota, Frank Schnorrer, Katja Rust, Todd G. Nystul, Zita Carvalho-Santos, Carlos Ribeiro, Soumitra Pal, Sharvani Mahadevaraju, Teresa M. Przytycka, Aaron M. Allen, Stephen F. Goodwin, Cameron W. Berry, Margaret T. Fuller, Helen White-Cooper, Erika L. Matunis, Stephen DiNardo, Anthony Galenza, Lucy Erin O'Brien, Julian A. T. Dow, FCA Consortium, Heinrich Jasper, Brian Oliver, Norbert Perrimon*, Bart Deplancke*, Stephen R. Quake*, Liqun Luo*, Stein Aerts*

† Equal contribution

* Corresponding authors: perrimon@genetics.med.harvard.edu (N.P.), bart.deplancke@epfl.ch (B.D.), steve@quake-lab.org (S.R.Q.), lluo@stanford.edu (L.L.), stein.aerts@kuleuven.be (S.A.)

This PDF file includes:

FCA Consortium Contributions
Materials and Methods
FCA Consortium Funding
Figures and Legends S1 to S37
Tables S1 to S6, provided as Excel files
Captions for Table S1 to S6
References

Other Supplementary Materials for this manuscript include the following:

Table S1 [excel]: for Fig1, analysis parameters
Table S2 [excel]: for Fig2, cell type annotation
Table S3 [excel]: for Fig5, cell type-specific transcription factors
Table S4 [excel]: for Fig6: sex-differences, manually removed cells
Table S5 [excel]: for Fig6: sex-differences cell level data
Table S6 [excel]: for Fig6: sex-differences cluster level data

FCA Consortium Contributions

Overall coordination

Hongjie Li, Jasper Janssens, Norbert Perrimon, Bart Deplancke, Stephen R. Quake, Liqun Luo, Stein Aerts

Logistical coordination

Hongjie Li, Jasper Janssens, Maxime De Waegeneer, Sai Saroja Kolluru, Robert C. Jones, Norbert Perrimon, Bart Deplancke, Stephen R. Quake, Liqun Luo, Stein Aerts, Aaron McGeever, Angela Oliveira Pisco, Jim Karkanias, Sheela Crasta, Tzu-Chiao Lu, Gil dos Santos, Clare Pilgrim, Alex McLachlan, David Osumi-Sutherland, Irene Papatheodorou, Nancy George, Jonathan Manning, Robert P Zinzen

Tissue dissection

Liqun Luo lab (head, body, antenna, haltere): Liqun Luo, Hongjie Li, Jiefu Li, David Vacek, Anthony Xie
Lucy O'Brien lab (gut): Lucy Erin O'Brien, Yu-Han Su, Erin Nicole Sanders, Samantha Gumbin, Paola Moreno-Roman, Aparna Sherlekar, Andrew Thomas Labott, Sang Ngo
Norbert Perrimon lab (Malpighian tubule): Norbert Perrimon, Ruei-Jiun Hung, Jun Xu
Yuh-Nung Jan lab (body wall): Yuh Nung Jan, Jacob S. Jaszczak, Ruijun Zhu, Ke Li, Yanmeng Guo, Kai Li, Liying Li, Tun Li, Han-Hsuan Liu, Caitlin E. O'Brien, Wanpeng Wang, Maja Petkovic
Rolf Bodmer lab (heart): Rolf Bodmer, Georg Vogler, Marco Tamayo, James Kezos, Katja Birker, Tanja Nielsen
Mariana Wolfner lab (male reproductive glands): Mariana F. Wolfner, Norene A. Buehner
Kristin Scott lab (leg, wing, proboscis & max palp), Kristin Scott, Amy Chang, Stefanie Engert, Amanda J González-Segarra, Meghan Laturney, Sarah Leinwand, Carolina Reisenman, Philip Shiu, Gabriella Sterne, Zepeng Yao
Heinrich Jasper lab (fat body, oenocyte): Heinrich Jasper, Xiaoyu Tracy Cai, Nadja Sandra Katheder
Tom Kornberg lab (trachea): Thomas B Kornberg, Wanpeng Wang
Margaret Fuller lab (testis): Margaret T. Fuller, Neuza Reis Matias, Cameron W. Berry, Susanna E. Brantley, Catherine C. Baker, Devon E. Harris, Yiu-Cheung E. Wong, Benjamin Bolival
Todd Nystul lab (ovary): Todd G. Nystul, Katja Rust
Katja Brueckner lab (hemocyte): Katja Brueckner, Jordan Augsburger, Anjeli Mase
Seung Kim lab (insulin-producing cell, corpora cardiaca cell): Seung K. Kim, Lutz Kockel

Library preparation and sequencing

Liqun Luo: Hongjie Li, Colleen N. McLaughlin, Qijing Xie,
Stephen Quake lab: Sai Saroja Kolluru, Robert C. Jones, Felix Horns
Biohub: Angela M. Detweiler, Jia Yan, Michelle Tan, Norma Neff, Rene V. Sit
NIH group: Harold E. Smith, Brian Oliver

Main Data analysis

Stein Aerts lab: Jasper Janssens, Maxime De Waegeneer, Kristofer Davie, Swann Floc'hlay, Katina Spanier
Bart Deplancke lab: Vincent Gardeux, Wouter Saelens, Fabrice David, Maria Litovchenko,
Jure Leskovec lab: Maria Brbić, Kumar Ayush
Liqun Luo lab: Hongjie Li

Case study analysis/writing

Common cell - hemocyte: Katja Brueckner, Jiwon Shim, Sudhir Tattikota, Jasper Janssens, Hongjie Li
Common cell - muscle: Frank Schnorrer, Jasper Janssens
Gut data integration: Wouter Saelens
Metabolic pathway: Carlos Ribeiro, Zita Carvalho-Santos, Darshan B. Dhakan, Rita Cardoso-Figueiredo,
Ovary data integration: Katja Rust , Todd G. Nystul
Sex differences: Brian Oliver, Soumitra Pal, Teresa Przytycka, Aaron M. Allen, Devika Agarwal, Stephen F Goodwin, Julian A. T. Dow

Testis annotation & trajectory: Margaret T. Fuller, Cameron W. Berry, Erika L. Matunis, Stephen DiNardo, Helen White-Cooper, Brian Oliver, Sharvani Mahadevaraju, Julie A. Brill, Henry M. Krause, Wouter Saelens, Bart Deplancke

Cell type annotation

SCope team: Stein Aerts, Jasper Janssens, Maxime De Waegeneer, Kristofer Davie

ASAP team: Bart Deplancke, Vincent Gardeux, Wouter Saelens, Fabrice David

Gut: Lucy Erin O'Brien, Anthony Galenza, Aparna Sherlekar, Erin Nicole Sanders, Yu-Han Su, Anna A. Kim, Kazuki Yoda, Norbert Perrimon, Joshua Shing Shun Li
Malpighian tubule: Norbert Perrimon, Julian A. T. Dow, Jun Xu, Jasper Janssens, Yifang Liu
Body wall: Yuh Nung Jan, Jacob S. Jaszczak, Ruijun Zhu, Ke Li, Yanmeng Guo, Liying Li, Hongjie Li
Heart: Rolf Bodmer, Georg Vogler, Hongjie Li, Jasper Janssens
Muscle: Frank Schnorrer, Jasper Janssens
Male reproductive glands: Mariana F. Wolfner, Nora C. Brown, Yasir Ahmed-Braimah, Helen White-Cooper, Mikaela Matera-Vatnick, Timothy L. Karr
Leg, wing, prob. and max palp: Kristin Scott, Zepeng Yao, Carlos Ribeiro, Ibrahim Tastekin
Antenna and haltere, Liqun Luo, Hongjie Li, Colleen N. McLaughlin, Andrew K. Groves, Shinya Yamamoto, Daniel Sutton, Rachel I. Wilson, Stephen L. Holtz
Fat body and oenocyte: Heinrich Jasper, Xiaoyu Tracy Cai, Nadja Sandra Katheder, Sudhir Gopal Tattikota, Carlos Ribeiro, Zita Carvalho-Santos, Rita Cardoso-Figueiredo, Hongjie Li, Jasper Janssens
Trachea: Thomas B Kornberg, Wanpeng Wang, Hongjie Li
Testis (see case study)
Ovary: Todd G. Nystul, Katja Rust, Ruth Lehman, Maija Slaidina, Torsten Banisch, Zita Carvalho-Santos, Mariana F. Wolfner, Wanpeng Wang, Brian Oliver, Sharvani Mahadevaraju
Hemocyte, Katja Brueckner, Jiwon Shim, Sudhir Gopal Tattikota, Jasper Janssens, Hongjie Li
Insulin-producing cell (IPC) and corpora cardiaca cell (CC): Seung K. Kim, Lutz Kockel, Maria Brbić
Head and body: Aaron M. Allen, Bruno Hudry, Caitlin E. McDonough-Goldstein, Christoph Treiber, Clare Pilgrim, Claude Desplan, David Sims, Devika Agarwal, Erika Donà, Fernando Casares, Gregory S.X.E. Jefferis, Majd M. Ariss, Megan Neville, Michelle Arbeitman, Mehmet Neset Özel, Nikolaos Konstantinides, Scott Waddell, Stephen F Goodwin, Thomas R. Clandinin, Jasper Janssens, Hongjie Li, Stein Aerts

Writing group

Hongjie Li, Jasper Janssens, Norbert Perrimon, Bart Deplancke, Stephen R. Quake, Liqun Luo, Stein Aerts

Principal investigators (A-Z):

Stein Aerts, Yasir Ahmed-Braimah, Rolf Bodmer, Julie A. Brill, Katja Brueckner, Fernando Casares, Thomas R. Clandinin, Bart Deplancke, Claude Desplan, Stephen DiNardo, Julian A. T. Dow, Margaret T. Fuller, Stephen F Goodwin, Andrew K. Groves, Bruno Hudry, Yuh Nung Jan, Heinrich Jasper, Gregory S.X.E. Jefferis, Timothy L. Karr, Seung K. Kim, Nikolaos Konstantinides, Thomas B Kornberg, Henry M. Krause, Jure Leskovec, Hongjie Li, Liqun Luo, Erika L. Matunis, Todd G. Nystul, Lucy Erin O'Brien, Brian Oliver, Norbert Perrimon, Teresa M Przytycka, Stephen R. Quake, Carlos Ribeiro, Katja Rust, Frank Schnorrer, Kristin Scott, Jiwon Shim, Scott Waddell, Helen White-Cooper, Rachel I. Wilson, Mariana F. Wolfner, Shinya Yamamoto, Robert P Zinzen

Materials and Methods

Fly sample information

				Number of cells after filtering				
tissue	**genotype**	**age**	**Dissection lab**	**10x male**	**10x female**	**10x mix**	**SS2 male**	**SS2 female**
head	w^{1118}	5d	Liqun Luo	33292	59275	4359	-	-
body	w^{1118}	5d	Liqun Luo	47409	49105	4013	-	-
antenna	w^{1118}	5d	Liqun Luo	15586	14446	7222	242	344
haltere	w^{1118}	5d	Liqun Luo	3148	3379	-	128	135
proboscis & maxillary palp	w^{1118}	5d	Kristin Scott	13765	12536	-	333	307
wing	w^{1118}	5d	Kristin Scott	8053	7836	-	207	313
leg	w^{1118}	5d	Kristin Scott	7120	7077	-	302	305
gut	w^{1118}	5d	Lucy O'Brien	5450	6338	-	292	302
body wall	w^{1118}	5d	Yuh-Nung Jan	6851	9700	-	249	176
heart	w^{1118}	5d	Rolf Bodmer	5515	5171	-	169	295
Male reproductive gland	w^{1118}	2-3d*	Mariana Wolfner	13143	-	-	238	-
testis	w^{1118}	1d*	Margaret Fuller	43454	-	-	374	-
ovary	w^{1118}	5d	Todd Nystul	-	31401	-	-	1011
Malpighian tubule	*drip-GAL4 > UAS-nlsGFP* (all nuclei,** see note)	5d	Norbert Perrimon	6185	7589	-	303	191
fat body	*Cg-GAL4 > UAS-lamGFP* (GFP enriched nuclei)	5d	Heinrich Jasper	10983	15943	-	693	656
oenocyte	*PromE800-GAL4 > UAS-unc84GFP* (GFP enriched nuclei)	5d	Heinrich Jasper	9420	4990	-	264	270
trachea	*Btl-GAL4 > UAS-lamGFP* (***GFP enriched nuclei)	5d	Tom Kornberg	7112	19794	-	339	380
insulin-producing cell (IPC)	*dilp2-GAL4 > UAS-unc84GFP* (GFP enriched nuclei)	5d	Seung Kim	-	-	-	345	313
corpora cardiaca cell (CC)	*Akh-GAL4 > UAS-unc84GFP* (GFP enriched nuclei)	5d	Seung Kim	-	-	-	351	241

For most samples, 5-day adults were used with two exceptions (see below). Male and female flies were collected on day 1 and kept together for mating, and on day 5, flies were sexed and dissected. *UAS-lamGFP* was from Bloomington Drosophila Stock Center (BDSC# 7378). *UAS-unc84GFP* was from (*48*).

*For the male reproductive gland, we used 2–3 day old virgin males in order to detect active transcripts which may be not detectable in 5 day old virgin flies. For the testis, we chose 0–1 day old males to be consistent with the phenotypic studies in the field. If virgin males are held away from females until they are 5 days old, the seminal vesicle fills up with huge numbers of mature sperm, and their condensed, inactive haploid nuclei would be a problem if they displaced nuclei from earlier germ cell stages.

**For the Malpighian tubule, we used *Drip-GAL4>UAS-nlsGFP* to label stellate cells and sequenced all nuclei from dissected tissues. During clustering analysis, we found that the stellate cells can be readily annotated based on the marker genes, *tsh, SecCl,* and *Drip*.

***For the trachea, flies cannot survive to adulthood using *btl-GAL4* driving *UAS-UNC84GFP* or *UAS-lamGFP*. In order to label and collect adult trachea cells, we crossed *btl-GAL4*, *tub-Gal80ts* flies with *UAS-lamGFP* at 18℃ and transferred the young adult flies to 29℃ for 5 days before dissection.

How many tissues to use for each sample?

During sample preparation, we estimated the required tissue number based on three factors: total cell/nucleus number in the tissue, targeted cell number for 10x Genomics and Smart-seq2, and the FACS recovery rate. Our FACS recovery rate is about 5%. For example, if a tissue contains 10,000 nuclei, we were able to collect 500 nuclei after FACS. So if we want to collect 10,000 nuclei after FACS, we will dissect 20 tissues. Please note that since we don't have the exact number of cells for many tissues, our dissection labs have prepared more samples than estimated. Here we list the numbers of tissues we prepared. If not specified, the number is used for each sex to target one 10x run, which is about 10,000 cells:

Head, 100 heads for a total 6 10x runs; body, 50 bodies for a total 6 10x runs; antenna, 300; haltere, 500; proboscis with maxillary palp, 100; wing, 200; leg, 120; gut, 200; body wall, 40; heart, 250; male reproductive gland, 200; testis, 600; ovary, 30; malpighian tubule, 300; fat body, 250; oenocyte, 250; trachea, 100; insulin-producing cell (IPC), 250 for one 384-well plate; corpora cardiaca cell (CC), 250 for one 384-well plate.

Single-nucleus RNA-seq

Fly dissection and single-nucleus suspension: Fly tissues were dissected by different dissection labs, flash-frozen using liquid nitrogen, stored at –80℃ , and shipped to Stanford University for processing in the Luo and Quake labs. When using nuclear GFP to label tissues, we compared *UAS-nlsGFP*, *UAS-UNC84GFP* and *UAS-lamGFP*, and found that there was no GFP signal from *UAS-nlsGFP* after nucleus isolation, while the other two gave good fluorescent signal of the nuclear labeling. Single-nucleus suspensions were prepared as detailed below, largely adapted from our recently published protocol (*11*).

1. Prepare w^{1118} flies or GAL4 driving UAS-nuclear-GFP flies.
2. Dissect tissue in cold Schneider's medium, and use P20 pipette (coat the tip with fly body fat) or forceps to transfer them into 100 µl Schneider's medium in a nuclease-free 1.5ml EP tube on ice. Label the tube clearly using permanent marker. Note: for tissues that float in the medium (e.g., adult antennae), before dissection, prepare three clean dishes: 1st with 100% ethanol, 2nd and 3rd with Schneider's medium. Rinse the fly in the 1st dish with 100% ethanol for 5 seconds, then rinse the fly in the 2nd dish, and dissect in the 3rd dish.

3. After dissection, spin down samples in 100 µl Schneider's medium using a bench top spinner.
4. Fresh: The sample can be processed for extraction of nuclei immediately following dissection. Frozen: Alternatively, the sample can be flash-frozen for long-term storage. Seal the 1.5 ml EP tube with parafilm and put into liquid nitrogen for >30s. Immediately store the sample at -80ºC freezer for long-term storage (several months).
5. Prepare fresh homogenization buffer (see details below) and keep on ice.
6. Thaw samples from -80ºC on ice if using frozen samples. Spin down samples in 100 µl Schneider's medium using the bench top spinner, discard medium as much as possible, and add 100 µl Homogenization butter.
7. Optional: if sample pieces are too big, e.g. whole body or whole head, use a pestle motor (Kimble 6HAZ6) to grind the sample for 30s–60s on ice.
8. Add 900 µl homogenization buffer, and transfer 1000 µl homogenized sample into the 1ml dounce (Wheaton 357538). Dounce sets should be autoclaved at 200ºC >5h or overnight.
9. Release nuclei by 20 strokes of loose dounce pestle and 40 of tight dounce pestle. Keep on ice. Avoid bubbles.
10. Filter 1000 µl sample through 5 ml cell strainer (35 µm), and then filter sample using 40 µm Flowmi (BelArt, H13680-0040) into 1.5 ml EP tube.
11. Centrifuge for 10 min at 1000g at 4ºC. Discard the supernatant. Do not disturb the pellet.
12. Re-suspend the nuclei using the desired amount (we normally use 500-1000 µl) of 1xPBS/0.5%BSA with RNase inhibitor (9.5 ml 1x PBS, 0.5 ml 10% BSA, 50 µl RNasin Plus). Pipet more than 20 times to completely re-suspend the nuclei. Filter sample using 40 µm Flowmi into a new 5 ml FACS tube and keep the tube on ice. Now the single-nucleus suspensions are ready for FACS.

According to our experience, the nuclei are stickier than whole cells. For users making single-nucleus suspension for the first time, we suggest taking 10 µl of the single-nucleus suspension, stain with Hoechst (Invitrogen 33342), and check on a cell counter slide to confirm if they are mostly individual nuclei. If nuclei are not sufficiently dissociated, adjust above steps (e.g., increase the number of strokes of the tight pestle when releasing nuclei).

	Amount	Storage	Item (add in this order)	Final concentration
1	10 ml	RT	H2O (nuclease free)	
2	0.856 g	RT	Sucrose (nuclease free)	250 mM
3	100 µl	4ºC	1M Tris PH 8.0	10 mM
4	250 µl	4ºC	1M KCl	25 mM
5	50 µl	4ºC	1M MgCl2	5 mM
6	100 µl	4ºC	10% Triton-x 100	0.1%
7	50 µl	-20ºC	RNasin Plus (Promega, N2615)	0.5%
8	200 µl	-20ºC aliquots	50x protease inhibitor (Promega, G6521)	1x
9	50 µl	-20ºC	20mM DTT	0.1 mM

FACS: We used the SONY SH800 FACS sorter for collecting nuclei. Nuclei were stained by Hoechst-33342 (1:1000; >5min). For wildtype tissues, Hoechst+ nuclei were collected; for collecting GFP+ nuclei, we first gated on Hoechst+ events and then chose the GFP+ population.

Since polyploidy is common for many fly tissues, we observed different populations of nuclei according to DNA content (Hoechst signal). Conversely, many haploid nuclei are present in testis. After FACS of nuclei from the testis plus seminal vesicle by level of Hoeschst and nuclear size, we observed 6 different populations with different Hoechst signal intensity, and confirmed that the Hoechst signal intensity correlated well with nuclear size. For the fly gut, we observed 5 different populations with different Hoechst signals. In order to include all cell populations with different nuclear sizes, we have included all nuclear populations from the FACS in samples for 10x sequencing, except for testis.

In the testis, 64 haploid spermatids are eventually produced for each germ line stem cell division. To avoid overrepresentation of small haploid spermatids in the testis sample, we used the following strategy to collect testis nuclei. For the first of the three total 10x runs for testis plus seminal vesicle, we collected nuclei from all 6 of the populations discerned by FACS for Hoechst x size. For the two subsequent 10x runs, we collected nuclei without the population of the smallest size (haploid spermatids)

Individual nuclei were collected either to 384-well plates for smart-seq2 or to one tube for 10x Genomics. For 10x Genomics, nuclei were collected into a 15ml tube with 500ul 1x PBS with 0.5% BSA as the receiving buffer (RNase inhibitor added). For each 10x Genomics run, 100k–400k nuclei were collected. Nuclei were spinned for 10min at 1000g at 4℃, and then resuspended using 40ul or desired amount of 1x PBS with 0.5% BSA (RNase inhibitor added). 2ul nucleus suspension was used for counting the nuclei with hemocytometers to calculate the concentration. When loading to the 10x controller, we always target at 10k nuclei for each channel. We observed that loading 1.5 folds more nuclei as recommended by the protocol allowed us to recover about 10k cells after sequencing. For example, if the concentration is 1500 nuclei per ul for one sample, we treat it as 1000 nuclei per ul when loading to the 10x controller.

Library preparation and sequencing: Smart-seq2 sequencing libraries were prepared following the protocol we previously described (*11*). Sequencing was performed using the Novaseq 6000 Sequencing system (Illumina) with 100 paired-end reads and 2x12 bp index reads.

10x Genomics sequencing libraries were prepared following the standard protocol from 10x Genomics 3' v3.1 kit with following settings. All PCR reactions were performed using the Biorad C1000 Touch Thermal cycler with 96-Deep Well Reaction Module. 13 cycles were used for cDNA amplification and 16 cycles were used for sample index PCR. As per 10x protocol, 1:10 dilutions of amplified cDNA and final libraries were evaluated on a bioanalyzer. Each library was diluted to 4 nM, and equal volumes of 18 libraries were pooled for each NovaSeq S4 sequencing run. Pools were sequenced using 100 cycle run kits and the Single Index configuration. Read 1, Index 1 (i7), and Read 2 are 28 bp, 8 bp and 91 bp respectively. A PhiX control library was spiked in at 0.2 to 1% concentration. Libraries were sequenced on the NovaSeq 6000 Sequencing System (Illumina).

Sequencing read alignment

Prior to read alignment, the raw FASTQ files were processed with the index-hopping-filter software from 10x Genomics (version 1.0.1) to remove index-hopped reads. More information about this software is available at https://support.10xgenomics.com/docs/index-hopping-filter.

A Cell Ranger (version 3.1.0) index was built from a pre-mRNA GTF which was derived from the Flybase version r6.31 GTF. A complete recipe on how to build this custom pre-mRNA GTF is available here: https://github.com/FlyCellAtlas/genome_references/tree/master/flybase/r6.31

For 10x, the filtered reads (index-hopped reads removed) were processed all the way up to the gene expression matrix using Cell Ranger (version 3.1.0). For Smart-seq2, reads were aligned to the *Drosophila melanogaster* genome (r6.31), the same as for 10x read alignment, using STAR (2.5.4). Gene counts were produced using HTseq (0.11.2) with default settings except '-m intersection-strict'. Gene counts were generated using the same GTF file as for 10x, covering both exonic and intronic regions. Low-quality nuclei having fewer than 10,000 uniquely mapped reads were removed.

Cell filtering and clustering: *Relaxed* version

To verify the accuracy and robustness of the data processing steps, we examined marker gene expression and compared multiple methods and parameter settings for the various preprocessing steps, including index hopping filtering, genome annotation and counting intronic reads, doublet detection (scrublet), read decontamination (DecontX), batch effect removal (harmony), dimensionality reduction (automated PC determination), and clustering (Leiden). At each step QC plots are generated (fig. S4) and the final loom files can be visualized in our SCope and ASAP analysis and visualization platforms, or be downloaded for custom analysis.

Two versions of the processed data were generated: a *Relaxed* and a *Stringent* version. Here we focus on describing the *Relaxed* version of the data. To know more about the difference between the two versions please read the next section.

The Scrublet software was chosen for doublet removal. Doublet scores were calculated from the raw expression matrix generated by Cell Ranger and using Scrublet (version 0.2.1, Docker image: vibsinglecellnf/scrublet:0.1.4). The strategy taken here to remove the doublets from each sample relies on the multiplet rate one can expect from running a Single Cell 3' 10x Genomics experiment. This number depends on the number of recovered cells. In order to estimate this rate as a function of the number of recovered cells, a linear regression was performed on the multiplet rate table (see Chromium Single Cell 3' Reagent Kits v2 User Guide • Rev F) in order to determine the slope and the bias terms. Those numbers were 0.008 and 0.0527 respectively. Given this model, for each sample the top N cells, ranked by the doublet score, were considered as doublet hence removed.

The data was further processed using the Python package Scanpy (version 1.4.4.post1, through Docker image: vibsinglecellnf/scanpy:0.5.0).

Two additional filters, cellwise and genewise, were applied. The cell filter is based on hard thresholds applied on some of the quality metrics (QC). All cells expressing less than 200 genes were filtered out. Moreover, cells exceeding a 15% mitochondrial content were removed. Regarding the gene filter, all genes not expressed in at least 3 cells were filtered out.

For the different analysis runs with VSN-Pipelines, the samples were concatenated using the anndata.concatenate (join=outer). Consequently, the combined matrix was normalized (scanpy.pp.normalize_per_cell, with counts_per_cell_after=10000) and log transformed (scanpy.pp.log1p). Highly variable genes were selected using sc.pp.highly_variable_genes (min_mean=0.0125, max_mean=3, min_disp=0.5). The data was further scaled so that each gene had unit variance and values exceeding a standard deviance of 10 were clipped. In order to determine the number of principal components (PC) to select, a cross-validation approach was performed using the pcacv module (available in the VSN-Pipelines). The scaled matrix was projected to a principal component analysis (PCA) space using the scanpy.tl.pca function (svd_solver=arpack). Batch correction was applied using the Harmony software (Docker image: vibsinglecellnf/pcacv:0.2.0) with default parameters and using sample as batch variable. The neighborhood graph was calculated from the corrected PCA space with scanpy.pp.neighbors and default parameters except for the number of PCs (see aforementioned). For visualization purposes, two non-linear dimensionality reduction methods were used: t-SNE and UMAP. The t-SNE embeddings were generated using scanpy.tl.tsne while the UMAP embeddings with sc.tl.umap. Default parameters were used for both methods except for the number of PCs (see aforementioned). Clustering was performed using the Leiden algorithm via scanpy.tl.leiden (default parameters) except for the resolution parameter where a range of values were selected. A default clustering was selected using a custom method available in the directs module from VSN-Pipelines (vibsinglecellnf/directs:0.1.0). The default clustering is selected as follows: for a range of min_cluster_size and min_samples, a density-based clustering is performed using HDBSCAN on the t-SNE embedding; an adjusted rand score is computed between this clustering and the previously generated Leiden clusterings; a clustering is assigned to each pair of parameters which maximizes the score; the final selected clustering is the one that maximizes the most the score over all pairs. Cluster markers for each of the generated clusterings were computed from the log normalized expression matrix by means of scanpy.tl.rank_genes_groups (method=wilcoxon, n_genes=0).

To ensure reproducibility of the 10x Genomics data processing, all the analyses from raw counts to final processed files (.loom and .h5ad) were performed using the VSN-Pipelines (https://githhub.com/vib-singlecell-nf/vsn-pipelines).

Cell filtering, decontamination and clustering: *Stringent* version

In the previous section, we described how the *Relaxed* version of the data was generated. The main reason to generate a *Stringent* version was that we identified a significant number of cells, we called "black hole" cells, which are expressing multiple general cell type markers e.g.: grh (epithelial cell), Mhc (muscle cell), onecut (neuron). These cells likely originated from droplets that were contaminated by ambient RNA.

DecontX was chosen in order to correct for this bias. Practically, the raw counts generated from the Cell Ranger pipeline were corrected using this algorithm, available in the celda R package (version 1.4.5, Docker image: vibsinglecellnf/celda:1.4.5). The corrected counts were then rounded using the R base::round function and newly generated empty cells were removed.

Additionally, we applied a more stringent filter on the cells. This cell filter is based on the median absolute deviation (MAD) from the median of the following quality control (QC) metrics across all cells: n_counts i.e.: number of counts per cell, n_genes i.e. number of genes per cell. A value is considered an outlier if it is greater than 3 MADs away (both directions) from the median of these two metrics. This filter strategy is applied in the log space of these QC metrics. Moreover, minima of 200 genes and 500 counts per cell are required for a cell to be considered in the downstream analysis. All cells exceeding a 5% mitochondrial content were removed.

Finally, after the highly variable gene selection, the number of UMIs per cell and the percentage of mitochondrial genes were regressed out using scanpy.pp.regress_out. All other steps described previously remained the same.

Relaxed versus Stringent dataset

As a more stringent filter was applied to generate the Stringent data, they were considered to be higher quality. For most analyses, we focused on the *Stringent* dataset, which should be used as a default for new users.

However, we noticed that in the testis data, the important hub cell cluster was filtered out by the stringent algorithms, likely due to the expression of many "somatic" transcripts including *Upd1* in late spermatocytes. Thus, the UMAP for testis presented in Figure 2C is plotted using Relaxed dataset.

SCope features and applications

SCope platform crowd annotation system was used to gather all annotations that were added during the Jamborees by all tissue experts. All tissue analysis results across all clustering resolutions were used as a basement to annotate the cells of the atlas. The system allows for tracking the author of the annotations as well as their confidence through a like/dislike feature. The latter feature was crucial for building a consensus annotation. Annotated Loom files can be directly downloaded from SCope.

ASAP features and applications

The ASAP platform (*18*) was used to perform more detailed analyses on the datasets. In particular, ASAP was used to perform sub-clustering and additional differential expression / marker gene discovery. Since the platform also allows annotating (e.g., a color gradient) cells according to the expression of a particular gene set (rather than a single gene), ASAP was also used to study the activity state of KEGG pathways. Finally, because ASAP allows users to share a project (or its copy) privately with a group, all FCA-related projects have been made public so that researchers can share/clone them freely, and annotated Loom files can then be directly downloaded in ASAP.

Jamboree annotation

We have tried two strategies to make sure our "jamboree" annotations are accurate. First, all tissue jamborees were led by Drosophila experts of corresponding tissues. Most annotations were based on ground truth knowledge, and for some uncertain annotations, we allowed experts to include notes besides the annotation. Second, we have implemented an upvote system, allowing experts to vote for clusters that have been assigned to different cell types. We also want to point out that there is no unified standard as a cutoff for FCA annotation, because some cell types can be specified by a single marker (for example, one type of olfactory receptor neuron can be determined by a single olfactory receptor gene), while some other cell types are specified by several different markers. To best document our jamboree annotation records, we have now included a supplemental table to show key information, including names, markers, references if any, and notes (Table S2).

For future annotation, please check flycellatlas.org website, where we provide information to users about how to provide new cell type annotations and where we will post our plan for updating these annotations.

Integration of 10x Genomics and Smart-Seq2 data (Fig. 1D)

We integrated 10x Genomics and Smart-Seq2 data using Harmony (*16*). To facilitate and improve integration, we first selected most relevant genes by performing differential gene expression on annotated 10x Genomics data (t-test; Benjamini-Hochberg corrected p-value < 0.1). To integrate individual tissues, we used genes differentially expressed between cell types of a given tissue. To integrate entire cell atlases, we used genes differentially expressed between tissues. After selecting differentially expressed genes, we batch-corrected datasets using Harmony to remove the influence of the sequencing technology. We included an additional step of batch-correction for those tissues in which gender specific clusters were present. In total, we performed additional batch-correction based on the gender for 12/15 tissues.

We next systematically validated integration in the following way. If the marker genes were known, we visually inspected whether marker genes are expressed at the same tSNE location for 10x Genomics and Smart-Seq2 data after integration. In case marker genes were not known, we found differentially expressed genes based on annotations of 10x Genomics data and selected 3-5 genes that are as cluster specific as possible. Finally, for each tissue and cell type we came up with the list of genes and validated whether these genes are expressed at the same location in the tSNE space for 10x Genomics and Smart-Seq2 data. Besides Harmony, we considered three other integration approaches and finally decided to use Harmony based on our validation procedure.

Annotating Smart-Seq2 data (fig. S20, S21)

After integrating 10x Genomics and Smart-Seq2 data, we next aimed at transferring cell type annotations from 10x Genomics to unannotated Smart-Seq2 data. To develop an approach and quantitatively compare performance of different classification methods, we used Smart-Seq2 cells from olfactory receptor neurons (ORN) (*11*) annotated using MARS (*49*) and manually validated based on the marker-gene expressions. We integrated this dataset with ORN antenna 10x Genomics dataset that was annotated on the same granularity level. The classification accuracy was high (0.88) with a linear logistic regression model and did not improve by using non-linear models. Therefore, we decided to use logistic regression as the base classifier due to its simplicity and interpretability. Finally, for each tissue we used a 10x Genomics dataset as the train set and trained a logistic regression classifier to distinguish different cell types of annotated 10x Genomics data. We then applied the classifier on the Smart-Seq2 dataset to obtain cell type annotations. To confirm that Smart-Seq2 annotations are indeed correct, we checked expressions of known marker genes and validated if they agree with the predicted Smart-Seq2 annotations.

Comparison of 10x Genomics and Smart-Seq2 data (Fig. 1E)

To compare the number of detected genes between 10x Genomics and Smart-Seq2 data (Fig. 1E), we considered a gene detected if a single read maps to it. In particular, for 10x Genomics data we used UMI greater or equal to 1 as a threshold, while for Smart-Seq2 data we used log2(CPM+1) greater or equal to 1 as a threshold. Given these thresholds, we counted the number of genes detected in at least 1% of cells. To obtain examples of genes that are detected using Smart-Seq2, but not using 10x Genomics (fig. S20G) we obtained a list of genes that are expressed in less than 20 cells in 10x Genomics data, and two to four times more cells in Smart-Seq2 data depending on a tissue.

Brain-Head integration (Fig. 3E)

Single cell RNA-seq dataset from Davie et al. was downloaded from GEO (GSE107451) and processed using VSN. Next, the data was integrated with the single nucleus data from the FCA using Seurat. Data was normalized using SCT normalization (*50*) and batch correction was performed as described (*51*). 150 components were selected for clustering and UMAP/tSNE visualization. Annotations were added using computational approaches. First, we transferred annotation from annotated cells to clusters that contained at least 25% of annotated cells. Next, we used a classifier from Ozel et al. (*22*) to annotate optic lobe cell types. Finally, we trained an SVM classifier on the Davie et al. data, using scikit-learn in Python, following

10 fold cross-validation, optimizing C, kernel and gamma parameters. All computed annotations were then manually curated in jamborees.

Common cell type analysis – Hemocyte (Fig. 4D)

With the cross-tissue analysis, we extracted 8,391 Hml$^+$ cells from most body parts, including the fat body, heart, body wall, oenocytes, legs, the Malpighian tubule, tissues in the head, and reproductive organs. Harmony was used to remove batch effects with different parameters to control against overcorrection. We tested lambda (ridge regression penalty parameter) and theta (diversity clustering penalty parameter) in a grid with each parameter ranging from 0 to 3. In the end, the T1L2 combination was found to preserve cell types while not overtly separating cells in batches (based on visual exploration). To explore hemocytes in adults, we annotated cell clusters according to the expression of previously published markers in larval hemocytes and identified twenty-one clusters of Hml$^+$ cells (Figure 4D). Crystal cells are readily segregated by high PPO1, PPO2, and lozenge expressions, while plasmatocytes are largely combined as a population most akin to embryonic and larval hemocytes. Plasmatocytes are categorized into five clusters based on their gene expressions and we named the clusters with representative marker genes: Pxn^{High}, Nplp2/Tep4^{High}, Cecropin^{High}, LysX/trol/Pvf2^{High}, and nAChRalpha3^{High}. LysX/trol/Pvf2^{High} plasmatocytes exhibit lower Hml compared to other plasmatocytes whereas Pxn^{High} shows the highest Hml with phagocytosis markers including crq, Sr-CI, and NimC1. Nplp2/Tep4^{High} plasmatocytes show a prohemocyte marker, Tep4, and an intermediate prohemocyte marker, Nplp2, along with phagocytosis markers. Cecropin^{High} plasmatocytes display immune- or stress responsive genes such as upd3, Mmp1, Mmp2, and puc. Further, we observed Antp and collier expressing Hml$^+$ cells reminiscent of the posterior signaling center in the lymph gland . Yet, lamellocytes are not observed in adults as previously suggested (Bosch et al., 2019) (Figure 4D). In addition to Hml$^+$ cells with classical hemocyte gene expressions, we noticed Hml$^+$ cells originating from a single tissue, including the testis and antenna, constitute independent clusters significantly enriched with resident tissue marker genes. Overall, single-cell transcriptome profiles of adult hemocytes provide ample resources for understanding adult immunity, hematopoiesis and repertoires of tissue-resident hemocytes.

Hemocytes in adults are largely resident and the majority is found in the thorax or head while a small fraction circulates the hemolymph (*27*). Thus, cross-tissue dissection of adult hemocytes categorized represent hemocytes in adults. Although *Hml* is a well-known marker for plasmatocytes in embryonic- and larval stages, the expression of *Hml* is heterogenous during development which could hinder labeling the entire population of adult hemocytes.

Common cell type analysis - Muscle (Fig. 4E)

Muscle cell clusters were identified by their expression of common sarcomeric gene products, including *Mhc, sls, bt* and *Unc-89* (*52*). With the cross-tissue analysis, we extracted 63,441 muscle cells from most body parts. Harmony was used to remove batch effects with different parameters to control against overcorrection. We tested lambda (ridge regression penalty parameter) and theta (diversity clustering penalty parameter) in a grid with each parameter ranging from 0 to 3. In the end, the T1L2 combination was found to preserve cell types while not overtly separating cells in batches (based on visual exploration). The abundant indirect flight muscle nuclei cluster was uniquely identified by expression of flight muscle-specific markers *TpnC4, Act88F* and *fln* (*53*). Furthermore, the here identified specific expression of different troponinC gene isoforms (*TpnC4, TpnC73F, TpnC41C, TpnC47D, TpnC25D*) was used to further annotate the different muscle clusters taking into account their body part of origin (*54*).

Transcription factors and cell type specificity analysis (Fig. 5A-D)

Cell-type specific TFs were identified using the tau factor. First, calculated average expression profiles in log2CPM space for every cell type and subsequently Z-normalised per gene. We then calculated the tau value for each TF (Flybase r6.36 TF list) using the tspex Python package (version 0.6.2), leading to the identification of 500 TFs with a score higher than 0.85. These factors were plotted in Fig. 5A and are available in **Table S3**. Since the tau factor is calculated on average expression profiles, single-cell information regarding the number of cells where expression is detected is lost. To take this into account, we have split the high tau genes into three categories depending on the percentage of cells in the cell type where at least 1 UMI for the TF was detected (>50%, 50%<x<5% and <5%).

Regarding the analysis showing the TF specificity heatmap (Fig 5C), we used the log normalized gene by cell expression matrix. The cells' expressions were averaged by the broad annotations. We then calculated the tau value for each TF (Flybase r6.36 TF list) using the tspex Python package (version 0.6.2). The values shown in the heatmap are the feature-scaled values using the zscore function available in the package. Only genes passing the thresholds of tau greater than 0.85, log normalized expression greater than or equal to 0.5 and log normalized scaled expression greater than or equal to 1 were retained. The plotting was performed using the ComplexHeatmap R package.

The network shown in Fig 5B is based on 5 different .sif files (network files). The first one is the network based on TFs and broad annotations where links passing the aforementioned thresholds were kept. The second one is the network based on TFs and narrow annotations where 0.85, 2 and 5 thresholds were applied respectively. The other networks represent the narrow-to-narrow, broad-to-narrow and broad-to-broad annotation associations. Since the annotations were mainly driven by the EBI OLS system, most of them are associated with a curated FBbt term. We leverage this graph-based ontology structure in order to compute a semantic similarity between annotations using the ontologySimilarity R package (version 2.5). For broad-to-narrow and broad-to-broad annotation associations, the ones with a semantic similarity below 0.4 were removed except for a few of the broad-to-narrow associations that resulted in a loss of broad terms (fat cell to muscle cell, cardial cell to multidendritic neuron and neuron to multidendritic neuron). For narrow-to-narrow connections, after the expression-based filter, only terms that had a TF assigned were kept and moreover we selected for each term the two most connected terms.

Those 5 processed networks were used as input in the Cytoscape software (version 3.8.0) to build the visual network depicted in Fig 5B. The width of the edges represents the log normalized scaled expression (z-score) while the tau values are represented by the colour intensity of the gene nodes.

UpSetPlot (Fig. 5F)

Average expression profiles for tissues and broad cell types were calculated in log2CPM space. Next, all genes with log2CPM>1 were selected as being highly expressed in the tissue/broad cell type. For every gene the evolutionary age was determined using the GenTree database (http://gentree.ioz.ac.cn/). Finally, sets of genes with their evolutionary age were then plotted in an upset plot using Python (UpSetPlot version 0.4.4).

Sex-differences analysis (Fig. 6A-6D)

For the sex bias analysis, we CPM normalized the gene expression matrix. Next, we filtered out the cells from sex specific samples, i.e., testis, ovary and male reproductive glands and also the cells which were marked to be of ‘mix’ sex or marked ‘artefact’ or ‘unannotated’ in the annotation. Since ‘body’ samples also contain sex specific tissues, we further removed the cells annotated as germ cells or cells assigned to other sex specific clusters.

To be as stringent as possible, we further removed cells that were either (i) co-clustered in the t-SNE with these sex-specific cell types or organs, or (ii) might be improperly annotated as evidenced by co-expression of mutually exclusive cell-type specific markers. These cells were identified using the SCope web interface and "lasso" tool and removed. The list of cells removed by this manual procedure is included as in **Table S4**.

At the end of the filtering, 270,486 cells from 176 annotated clusters remained and were used for our analysis. **Table S5** gives the details of these cells and annotations. These were grouped by annotation and for each gene in each annotated cluster, we computed i) it's sex bias B (B = log2((male_avg+1e-9) / (female_avg+1e-9))) where male_avg and female_avg denote the average expression (computed from the normalized expression matrix) of the male and female cells, respectively, in the cluster and p-value for the bias (multiple tests corrected) using Wilcoxon test (scanpy function sc.tl.rank_genes_groups() with default parameters) of the difference in male and female means, and ii) average dsx expression (normalized).

For each annotated cluster and gene, we denoted the gene to be male-biased in this cluster, if sex-biased B was > 1 (i.e., 2-fold change in favor of male) with FDR < 0.05. Similarly, female-biased if sex-biased B was < -1 (i.e., 2-fold change in favor of female) with FDR < 0.05. A gene was considered sex biased if it was either male or female biased. Using this definition, we obtained the list of 9179 genes which are sex-biased in at least one annotated cluster. Next, for each cluster we computed what percentage of these sex biased genes were male (respectively female) biased in the given cluster. We define these fractions as male-bias (respectively female-bias) of the cluster. This information is kept in the data file **Table S6**.

Data used for the SNE visualizations on panel B is kept in the data file **Table S5**. This table also includes the dsx expression for each cell, extracted from the normalized expression matrix. The *dsx* expression level displayed on panel B uses log scale: (log2(dsx+1)). The cells with zero *dsx* expression are shown in gray and remaining using the color scale shown in the legend. For the bottom two subpanels each projected cell is colored according to the sex bias (as defined above) of the cluster it belongs to. For comparison with the top panels, we show the female-bias for female cells only on the left and male-bias for the male cells only on the right. For all four subpanels, if the displayed value is outside the scale, we use the closest extreme color (using sign < or >).

For the cut-off for *dsx* presence in panel D, we used 0.1 which is equal to maximum of average dsx expression (rounded to single decimal digit) of all germ cells which are known to not express dsx but show trace expression in FCA data (we note that these clusters are otherwise removed from this analysis and only used to decide the threshold for other clusters in this analysis).

Trajectory inference of testis subsets (Fig. 6E–G)

We used slingshot to infer a possible branching trajectory in subsets of the testis cells. Specifically, 1) for the spermatogonia-spermatocyte trajectory we used clusters annotated as spermatogonia or spermatocytes, 2) for spermatids we used clusters annotated as early/late spermatids, and 3) for early cyst cells, we used cyst stem cells, early cyst cells and the two spermatocyte cyst cell branches. As input for slingshot, we used Seurat's FindClusters function with resolution 0.4 to find clusters, and the first 20 PCA components as dimensionality reduction. We also provided the start cell of the trajectory as "cyst stem cell", "spermatogonium", and "early elongation stage spermatid". To determine differentially expressed genes, we used the "calculate_overall_feature_importance" function from dyno (https://github.com/dynverse/dyno) and filtered genes based on a feature importance of at least 0.1 and a log2fold change along any point in the trajectory of at least 0.5. To map the trajectory onto the UMAP embedding, we used the project_trajectory function, also implemented in dyno.

Metabolic clustering using ASAP

For probing the FCA data for an enrichment in Fatty acid synthesis (FAS) and Fatty acid degradation (FAD) metabolic genes, we first downloaded the latest KEGG assignments of genes of *Drosophila melanogaster* (DM) which were mapped to KEGG pathways (FAS: map00061, and FAD: map00071) on December 2020. We next used the ASAP (Automated Single-cell Analysis Pipeline) platform to probe the FCA datasets for a transcriptional enrichment of the genes of these metabolic pathways (*18*). ASAP generates a score from the difference of expression of the genes in the FAS or FAD gene sets as compared to background genes. In short, for each gene in the gene set, the function will take n random genes from the same expression quantile and add them to a background gene set. The gene set score is calculated as the difference of average expression of the genes in the module score and the genes in the background, for each cell. Scores close to zero indicate a similar expression, positive scores indicate higher expression and negative scores indicate lower expression of the genes in the gene set than the background genes. This function was adapted from the AddModuleScore function from the Seurat package , and was entirely recorded in Java. We have used the non-normalized parsed Fat body v2 data as input matrix, 24 bins, 100 background genes and set the seed to 42. We plotted the results using the visualization feature implemented in ASAP and colored the cells according to the score values (*18*). Finally, we used the FCA 0.4 resolution clustering information available on Scope to delineate the frontiers between the different cell clusters.

Transcription factor pleiotropy analysis

Markers were calculated with the wilcoxon test, comparing every cell type against all other cells. Next only genes with pval adj<0.05 and average $\log_2$[foldchange] > 1 were selected as selective markers.

Ovary data integration (fig. S37)

Four scRNA-seq datasets of the adult ovary were used for the data integration: current FCA data and three other published datasets (*41*, *42*, *55*) merged and batch corrected using Seurat v4.0.1. Datasets were processed with Seurat v4.0.1 in RStudio Version 1.4.1103. Batch correction was performed as described (*51*) 4. Clustering of unannotated cell types was performed using the FindClusters command in Seurat v4.0.1 with a resolution factor of 0.6. Image processing was performed with FIJI. Fly lines were ordered from BDSC: *sick-Gal4* (#76195), *Wnt4-Gal4* (#67449), *UAS-RedStinger, UAS-Flp, Ubi-(FRT.STOP.FRT) -Stinger* (#28281).

FCA Consortium Funding:
The sequencing experimental work was supported by the Chan Zuckerberg Biohub (S. Quake), Genentech Inc (H. Jasper), National Institutes of Health (B. Oliver), and Howard Hughes Medical Institute and a National Institutes of Health grant (L. Luo). Computational work was supported by the KU Leuven and the Flemish Supercomputer Center (VSC) (S. Aerts) and EPFL (B. Deplancke).

H. Li is a CPRIT Scholar in Cancer Research (RR200063) and supported by National Institutes of Health (R00AG062746). L. Luo is a Howard Hughes Medical Institute (HHMI) investigator and supported by the National Institutes of Health (R01DC005982). S. Aerts was supported by KU Leuven (grant no. C14/18/092) and FWO (grant no. G094121N). J. Janssens is supported by a PhD fellowship of The Research Foundation – Flanders (FWO, 1199518N). B. Deplancke, V. Gardeux, and F. David were supported by an EPFL Open Science Grant and a Precision Health and related Technologies Grant (no. PHRT-502). F. Schnorrer is supported by the Centre National de la Recherche Scientifique (CNRS), Aix-Marseille University (ANR-11-IDEX-0001-02), the European Research Council under the European's Union Horizon 2020 Programme (ERC-2019-SyG 856118), the French National Research Agency (ANR-18-CE45-0016-01) and the Turing Centre for Living Systems (ANR-16-CONV-0001). S. Quake is a Chan Zuckerberg Biohub Investigator. N. Perrimon is a Howard Hughes Medical Institute (HHMI) investigator. C. McLaughlin is a HHMI fellow of the Damon Runyon Cancer Research Foundation (DRG 2390- 20). M. T. Fuller and C. W. Berry were supported by NIH grants 1R01GM122951 and R35GM136433, the Reed-Hodgson Professorship in Human Biology to MTF and NIH Training grant T32AR007422 for CWB. S. K. Kim and L. Kockel were supported by NIH awards (R01 DK107507; R01 DK108817; U01 DK123743; P30 DK116074 to S.K.K.), the JDRF Northern California Center of Excellence (to S.K.K. and M. Hebrok), the H.L. Snyder Foundation and Elser Trust, and the Stanford Diabetes Research Center. K. Rust was supported by the Deutsche Forschungsgemeinschaft (DFG, project number 419293565) and the Promoting Scientific Independence (PSI) Program of the Philipps-University Marburg, Germany. C. Ribeiro is supported by the Champalimaud Foundation, "la Caixa" Banking Foundation (LCF/PR/HR17/52150002), Fundação para a Ciência e Tecnologia (02/SAICT/30081/2017), and the Global Consortium for Reproductive Longevity and Equality through the Buck Institute, made possible by the Bia-Echo Foundation (GCRLE-1420). H. Krause was supported by a grant from the Canadian Institutes of Health Research (MOP-133743). J. A. Brill was supported by the Natural Science and Engineering Research Council (RGPIN-2016-06775). B. Oliver was supported in part by the Intramural Research Program of the NIH, The National Institute of Diabetes and Digestive and Kidney Diseases (DK015600). T. Przytycka was supported in part by the Intramural Research Program of the NIH, National Library of Medicine, (LM200887). A. K. Groves is supported by the National Institutes of Health (R01DC014932). S. Yamamoto is supported by the National Institutes of Health (U54NS093793, R01DC014932, R24OD022005, U54OD030165, R01AG071557, R01HG011795). M. Wolfner was supported by NIH grant R37HD038921, and by an NIH grant of which A.G. Clark is joint-PI, R01HD059060. Mehmet Neset Özel, Nikolaos Konstantinides and Claude Desplan were supported by NIH grant R01EY017916. Claude Desplan was also supported by NYU Abu Dhabi Research Institute grant to the Center for Genomics and Systems Biology (ADHPG-CGSB). R. Lehmann was supported as a Howard Hughes Medical Institute (HHMI) investigator and by the National Institutes of Health (R37 HD41900). E. Donà was supported by a Sir Henry Wellcome Postdoctoral Fellowship (110232/Z/15/Z). G. S. X. E. Jefferis was supported by the MRC (MC-U105188491) and an ERC Consolidator grant (649111). S.L. Holtz and R.I. Wilson are supported a grant from the NIH (R01NS101157). S.L.H. was also supported by a fellowship from the NIH (F31NS106982). R.I.W. is an investigator of the Howard Hughes Medical Institute (HHMI). S. DiNardo is supported by NIH R35GM136270. Scott Waddell and Christoph D. Treiber were funded by a Wellcome Principal Research Fellowship (200846/Z/16/Z), Wellcome Collaborative Award (209235/Z/17/Z) and European Research Council Advanced Grant (789274) to S.W. R. Bodmer is supported by NIH HL054732, AG045428, AG058075, HL149992, G. Vogler is supported my HL54732 and DOD W81XWH-21-1-0259, M. Tamayo is supported by DOD W81XWH-21-1-0259, K. Birker is supported by AHA 835002, J. Kezos is supported by NIH F32 Hl56607. T. Kornberg is supported by NIH R35GM122548. I.Papatheodorou, N. Georg, J. Manning are supported by EMBL States, BBSRC/NSF BB/T014563/1 and WT Single Cell Atlas: 221401/Z/20/Z. "The research was funded in part by the Wellcome Trust [221401/Z/20/Z]. For the purpose of open access, the author has applied a CC BY public copyright licence to any Author Accepted Manuscript version arising from this submission." "This work was supported by the Biotechnology and Biological Sciences Research Council (BBSRC) [Grant number: BB/T014563/1]" Z. Carvalho-Santos is financed by national funds through the FCT in the framework of the financing of the Norma Transitória DL 57/2016. I. Tastekin is financed by Marie Skłodowska-Curie Actions postdoctoral fellowship MSCA-IF-EF-ST 867459. R. Cardoso-Figueiredo is financed by the FCT doctoral fellowship SFRH/BD/143862/2019. D. Dhakan is financed by the La Caixa Foundation, LCF/PR/HR17/52150002. Zepeng Yao was supported by a Jane Coffin Childs Fellowship. T. G. Nystul is supported by NIH R35GM136348. Erika L. Matunis is supported by NIH R35GM136665 and HD052937. Thomas R. Clandinin was supported by 5R01EY02263808, 5U19NS104655-04, 3R01NS11006003S1, and by 5P30EY02687704. Jiwon Shim was supported by the Samsung Science and Technology Foundation (SSTF-BA1701-15). Aaron M. Allen, Megan C. Neville and Stephen F. Goodwin were supported by a Wellcome Investigator Award (106189/Z/14/Z) and a Wellcome Collaborative Award (209235/Z/17/Z) to S.F.G. Joshua Shing Shun Li was is supported by a Croucher fellowship for Postdoctoral Research from the Croucher Foundation. Devika Agarwal was supported by the Wellcome Collaborative Award (209235/Z/17/Z) to S.W. , S.F.G and David Sims. Helen White-Cooper was supported by a the Biotechnology and Biological Sciences Research Council (BBSRC) (Grant number BB/P001564/1). O'Brien Lab information: Lucy O'Brien was supported by the American Cancer Society (ACS) RSG-17-167-01-DDC and the National Institutes of Health (NIH) (R01GM116000-01A1). Erin Nicole Sanders was supported by NSF GRFP DGE-1656518 and by a Stanford Developmental Biology and Genetics NIH Training Grant (2T32GM00779038). Paola Moreno Roman was supported by a Stanford Bio-X Bowes Graduate Fellowship and by a Stanford DARE (Diversifying Academia Recruiting Excellence) Fellowship and the National Institutes of Health (NIH) (R01GM116000-01A1). Anna A. Kim was supported by the Swedish Research Council under grant number 2017-06156 and a seed grant from the Stanford Bio-X. Yu-Han Su was supported by the National Institutes of Health (NIH) (R01GM116000-01A1). Anthony Galenza was supported by the National Institutes of Health (NIH) (R01GM116000-01A1). Sang Ngo was supported by the American Cancer

Society (ACS) RSG-17-167-01-DDC and the National Institutes of Health (NIH) (R01GM116000-01A1). Aparna Sherlekar was supported by the American Cancer Society (ACS) RSG-17-167-01-DDC and the National Institutes of Health (NIH) (R01GM116000-01A1). Andrew Thomas Labott was supported by the National Institutes of Health (NIH) (R01GM116000-01A1). Samantha Gumbin was supported by a Stanford Graduate Fellowship, Smith Fellow.

Supplementary Figures and Legends

FCA Figure S1

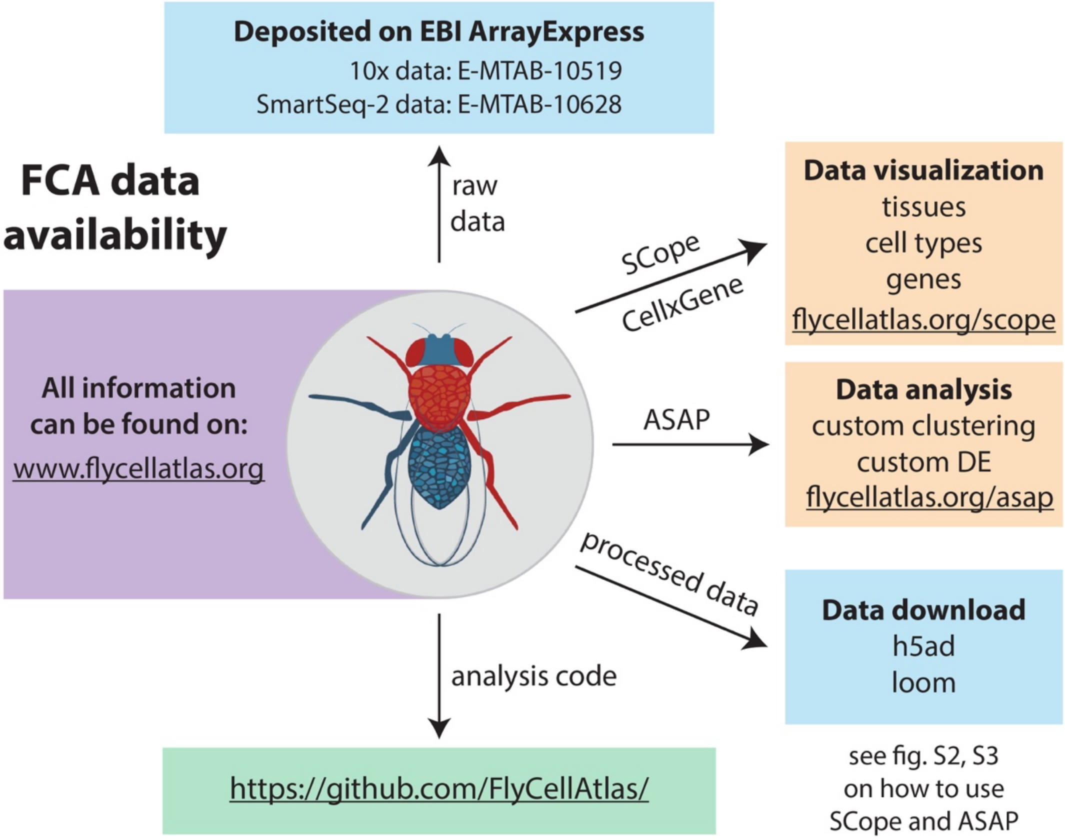

Figure S1. Summary of FCA data availability. See fig. S2 and S3 for more details.

FCA Figure S2

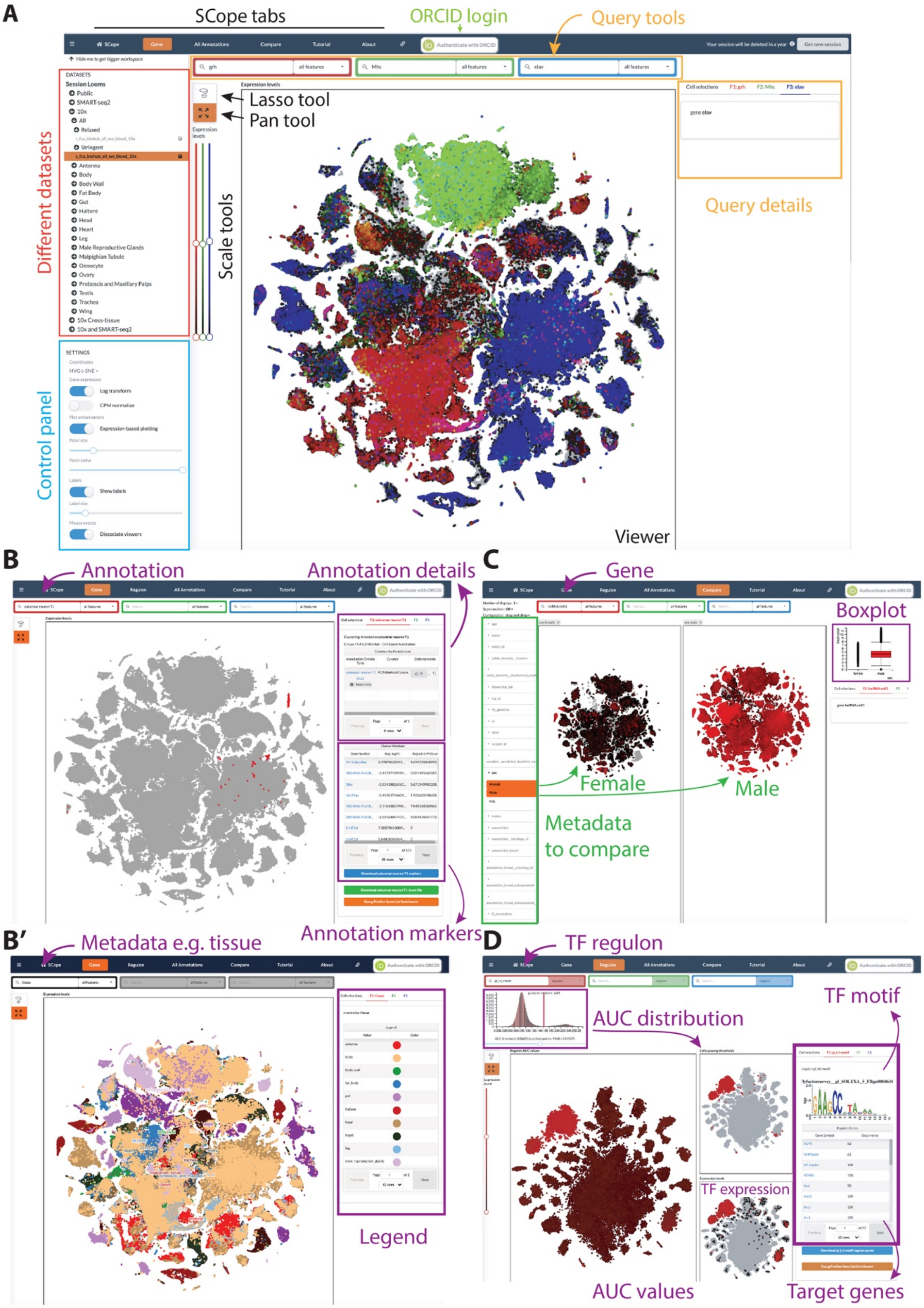

Figure S2. How to use SCope for visualizing the FCA datasets. This is a short overview of how the FCA datasets are accessible through the SCope platform (https://flycellatlas.org/scope).

(A) At the top, different modes can be selected, "Gene" being the default option. Further, a user can login with their ORCID. Navigation between different datasets is possible through the hierarchical tree on the left, showing both Relaxed and Stringent datasets for every tissue. The selected tissue is visualized in the main viewer, whose settings can be adapted in the Control panel: different embeddings can be selected by clicking on “Coordinates” (choices are tSNE, UMAP, PCA, SCENIC tSNE and SCENIC UMAP), and the appearance of the points can be modified (size and transparency [alpha]). Gene expression can be plotted using up to three query boxes, by default one for each primary color. Colors can be modified using the Scale tools or by selecting different normalization options in the Control panel. A user can select cell subpopulations for closer inspection with the Lasso tool, and move and zoom in the viewer using the Pan tool.

(B) The “Gene” mode also allows the user to look for annotations. Cells belonging to the selected annotation will be colored, and annotation details including marker genes will pop up on the right. The marker genes can be sorted by AvgLogFC or adjusted p-value. Download buttons are present to download marker genes or a subset of the loom file. Finally, the marker genes can be sent to gProfiler for gene ontology enrichment. Similarly, clusters and their marker genes can be queried in different resolutions.

(B’) Metadata can also be queried in the “Gene” mode, coloring cells based on metadata (e.g. tissue, sex) with a legend on the right and labels over the median location.

(C) The “Compare” mode, allows to split the data based on metadata, allowing to compare gene expression. Additionally, a boxplot appears for more quantitative comparisons.

(D) The “Regulon” mode allows to visualize gene regulatory networks linked to TFs. A regulon (GRN) consists of a TF and its motif, with predicted target genes that are co-expressed and whose locus is enriched for the TF motif. Network activity in cells is scored as AUC with AUCell. The AUC distribution is shown as a histogram, and an optimal threshold can be set manually. The viewer shows both the raw AUC values (left), the cells passing the AUC threshold (top right), and the raw TF expression (bottom right). The “Regulon" tab is present for all tissues, but not for the combined dataset.

For more details, please refer to this video tutorial for using SCope (https://www.youtube.com/watch?v=yNETQVaSJYM&t=349s).

FCA Figure S3

A

Access FCA datasets directly from ASAP (asap.epfl.ch)
Top bar > Data > FlyCellAtlas

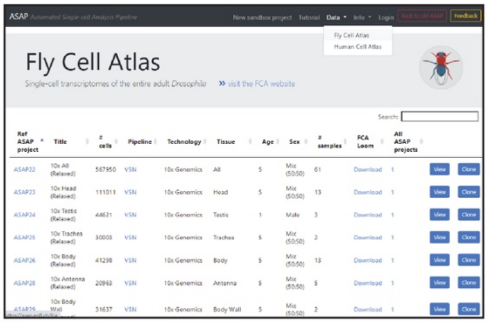

ASAP *Automated Single-cell Analysis Pipeline* — New sandbox project · Tutorial · Data ▾ · Info ▾ · Login · Back to old ASAP · Feedback

Data menu: Fly Cell Atlas · Human Cell Atlas

Fly Cell Atlas

Single-cell transcriptomes of the entire adult *Drosophila* » visit the FCA website

Search:

Ref ASAP project	Title	# cells	Pipeline	Technology	Tissue	Age	Sex	# samples	FCA Loom	All ASAP projects		
ASAP22	10x All (Relaxed)	567950	VSN	10x Genomics	All	5	Mix (50:50)	61	Download	1	View	Clone
ASAP23	10x Head (Relaxed)	111011	VSN	10x Genomics	Head	5	Mix (50:50)	13	Download	1	View	Clone
ASAP24	10x Testis (Relaxed)	44621	VSN	10x Genomics	Testis	1	Male	3	Download	1	View	Clone
ASAP25	10x Trachea (Relaxed)	30003	VSN	10x Genomics	Trachea	5	Mix (50:50)	2	Download	1	View	Clone
ASAP26	10x Body (Relaxed)	41298	VSN	10x Genomics	Body	5	Mix (50:50)	13	Download	1	View	Clone
ASAP28	10x Antenna (Relaxed)	20963	VSN	10x Genomics	Antenna	5	Mix (50:50)	5	Download	1	View	Clone
ASAP29	10x Body Wall	31637	VSN	10x Genomics	Body Wall	5	Mix (50:50)	2	Download	1	View	Clone

Or from ASAP links on the FCA main portal (flycellatlas.org)
Top bar > Data

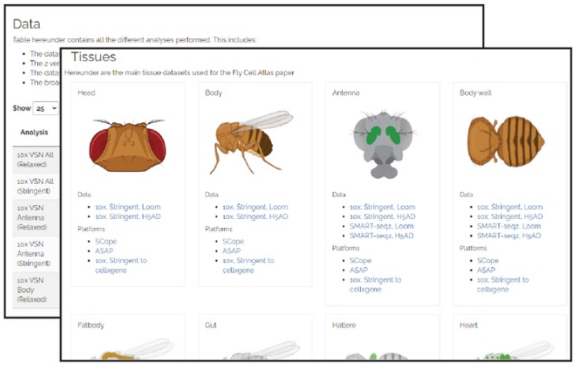

Data

Table hereunder contains all the different analyses performed. This includes:

- The data
- The 2 ver
- The data
- The broa

Show 25 ▾

Analysis
10x VSN All (Relaxed)
10x VSN All (Stringent)
10x VSN Antenna (Relaxed)
10x VSN Antenna (Stringent)
10x VSN Body (Relaxed)

Tissues

Hereunder are the main tissue datasets used for the Fly Cell Atlas paper

Head

Data
- 10x, Stringent, Loom
- 10x, Stringent, H5AD

Platforms
- SCope
- ASAP
- 10x, Stringent to cellxgene

Body

Data
- 10x, Stringent, Loom
- 10x, Stringent, H5AD

Platforms
- SCope
- ASAP
- 10x, Stringent to cellxgene

Antenna

Data
- 10x, Stringent, Loom
- 10x, Stringent, H5AD
- SMART-seq2, Loom
- SMART-seq2, H5AD

Platforms
- SCope
- ASAP
- 10x, Stringent to cellxgene

Body wall

Data
- 10x, Stringent, Loom
- 10x, Stringent, H5AD
- SMART-seq2, Loom
- SMART-seq2, H5AD

Platforms
- SCope
- ASAP
- 10x, Stringent to cellxgene

Fatbody

Gut

Haltere

Heart

B

Selecting any tissue/project will then open the project in ASAP and jump directly to the precalculated UMAP (that can be changed to t-SNE/PCA). In this view, you can:

Clone / share the project
(to modify it)

Browse the cells interactively
or select cells using lasso

Color the plot according to
- gene expression
- metadata (sex, batch, etc..)
- cell type annotation
- clustering

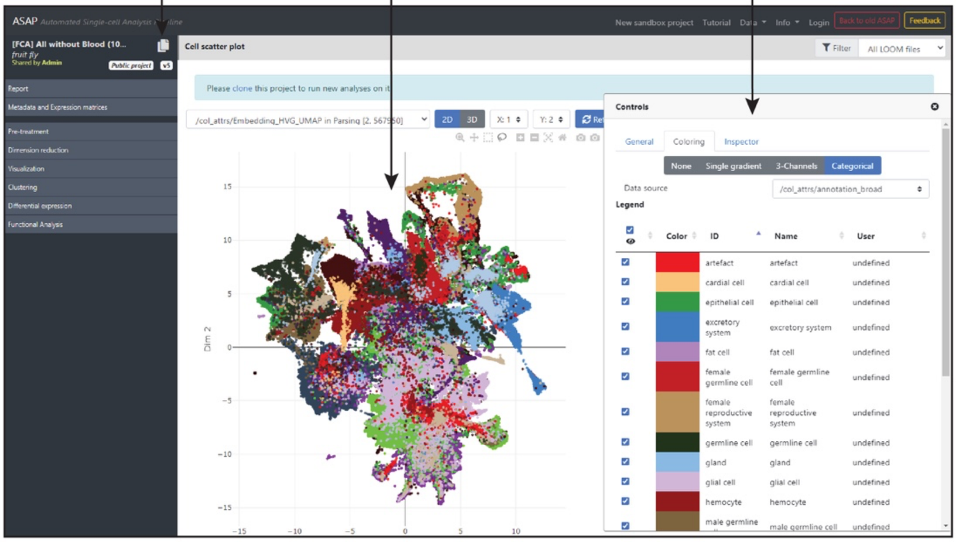

ASAP *Automated Single-cell Analysis Pipeline* — New sandbox project · Tutorial · Data ▾ · Info ▾ · Login · Back to old ASAP · Feedback

[FCA] All without Blood (10...
fruit fly
Shared by Admin — Public project · v5

- Report
- Metadata and Expression matrices
- Pre-treatment
- Dimension reduction
- Visualization
- Clustering
- Differential expression
- Functional Analysis

Cell scatter plot — Filter · All LOOM files ▾

Please clone this project to run new analyses on it

/col_attrs/Embedding_HVG_UMAP in Parsing [2, 567950] ▾ · 2D · 3D · X: 1 · Y: 2 · Re

Controls

General · Coloring · Inspector

None · Single gradient · 3-Channels · Categorical

Data source: /col_attrs/annotation_broad

Legend

☑	Color	ID	Name	User
☑	🟥	artefact	artefact	undefined
☑	🟧	cardial cell	cardial cell	undefined
☑	🟩	epithelial cell	epithelial cell	undefined
☑	🟦	excretory system	excretory system	undefined
☑	🟪	fat cell	fat cell	undefined
☑	🟥	female germline cell	female germline cell	undefined
☑	🟫	female reproductive system	female reproductive system	undefined
☑	⬛	germline cell	germline cell	undefined
☑	🟦	gland	gland	undefined
☑	🟪	glial cell	glial cell	undefined
☑	🟥	hemocyte	hemocyte	undefined
☑	🟫	male germline	male germline cell	undefined

Run additional analyses online such as cell filtering (e.g. subclustering), clustering, differential expression, ...

C

Case study: you can filter cells and select only one cluster for subclustering and marker gene discovery

1. Pre-treatment > Cell Filtering
Select cluster(s) of interest to keep
(here adult oenocyte)

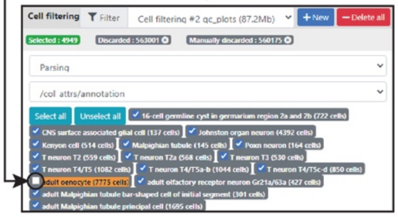

Cell filtering · Filter · Cell filtering #2 qc_plots (87.2Mb) ▾ · + New · − Delete all

Selected : 4949 · Discarded : 563001 · Manually discarded : 560175

Parsing ▾

/col attrs/annotation ▾

Select all · Unselect all

- ☑ 16-cell germline cyst in germarium region 2a and 2b (722 cells)
- ☑ CNS surface associated glial cell (137 cells)
- ☑ Johnston organ neuron (4392 cells)
- ☑ Kenyon cell (514 cells)
- ☑ Malpighian tubule (145 cells)
- ☑ Poxn neuron (164 cells)
- ☑ T neuron T2 (559 cells)
- ☑ T neuron T2a (568 cells)
- ☑ T neuron T3 (530 cells)
- ☑ T neuron T4/T5 (1082 cells)
- ☑ T neuron T4/T5a-b (1044 cells)
- ☑ T neuron T4/T5c-d (850 cells)
- ☐ adult oenocyte (7775 cells)
- ☑ adult olfactory receptor neuron Gr21a/63a (427 cells)
- ☑ adult Malpighian tubule bar-shaped cell of initial segment (301 cells)
- ☑ adult Malpighian tubule principal cell (1695 cells)

2. Dimension Reduction
PCA > UMAP > Clustering
(here 19 subclusters are found)

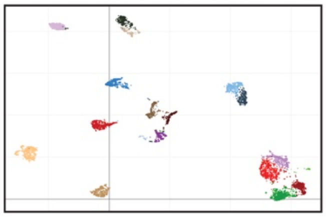

3. Differential expression
Marker genes of each subcluster
(here top 10 up-/down-regulated)

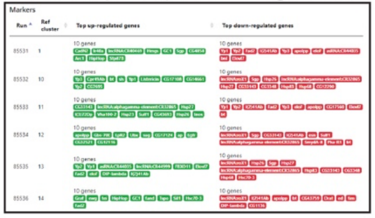

Markers

Run	Ref cluster	Top up-regulated genes	Top down-regulated genes
85531	1	10 genes CadN2 · ln46a · lncRNA:CR40469 · Hmgs · GC1 · Sgp · CG4858 · Arc1 · HipHop · [illegible]	10 genes Yp1 · Yp2 · Fad2 · l(2)41Ab · Yp3 · apolpp · eloF · asRNA:CR44035 · [illegible] · Elovl7
85532	10	10 genes Yp3 · Cpr49Ab · bt · sls · Yp1 · Listericin · CG17108 · CG14661 · Yp2 · CG7695	10 genes lncRNA:roX1 · Sgp · Hsp26 · lncRNA:alphagamma-element:CR32865 · Hsp27 · CG33143 · CG3348 · Hsp83 · Hsp68 · CG12290
85533	11	10 genes CG33143 · lncRNA:alphagamma-element:CR32865 · Hsp27 · l(3)72Dp · Vha100-2 · Hsp23 · Sulf1 · CG43693 · Hsp26 · [illegible]	10 genes Yp1 · Yp2 · l(2)41Ab · Fad2 · Yp3 · eloF · apolpp · CG17560 · Elovl7 · bt
85534	12	10 genes apolpp · Gbs-70E · [illegible] · Ubx · sug · CG17124 · ap · [illegible] · CG32521 · CG12116	10 genes lncRNA:roX1 · Sgp · CG33143 · l(2)41Ab · esn · Sulf1 · lncRNA:alphagamma-element:CR32865 · [illegible] · [illegible] · bt
85535	13	10 genes Yp2 · Yp1 · asRNA:CR44035 · lncRNA:CR44999 · FBXO11 · Elovl7 · Fad2 · eloF · DIP-lambda · l(2)41Ab	10 genes lncRNA:roX1 · Hsp26 · Sgp · Hsp27 · lncRNA:alphagamma-element:CR32865 · Hsp83 · CG33143 · CG3348 · Hsp68 · Hsc70-3
85536	14	10 genes [illegible] · ewg · [illegible] · HipHop · GC1 · [illegible] · [illegible] · [illegible] · Hsc70-3 · Fad2	10 genes lncRNA:roX1 · l(2)41Ab · apolpp · bt · CG43759 · Drat · ed · [illegible] · DIP-lambda · CG1136

Figure S3. How to use ASAP for analyzing the FCA datasets. This is a short overview of how the FCA datasets are accessible through the ASAP platform.

(A) The datasets can be accessed directly from the main ASAP website (https://flycellatlas.org/asap) where there is a dedicated page (Top bar > Data > FlyCellAtlas) listing all projects and different information (number of cells, technology used, tissue, etc…). The projects are also listed at the main Fly Cell Atlas portal (https://flycellatlas.org), and linked out to the main ASAP website, for direct view of the data. For each dataset, the user can view the project, i.e. visualize and interact with the results of the analysis pipeline and cell type annotation. The user can also clone the project in its user space to be able to modify it or create new analyses.

(B) This is the main view when the user accesses a project (from any source). The main visualization is a UMAP but t-SNE and PCA can be visualized as well. In this view, the user can color the cells according to many criteria such as gene expression, metadata (sex, age, batch, etc.), annotated cell type, clustering results, and more. The left menu contains the single-cell analysis standard pipeline to run additional/new analyses on the dataset. For example, the user can perform a new differential expression to find marker genes of each cluster or each annotation. The user can also select cells of interest (by rectangular or lasso selection) and find marker genes that are specific to this selection.

(C) This use case is featuring re-analysis of the "All" dataset (https://asap.epfl.ch/projects/ASAP22) by 1). Performing a new "Pre-treatment > Cell filtering" and selecting a cluster/annotation of interest. Here we selected the "adult oenocyte" cluster from the "annotation" metadata. It generates a new subset of 7775 cells (from 567950 cells, initially). 2). Then, we performed a new PCA with 50PCs on this subset (Dimension Reduction > PCA) and, once computed, we ran a UMAP (Dimension Reduction > UMAP) and a clustering (Clustering > Seurat) on the 50PCs of the PCA. Then, the figure shows the visualization of the UMAP, colored using the 19 clusters found by the clustering method. 3). Finally, we ran a differential expression analysis (Differential expression > Seurat – Wilcoxon) for all clusters (vs complementary) to find the marker genes of each subcluster. This view shows the top 10 up- and down-regulated genes, for each cluster (full table is also available). The user can change the thresholds (p-value, FDR, fold-change), highlight transcription factors or surface markers, or annotate the clusters. Of note, clicking on a gene will display a description of the gene and provide a link out to the Ensembl database.

FCA Figure S4

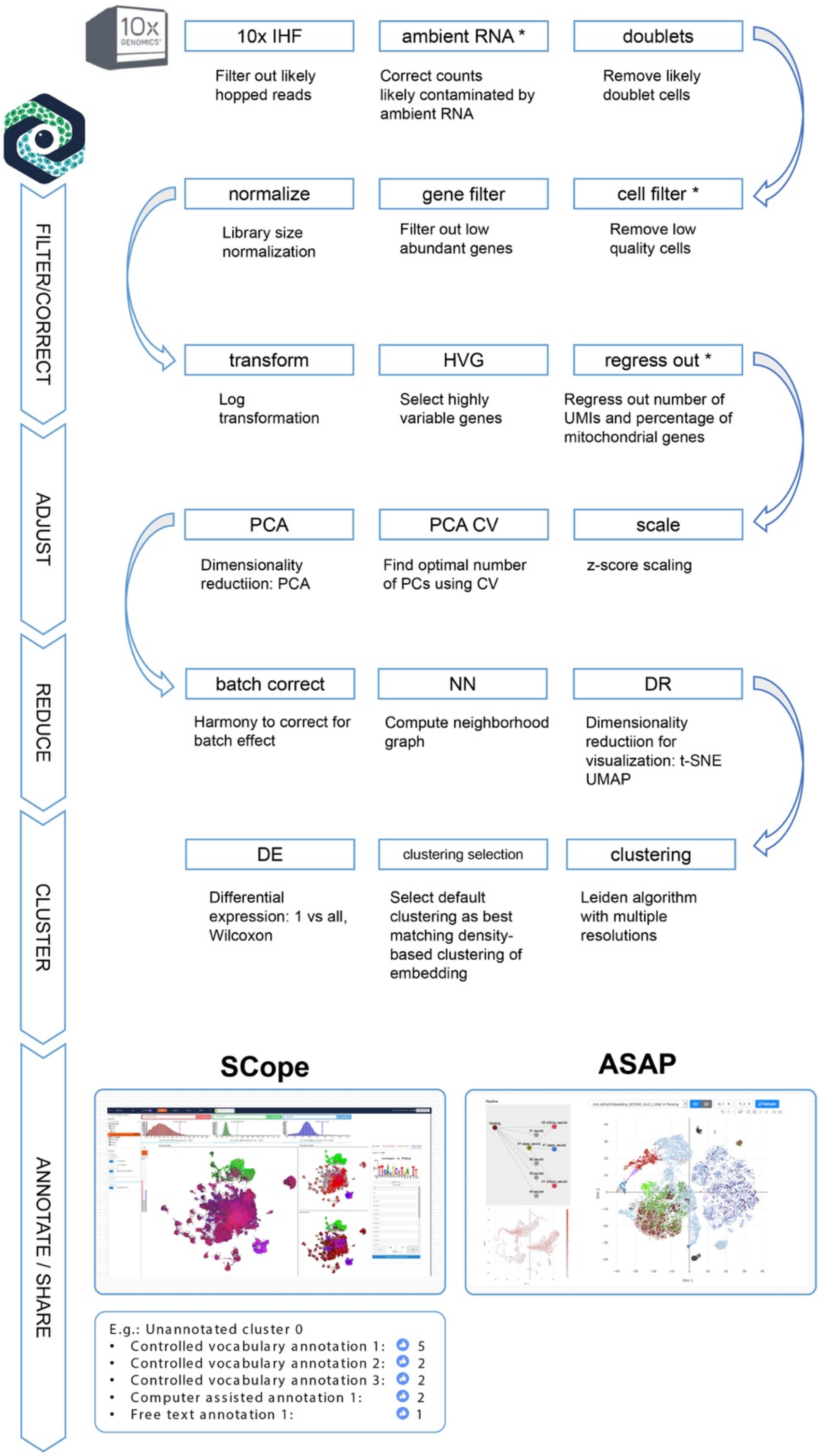
10x IHF
Filter out likely hopped reads
ambient RNA *
Correct counts likely contaminated by ambient RNA
doublets
Remove likely doublet cells
normalize
Library size normalization
gene filter
Filter out low abundant genes
cell filter *
Remove low quality cells
transform
Log transformation
HVG
Select highly variable genes
regress out *
Regress out number of UMIs and percentage of mitochondrial genes
PCA
Dimensionality reductiion: PCA
PCA CV
Find optimal number of PCs using CV
scale
z-score scaling
batch correct
Harmony to correct for batch effect
NN
Compute neighborhood graph
DR
Dimensionality reductiion for visualization: t-SNE UMAP
DE
Differential expression: 1 vs all, Wilcoxon
clustering selection
Select default clustering as best matching density-based clustering of embedding
clustering
Leiden algorithm with multiple resolutions
FILTER/CORRECT
ADJUST
REDUCE
CLUSTER
ANNOTATE / SHARE
SCope
ASAP

E.g.: Unannotated cluster 0

- Controlled vocabulary annotation 1: 5
- Controlled vocabulary annotation 2: 2
- Controlled vocabulary annotation 3: 2
- Computer assisted annotation 1: 2
- Free text annotation 1: 1

Figure S4. Steps for 10x data processing, from raw sequencing data to cluster analysis. Processed data are annotated and shared through SCope and ASAP. See Methods for detailed description.

FCA Figure S5

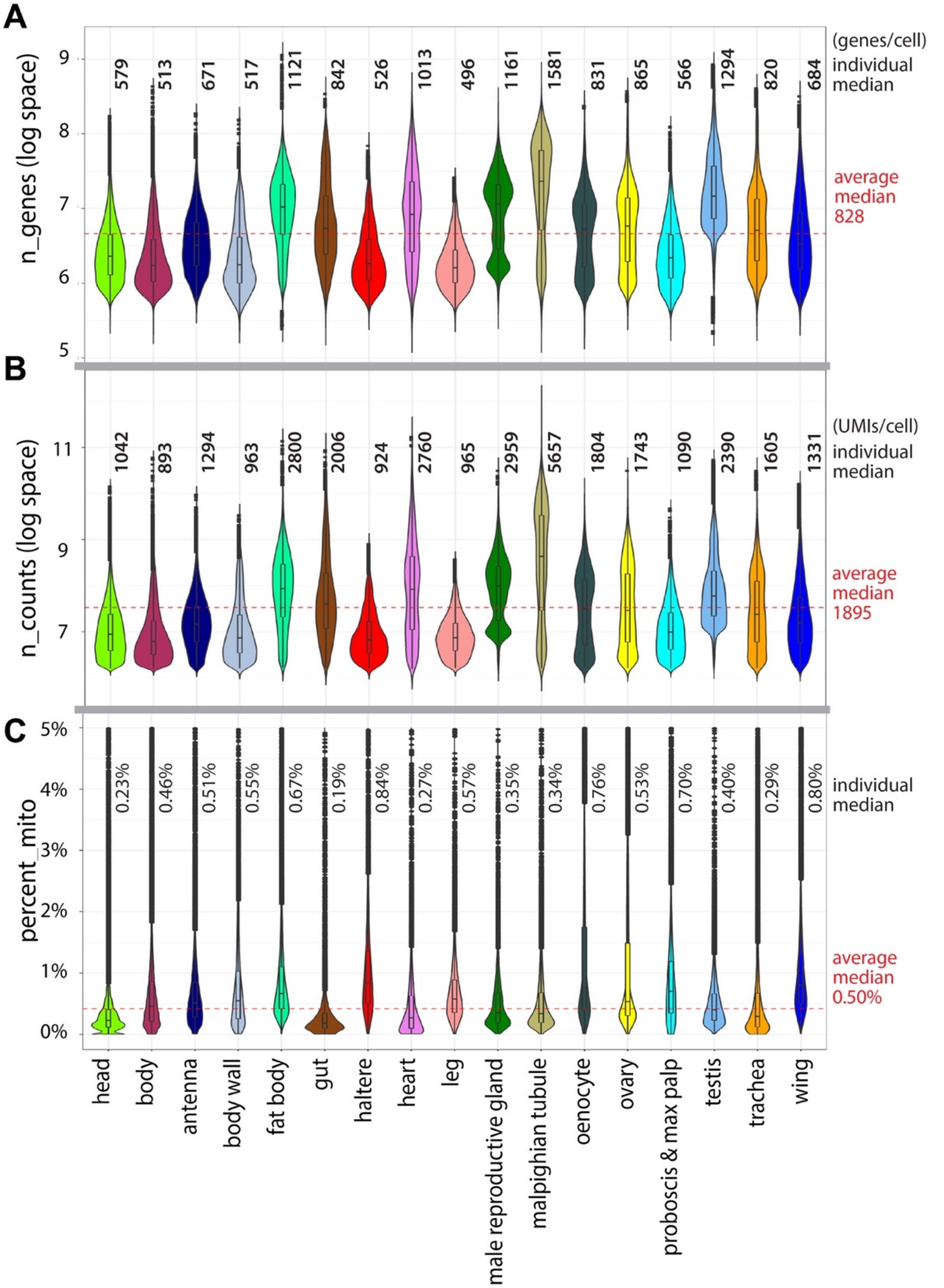

Figure S5. Quality control of 10x data.
(A) The average median UMI count is 1895 UMIs per cell.
(B) The average median gene detection is 828 genes per cell.
(C) The average median percentage of mitochondrial genes for all samples is 0.50%.
Numbers for individual tissues are indicated.

FCA Figure S6

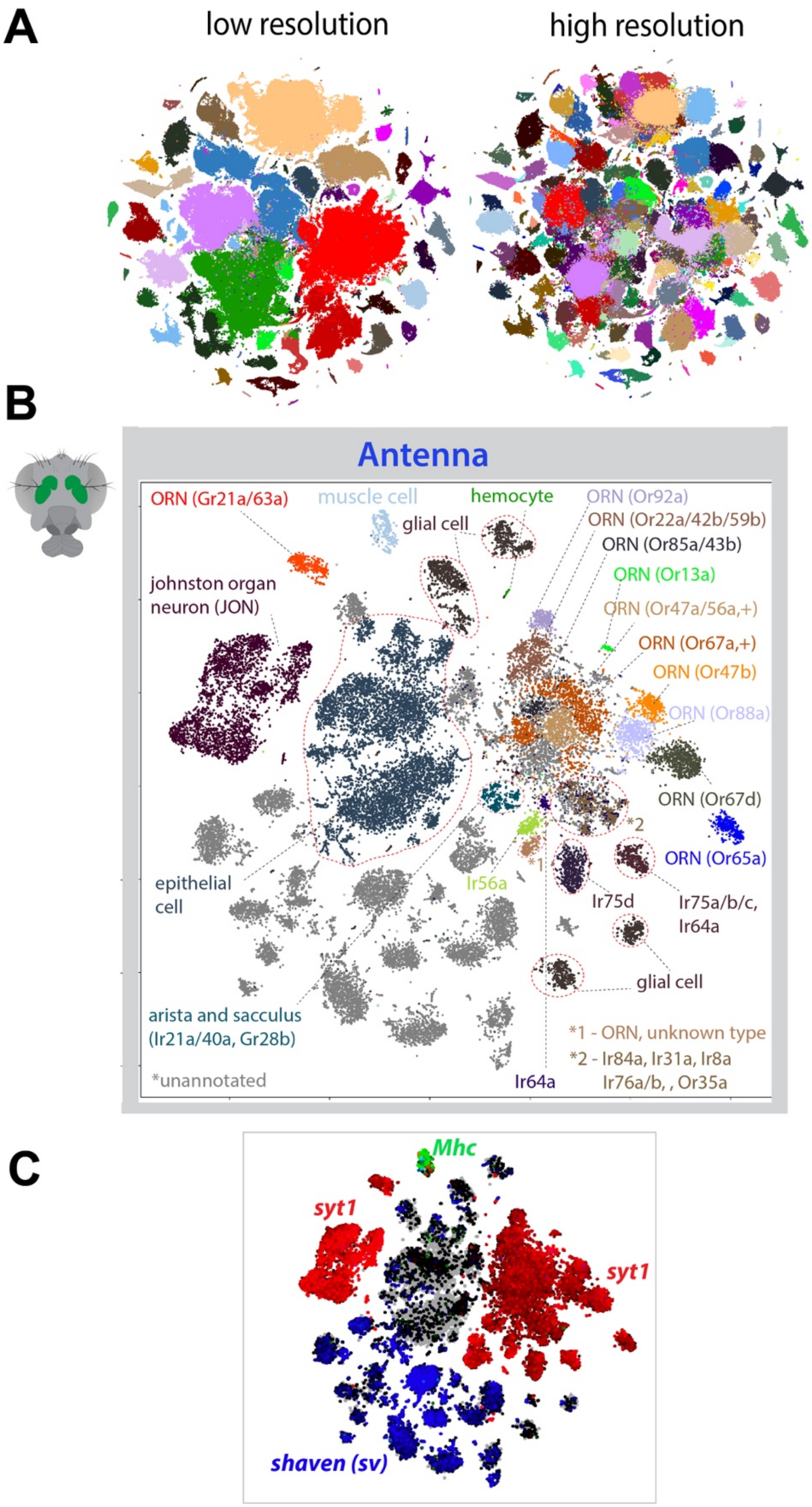

Figure S6. Different clustering resolutions and cell type annotation in the antenna.

(A) Different clustering resolutions (using Leiden) are used for annotating cell types, because some cell types are present at low clustering resolution, and others appear only at higher resolution.
(B) tSNE plot with annotations for the fly antenna from the *Stringent* 10x dataset. All three antennal segments were dissected for single-nucleus sequencing. ORN: olfactory receptor neuron.
(C) The unannotated clusters in the antenna are largely *shaven+,* likely to be different types of non-neuronal and non-glial supporting cells from different segments of the antenna.

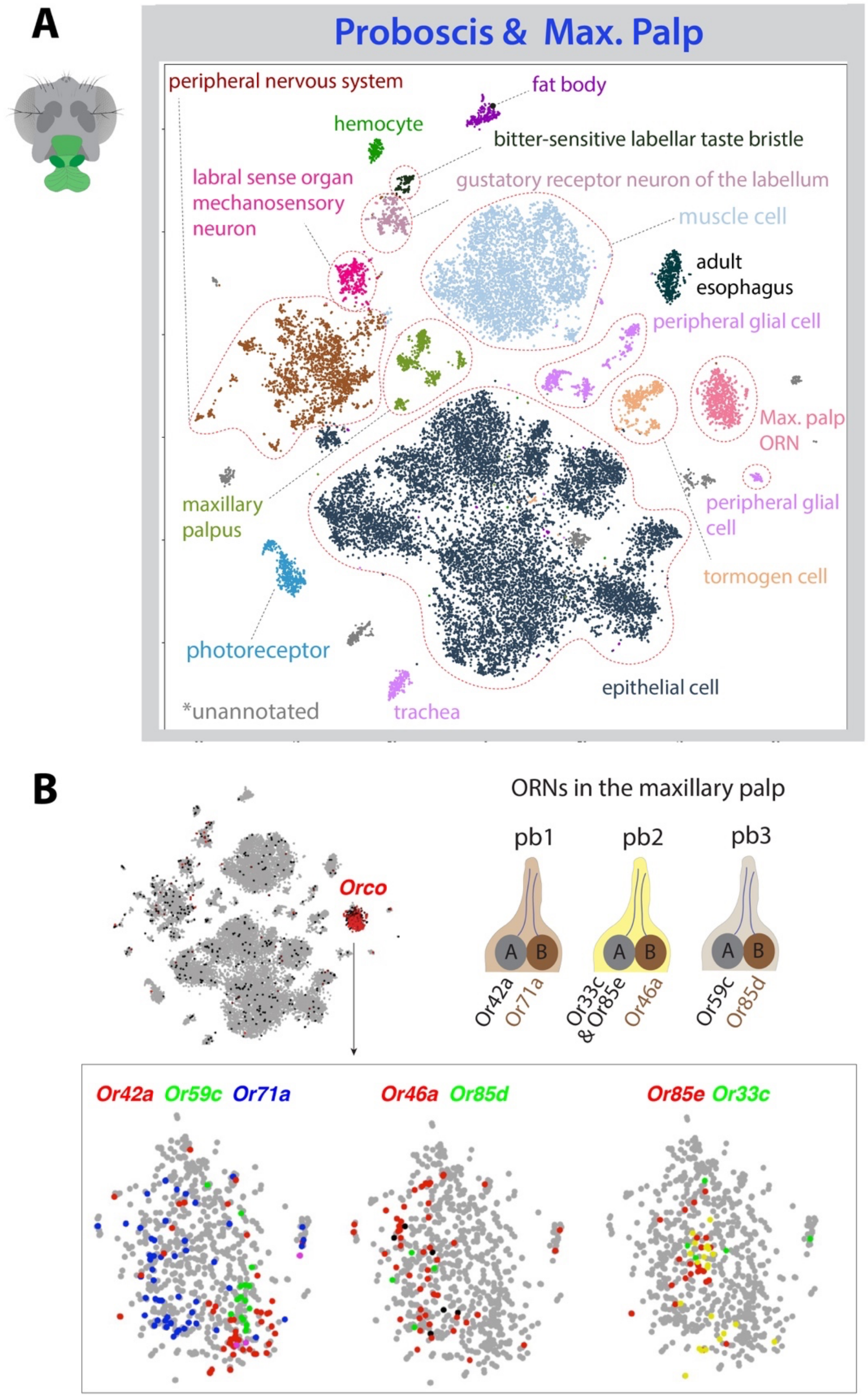

Figure S7. Cell type annotation in the proboscis and maxillary palp.

(A) tSNE plot with annotations for the fly proboscis and maxillary palp from the *Stringent* 10x dataset. ORN: olfactory receptor neuron.
(B) Expression of olfactory receptor co-receptor (*orco*) in one cluster annotated as maxillary palp ORNs. All 7 known olfactory receptor genes can be detected, including two receptors, Or33c and Or85e, that are co-expressed in the same ORN (*56*). Palpal basiconic 1 (pb1), pb2, and pb3 are three different types of sensilla in the maxillary palp.

FCA Figure S8

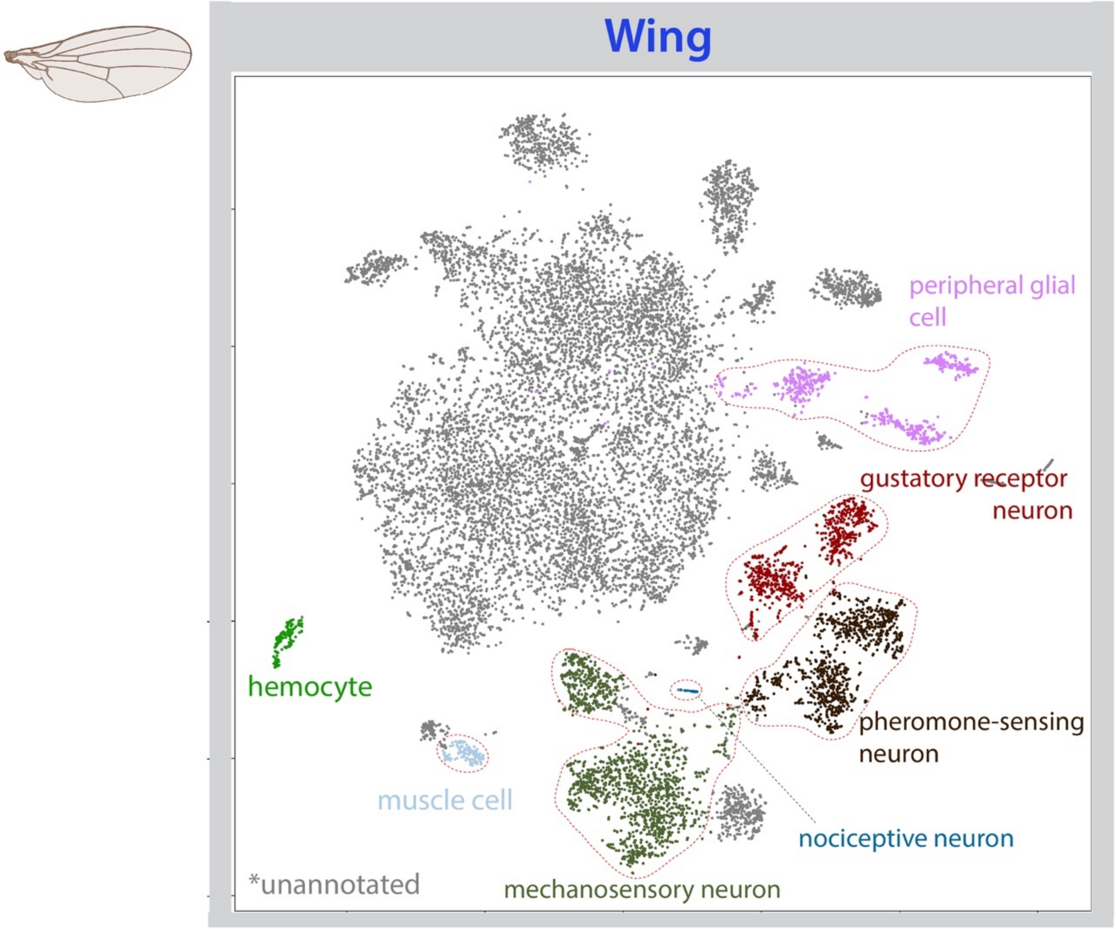

Figure S8. Cell type annotation in the wing. tSNE plot with annotations for the fly wing from the *Stringent* 10x dataset. Note a large group of cells are currently unannotated, which are likely to be epithelial cells.

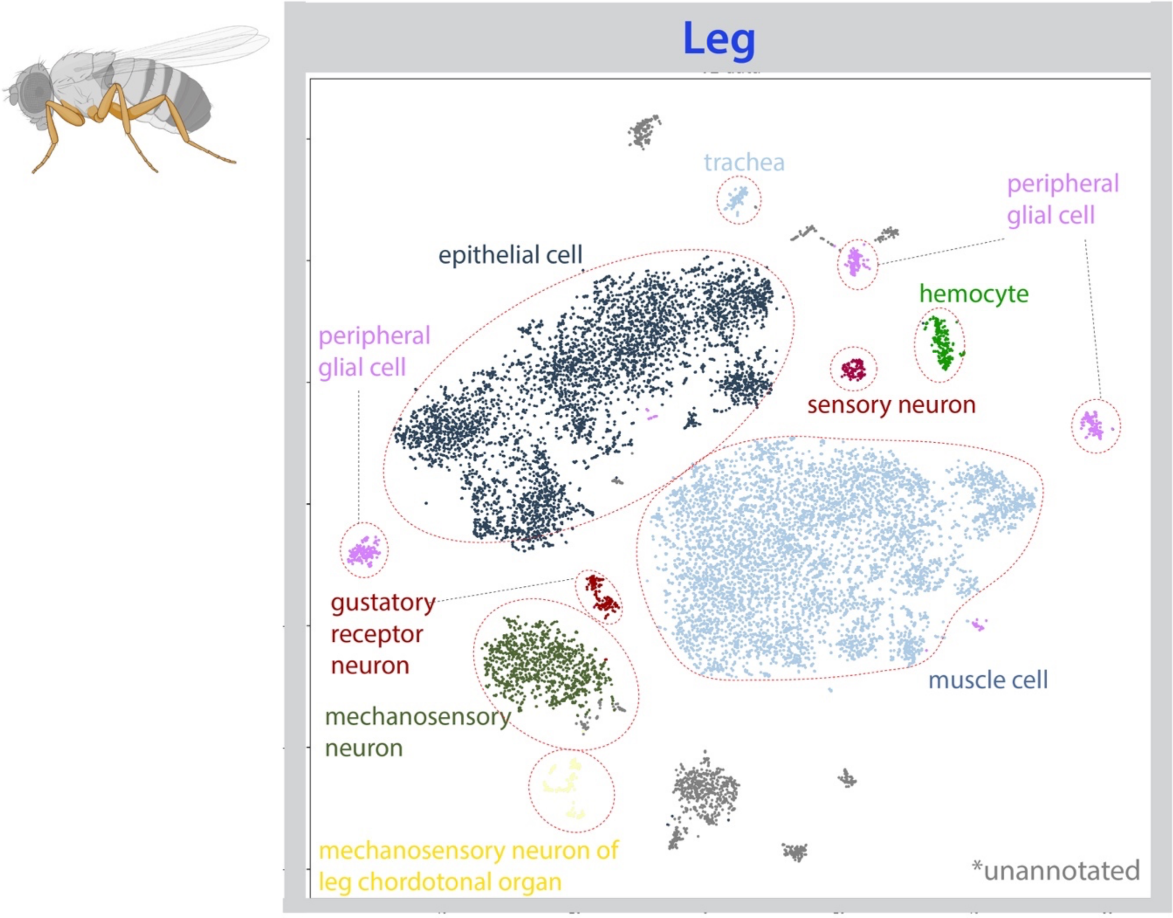

Figure S9. Cell type annotation in the leg. tSNE plot with annotations for the fly leg from the *Stringent* 10x dataset. All six fly legs were dissected and pooled for single-nucleus sequencing.

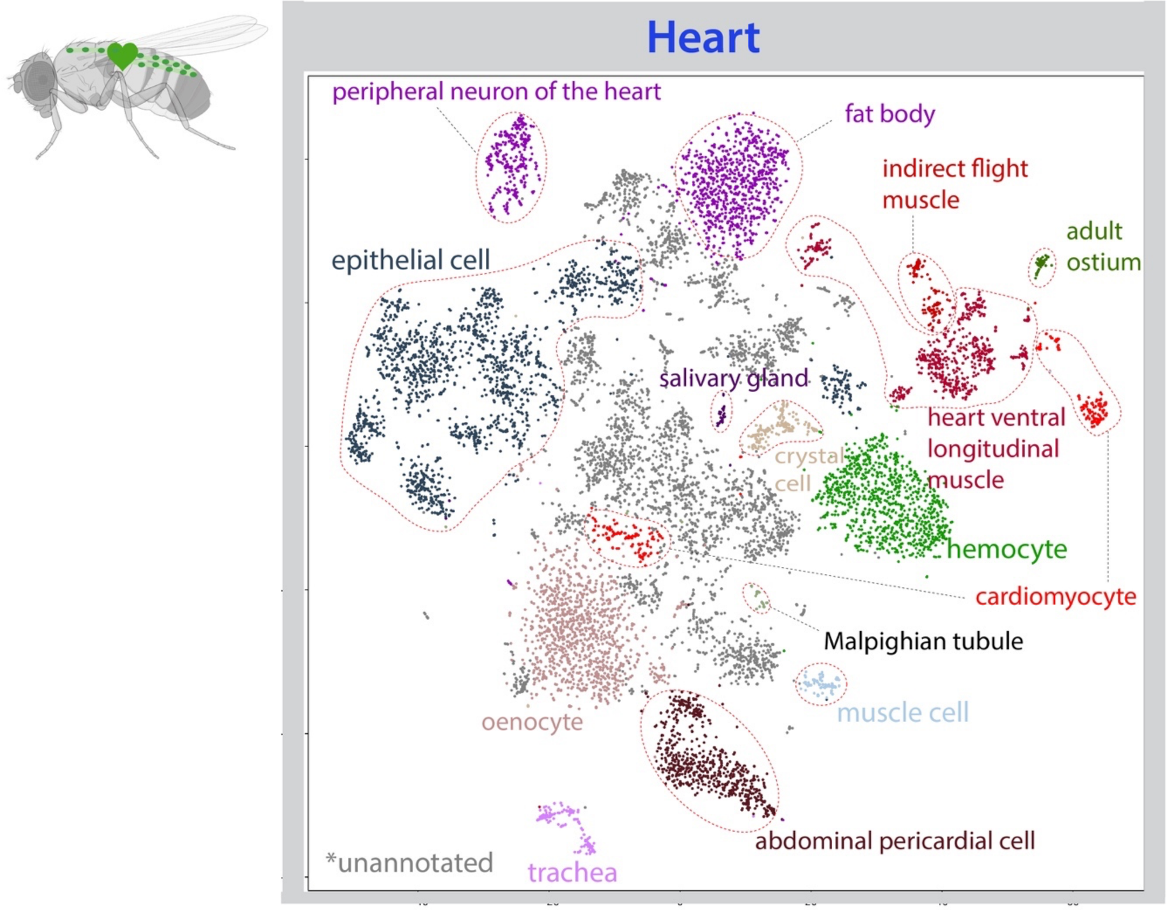

Figure S10. Cell type annotation in the heart. tSNE plot with annotations for the fly heart from the *Stringent* 10x dataset.

FCA Figure S11

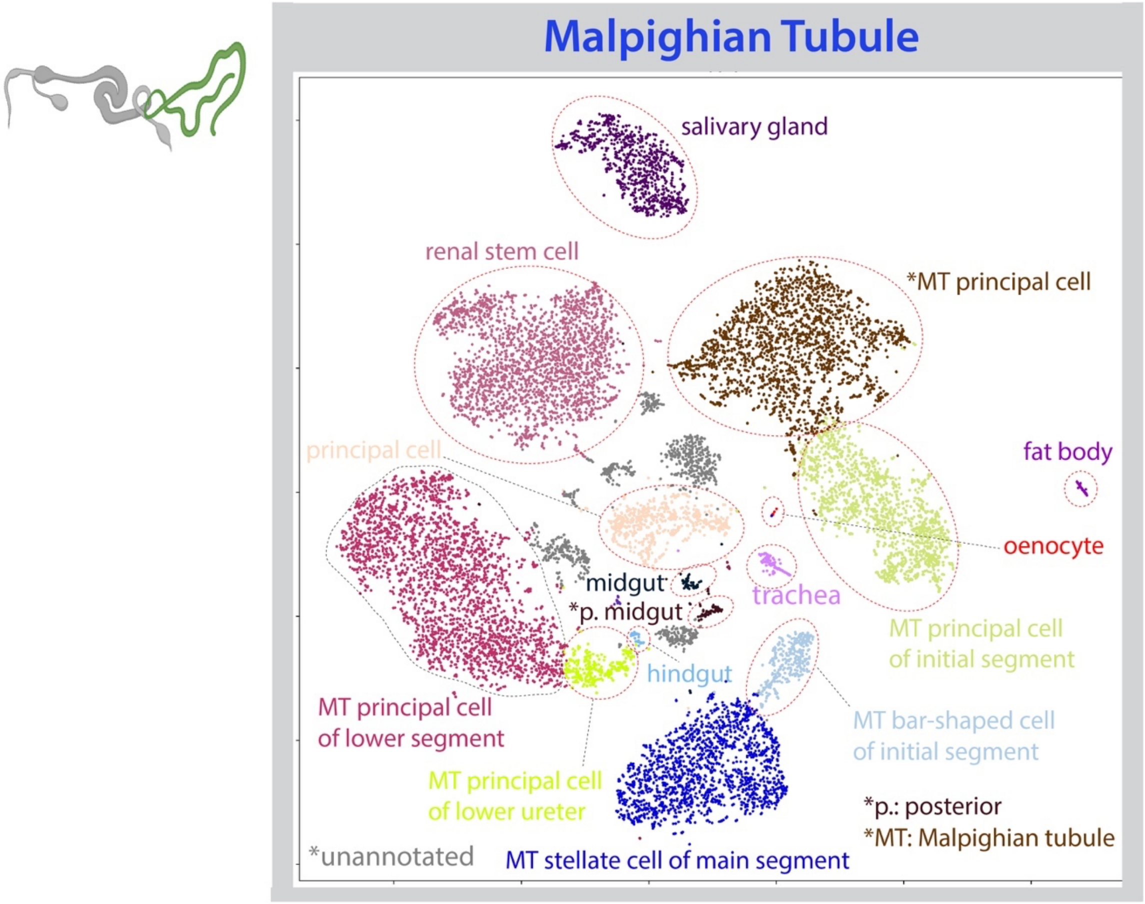

Figure S11. Cell type annotation in the Malpighian tubule. tSNE plot with annotations for the fly Malpighian tubule (MT) from the *Stringent* 10x dataset.

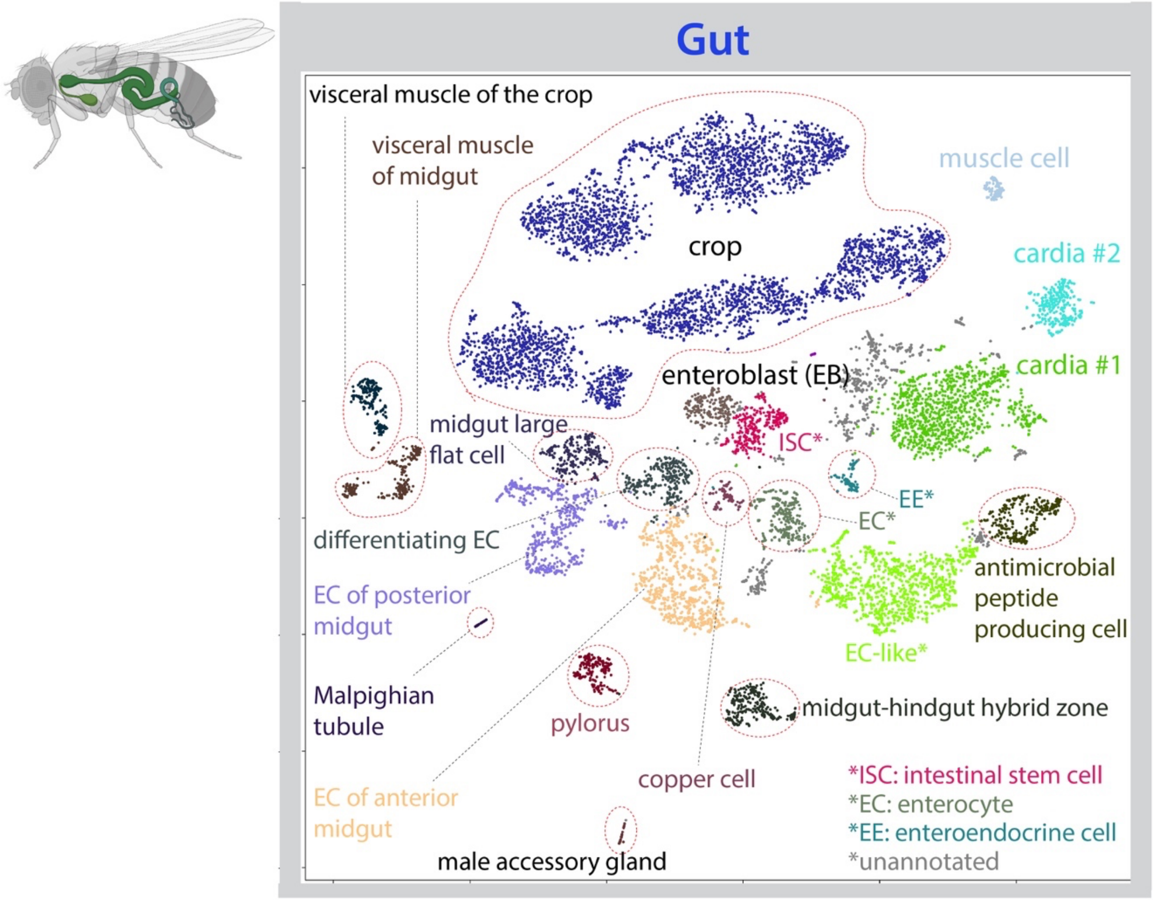

Figure S12. Cell type annotation in the gut. tSNE plot with annotations for the fly gut from the *Stringent* 10x dataset.

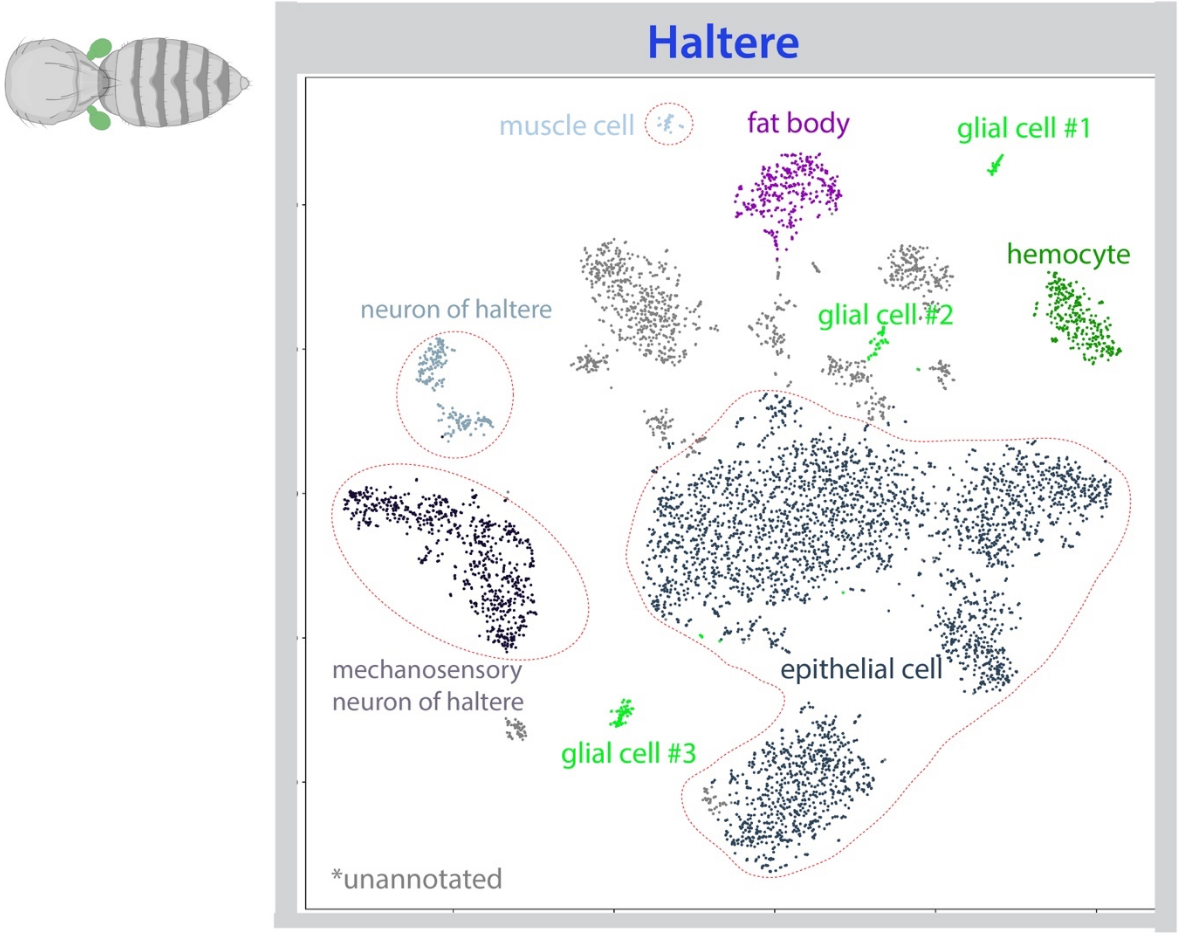

Figure S13. Cell type annotation in the haltere. tSNE plot with annotations for the fly haltere from the *Stringent* 10x dataset.

FCA Figure S14

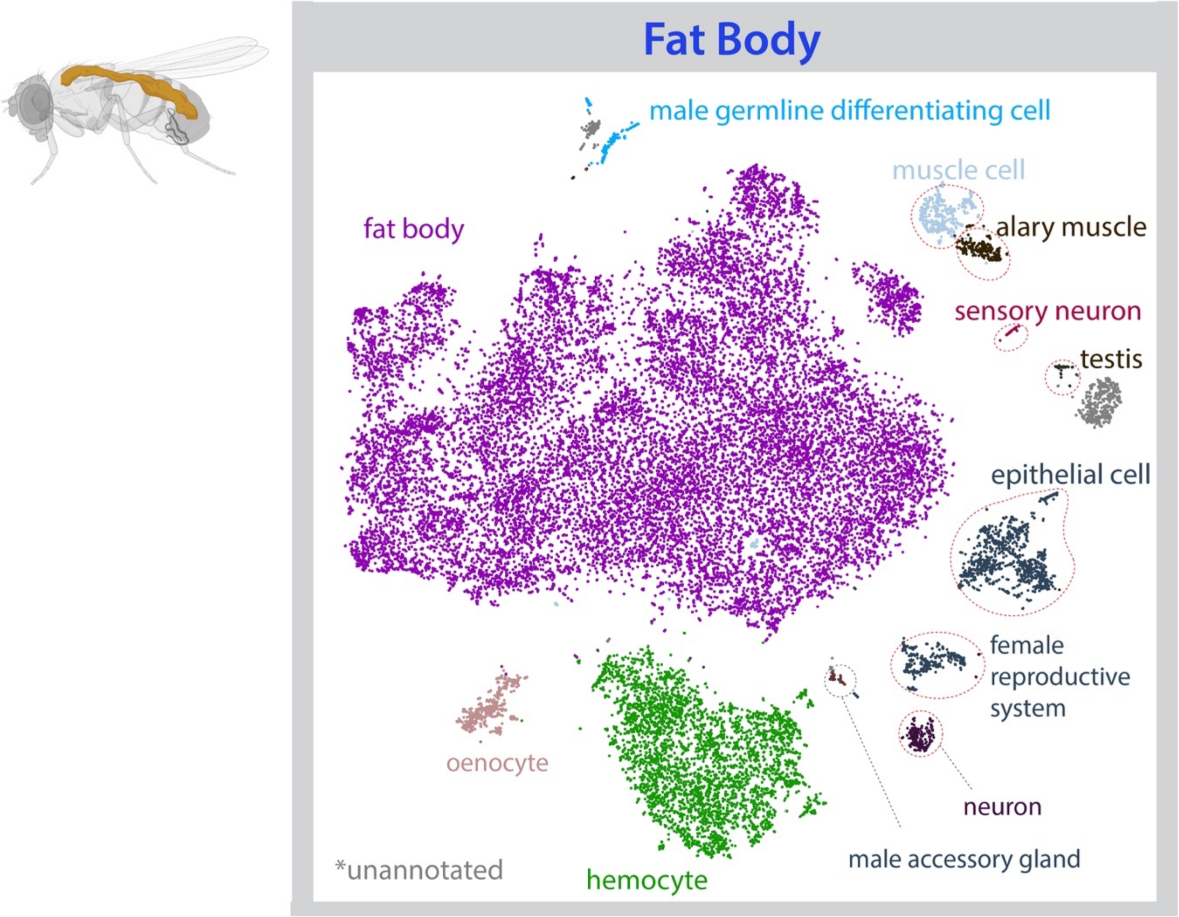

Figure S14. Cell type annotation in the fat body. tSNE plot with annotations for the fly fat body cells from the *Stringent* 10x dataset. Fat body cells are FAC-sorted based on the nuclear GFP signal; flies are *Cg-GAL4 > UAS-lamGFP*.

FCA Figure S15

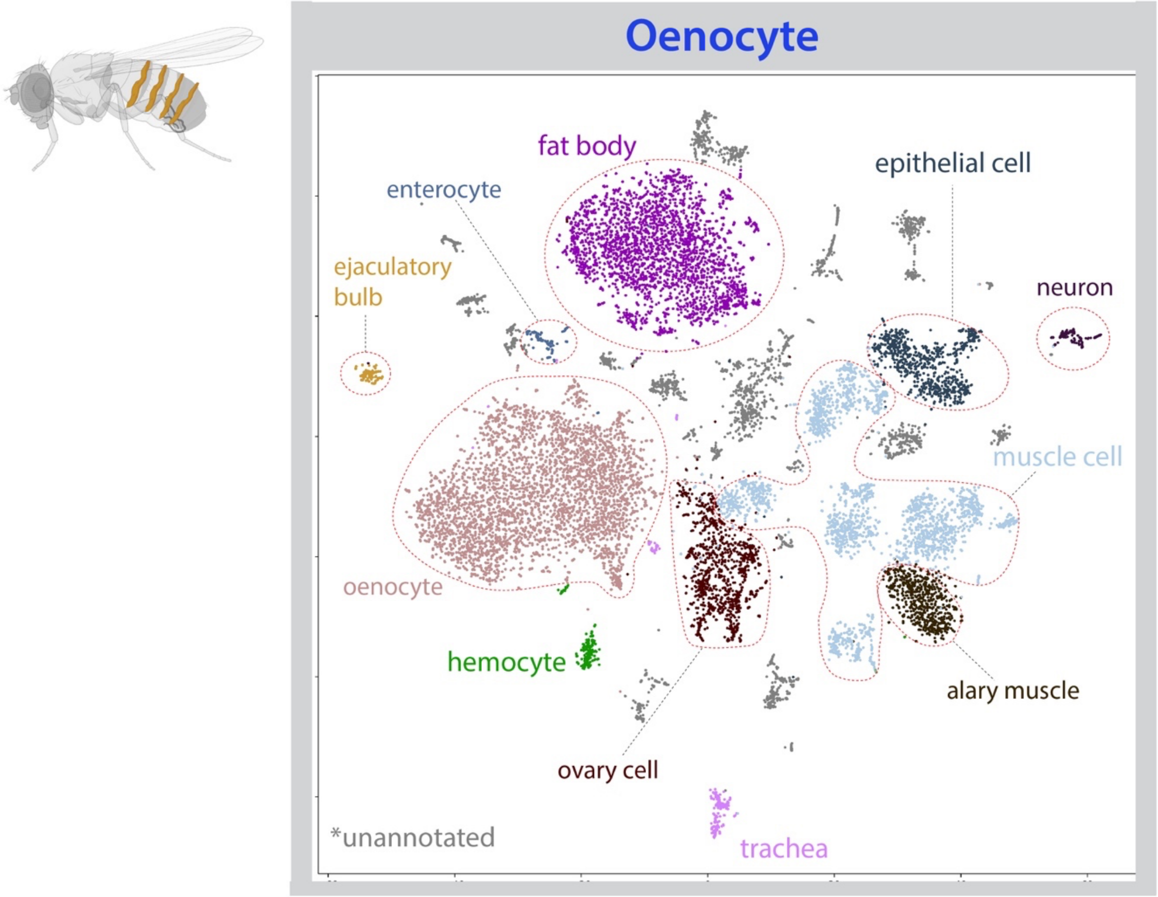

Figure S15. Cell type annotation in the oenocyte. tSNE plot with annotations for the fly oenocyte from the *Stringent* 10x dataset. Oenoctyes are FAC-sorted based on the nuclear GFP signal; flies are *PromE800-GAL4 > UAS-unc84GFP*.

FCA Figure S16

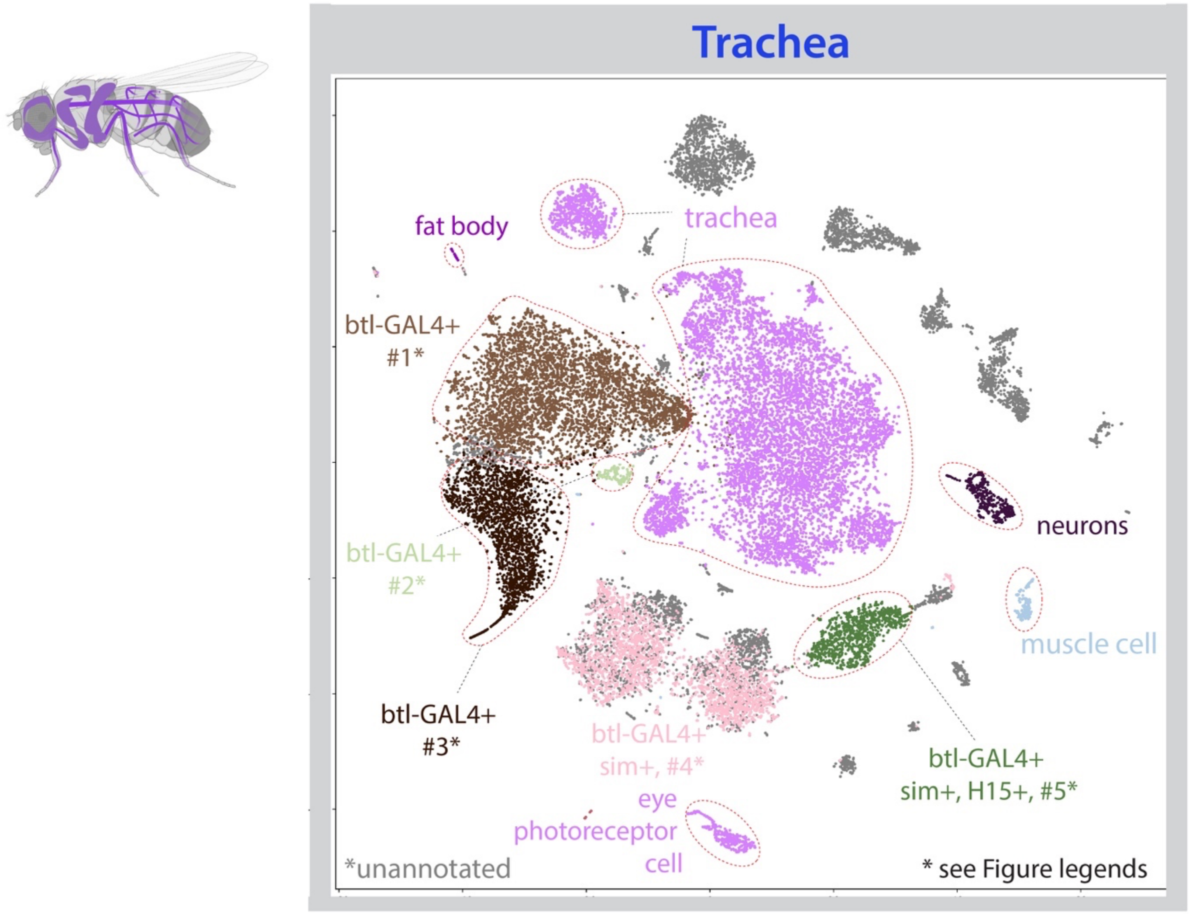

Figure S16.Cell type annotation in the trachea. tSNE plot with annotations for the fly trachea from the *Stringent* 10x dataset. Tracheal cells are FAC-sorted based on the nuclear GFP signal; flies are *btl-GAL4 > UAS-lamGFP*.

FCA Figure S17

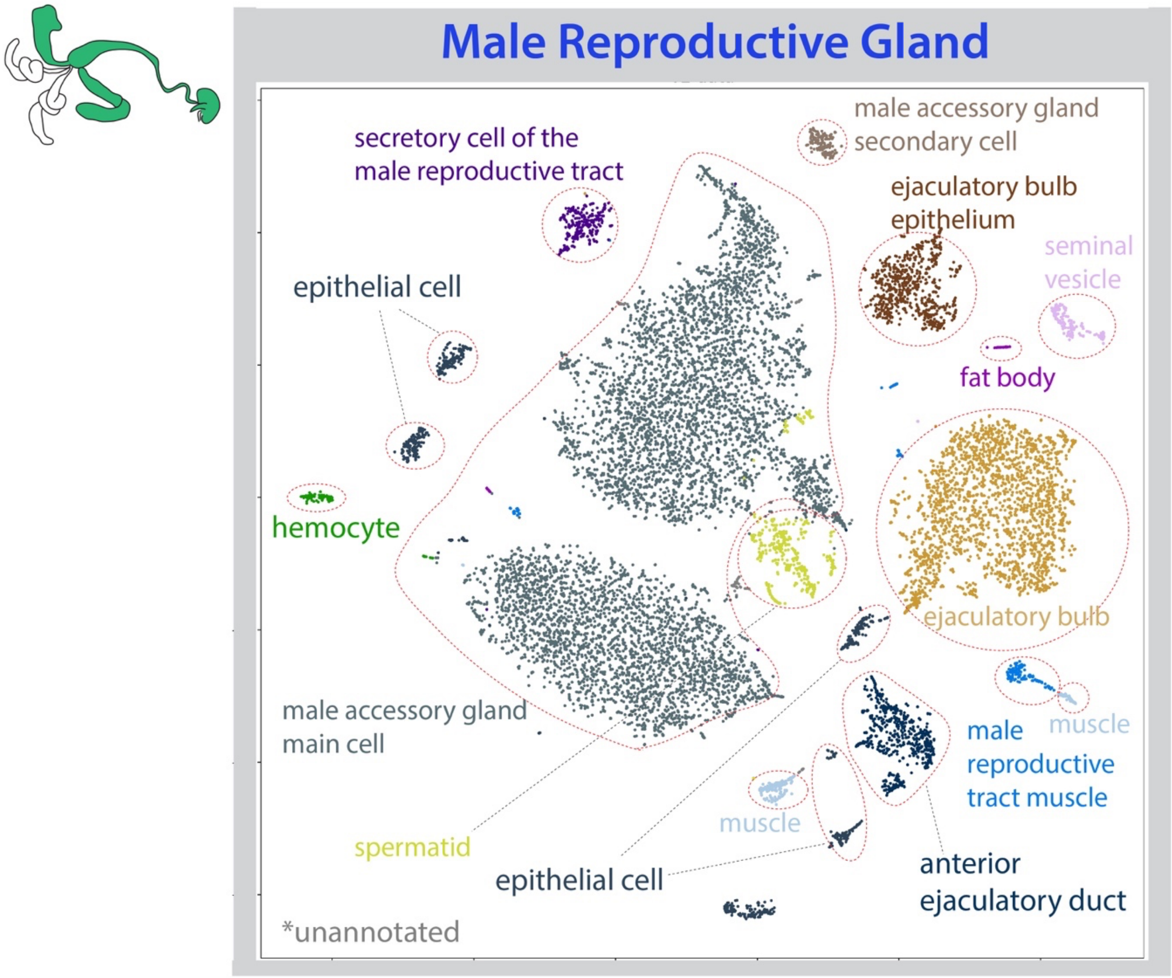

Figure S17. Cell type annotation in the male reproductive glands. tSNE plot with annotations for the fly male reproductive glands from the *Stringent* 10x dataset. The sequenced cells are from dissected male accessory glands, ejaculatory ducts and ejaculatory bulbs.

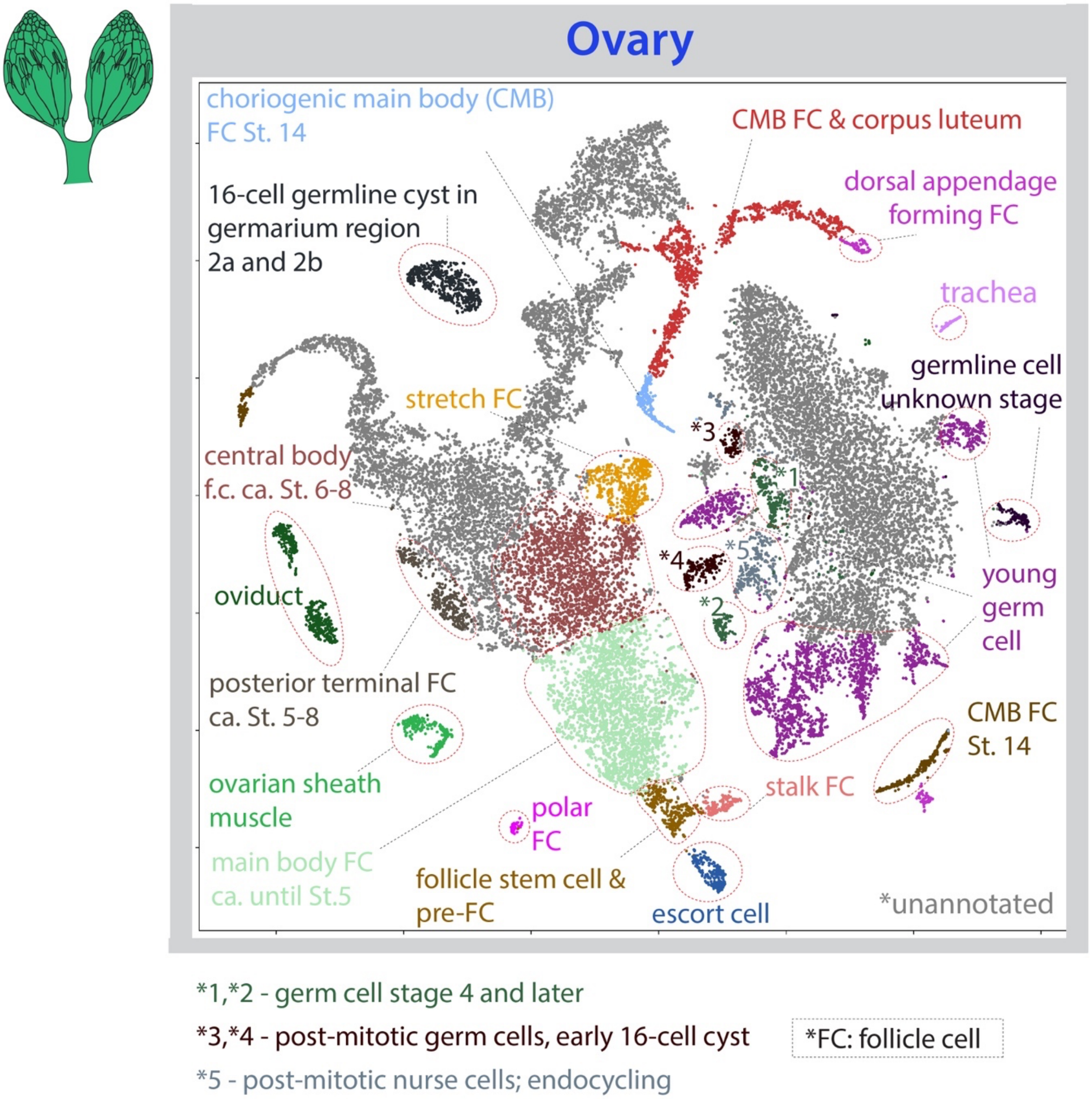

Figure S18. Cell type annotation in the ovary. tSNE plot with annotations for the fly ovary from the *Stringent* 10x dataset.

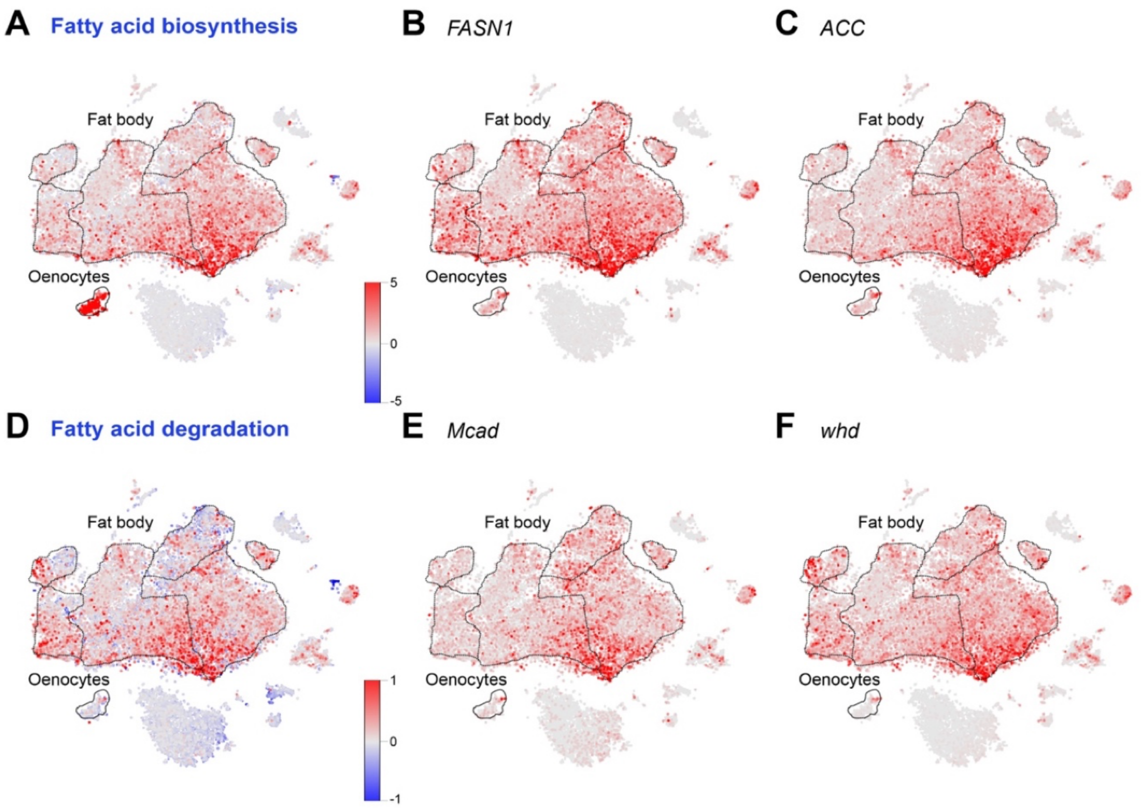

Figure S19. Metabolic pathway enrichment reveals the existence of cell subpopulations suggesting tissue specific functional specialization.

(A) Fatty acid biosynthesis pathway enrichment analysis as performed by ModuleScore (see Methods) in ASAP reveals strong homogeneous positive enrichment in oenocytes, while the fat body shows non-homogeneous enrichment across all cells. Red colors correspond to positive enrichment while blue colors correspond to negative enrichment.

(B, C) Similar profiles were obtained if using single genes in this pathway, *FASN1* and *ACC*.

(D) Fatty acid degradation pathway enrichment as revealed by ModuleScore analysis in ASAP shows low enrichment in oenocytes, while in the fat body there is a positive enrichment in specific subpopulations of cells. Red colors correspond to positive enrichment while blue colors correspond to negative enrichment.

(E, F) Similar profiles were obtained if using single genes in this pathway, *Mcad* and *whd.*

Color bar in **A** and **D** is for module score. The score is calculated as the difference of average expression of the genes in the module score and the genes in the background, for each cell. Scores close to zero indicate a similar expression, positive scores indicate higher expression, and negative scores indicate lower expression of the genes in the gene set than the background genes. See Methods for detail.

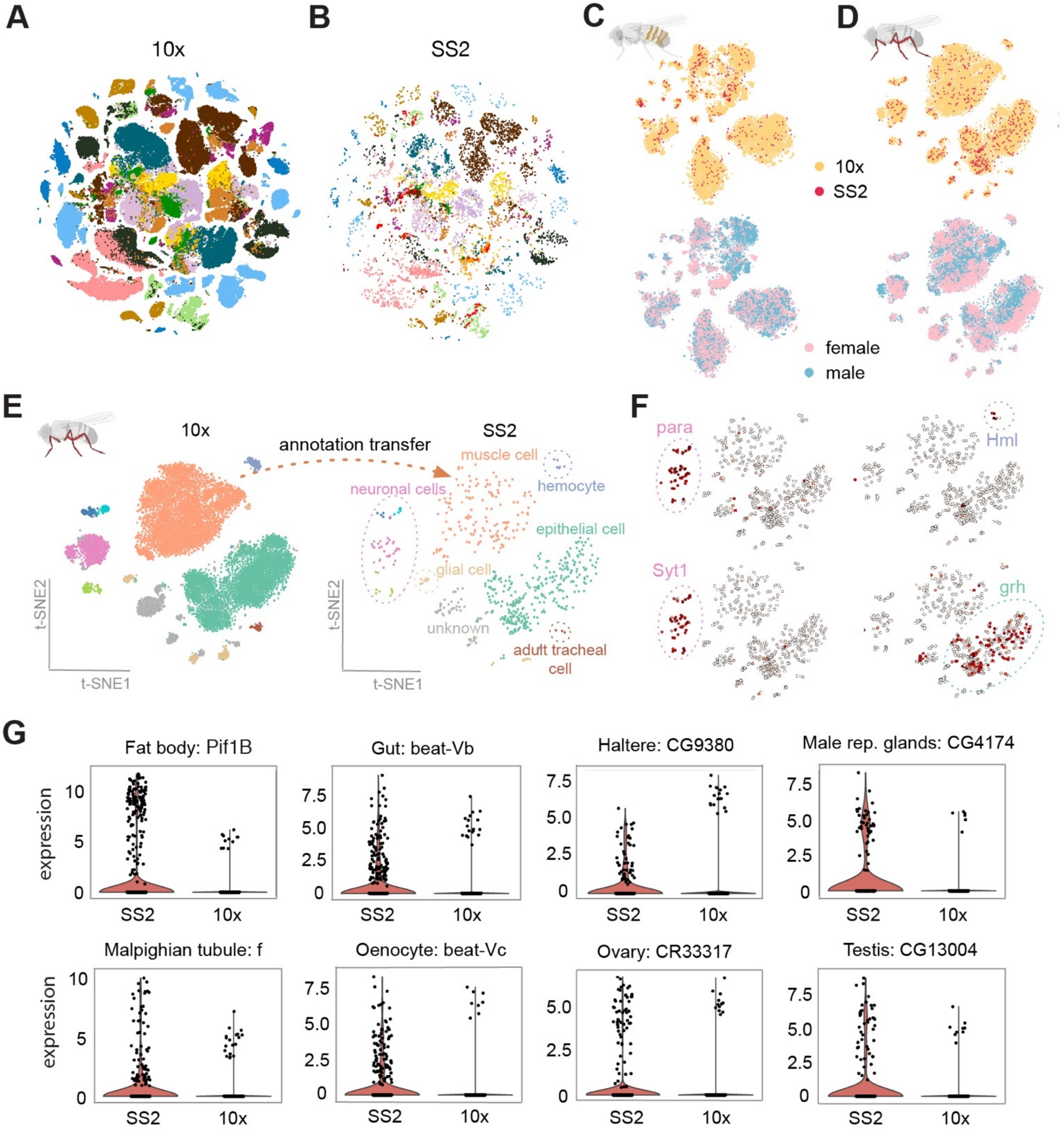

Figure S20. Integration of Smart-seq2 (SS2) and 10x Genomics data.

(A) tSNE visualization of individually dissected tissues using 10x Genomics and integrated with Smart-seq2 data. Colors denote different tissues.

(B) tSNE visualization of individually dissected tissues using Smart-seq2 and integrated with 10x Genomics data. Colors denote different tissues.

(C,D) Examples of integrated data for (C) oenocyte, and (D) leg. Cells are colored by technology (top) and by gender (bottom).

(E) Overview of computational pipeline for annotating Smart-seq2 data using leg as an example. After integrating 10x Genomics and Smart-seq2 data, we train a classifier on 10x Genomics data (left) and transfer annotations to Smart-seq2 data (right). Colors indicate different cell types.

(F) Validation of Smart-seq2 annotations by known marker genes. Cells annotated as neuronal cells correctly express *para* and *Syt1* neuronal markers, while cells annotated as hemocyte and epitelial correctly express *Hml* and *grh* markers, respectively.

(G) Examples of genes expressed in Smart-seq2 cells, but their expression is barely captured with 10x Genomics.

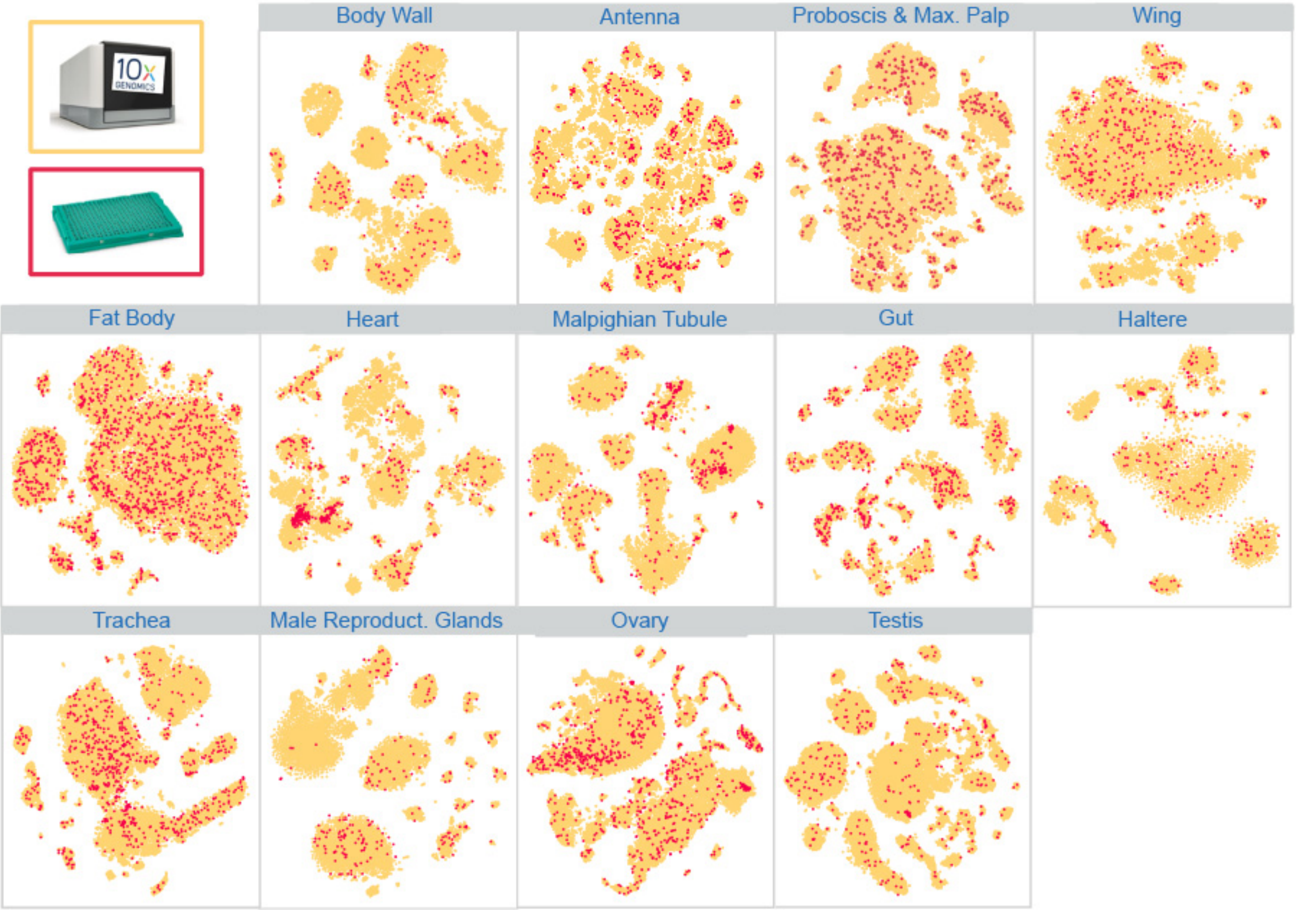

Figure S21. Tissue-level integration of 10x Genomics and Smart-seq2 datasets.
tSNE visualizations of 13 individually dissected tissues. Yellow color denotes cells from 10x Genomics and red color denotes cells from Smart-seq2. Remaining tissues (oenocyte and leg) are visualized in fig. **S17 C,D.**

FCA Figure S22

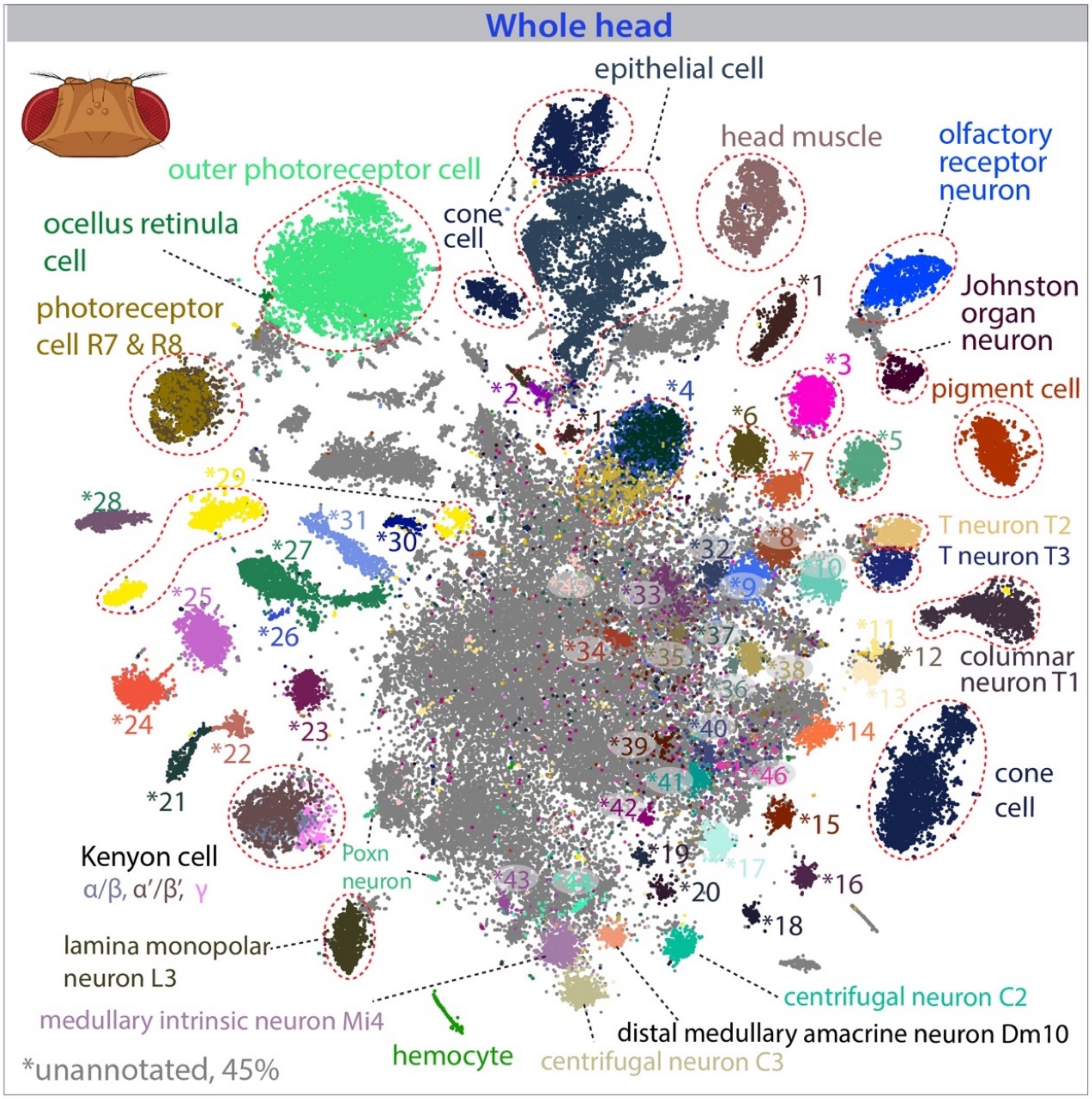

total 81 annotations

*1 adult lamina epithelial/marginal glial cell
*2 fat body
*3 medullary intrinsic neuron Mi1
*4 T neuron T4/T5 [see sub-types later]
*5 transmedullary neuron Tm1
*6 transmedullary neuron Tm2
*7 lamina monopolar neuron L5
*8 transmedullary neuron Tm4
*9 transmedullary neuron Tm3a
*10 T neuron T2a
*11 octopaminergic/tyraminergic neuron
*12 dopaminergic neuron
*13 medullary intrinsic neuron Mi15
*14 transmedullary Y neuron TmY8
*15 distal medullary amacrine neuron Dm8/Dm11
*16 lamina intrinsic amacrine neuron Lai
*17 transmedullary Y neuron TmY5a
*18 distal medullary amacrine neuron Dm9
*19 lamina wide-field 1 neuron
*20 lamina wide-field 2 neuron
*21 optic-lobe-associated cortex glial cell
*22 adult optic chiasma glial cell
*23 lamina monopolar neuron L4
*24 lamina monopolar neuron L1
*25 lamina monopolar neuron L2
*26 adult brain cell body glial cell
*27 ensheathing glial cell
*28 auditory sensory neuron
*29 adult brain perineurial glial cell
*30 subperineurial glial cell
*31 adult reticular neuropil associated glial cell
*32 transmedullary neuron Tm9
*33 transmedullary neuron Tm20
*34 lobula columnar neuron LC10
*35 transmedullary Y neuron TmY4
*36 transmedullary neuron Tm29
*37 lobula columnar neuron LC12
*38 lobula columnar neuron LC17
*39 distal medullary amacrine neuron Dm12
*40 distal medullary amacrine neuron Dm3
*41 medullary intrinsic neuron Mi9
*42 transmedullary Y neuron TmY14
*43 proximal medullary amacrine neuron Pm2
*44 proximal medullary amacrine neuron Pm4
*45 photoreceptor-like
*46 transmedullary neuron Tm5c

Figure S22. tSNE plot with annotations for the fly head from the *Stringent* 10x dataset. A large number of cells in the middle are unannotated cells, most of which are neurons from the central brain. The annotations not indicated in the plot are listed below the plot.

FCA Figure S23

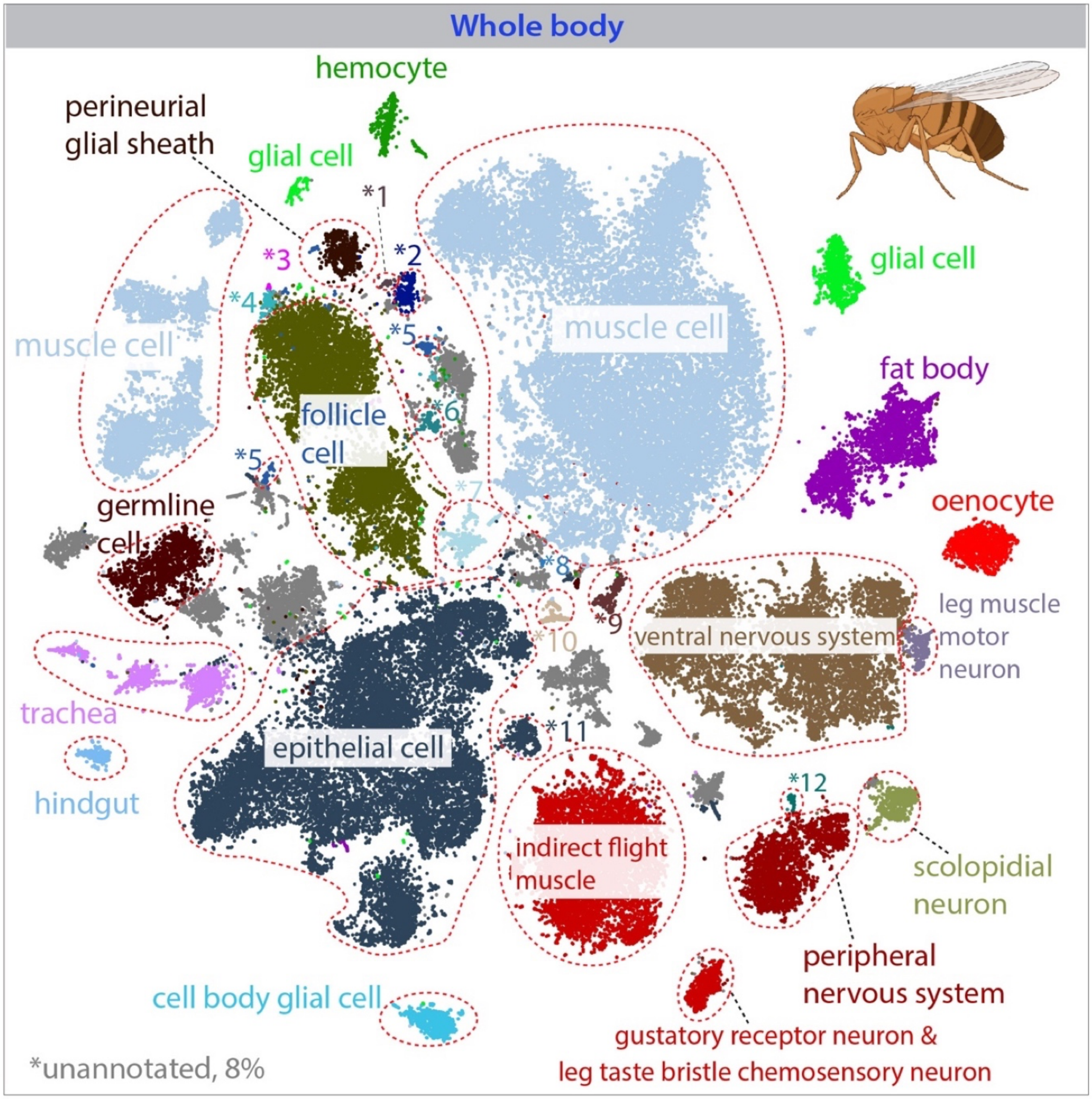

total 33 annotations

*1 CNS surface associated glial cell
*2 subperineurial glial cell
*3 polar follicle cell
*4 prefollicle cell and stalk follicle cell
*5 escort cell
*6 enteroendocrine cell
*7 eo support cell
*8 spermatocyte
*9 male accessory gland
*10 reticular neuropil associated glial cell
*11 female reproductive system
*12 multidendritic neuron

Figure S23. tSNE plot with annotations for the fly body from the *Stringent* 10x dataset. Note that only the top abundant cell types are annotated, and many of them can be further divided into different subtypes. The annotations not indicated in the plot are listed below the plot.

FCA Figure S24

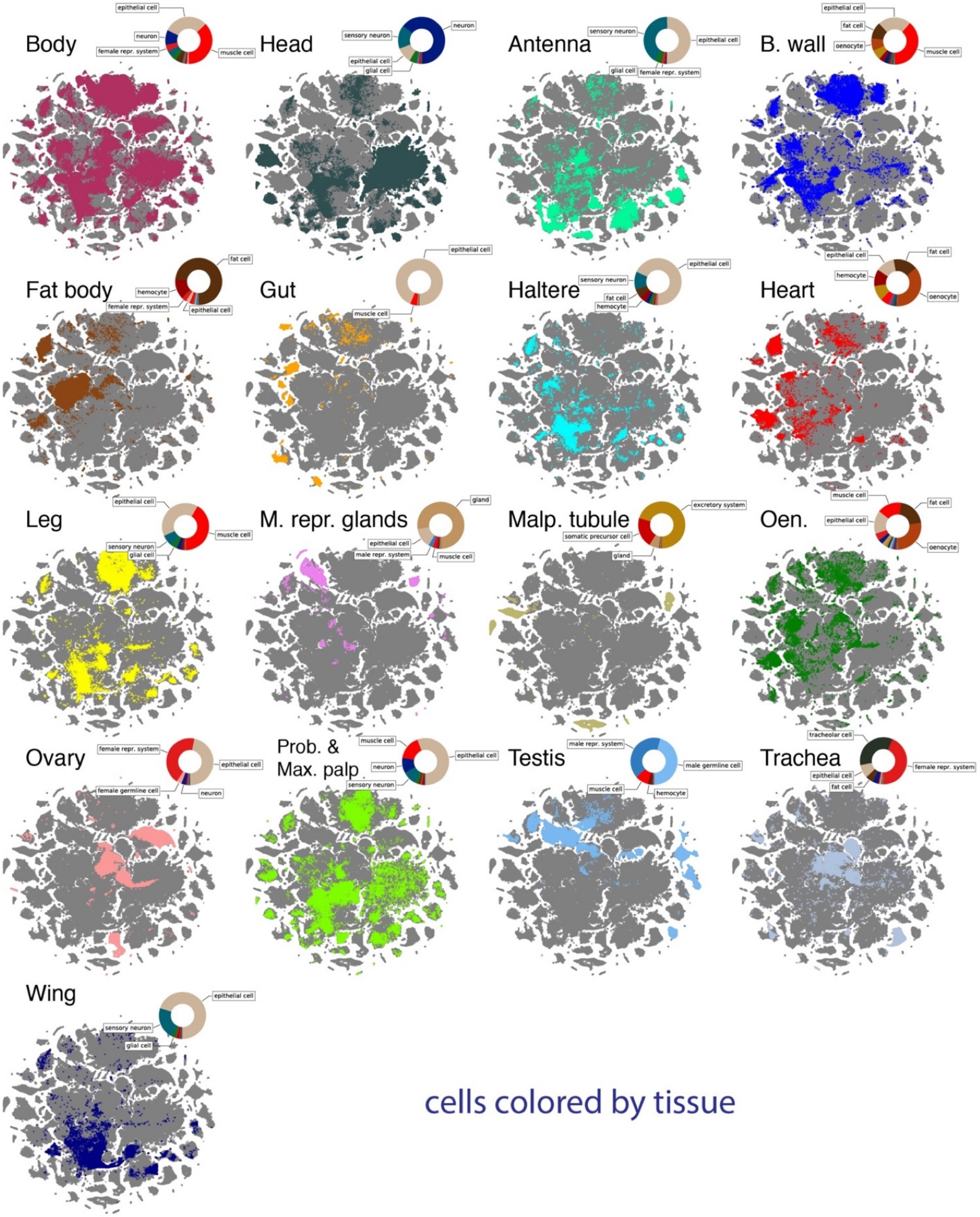

Figure S24. tSNE plots of all cells from the *Stringent* 10x dataset. Each tissue is highlighted in a different color. Pie charts show the top common cell types for each tissue, such as epithelial cells, neurons, and muscle cells, and so on. Note that some cells from two tissues overlap in one cluster, indicating these two tissues share one cell type. For example, the head and body share cell types, such as muscle, CNS neurons, and epithelial cells (see fig. S25). B. wall for body wall; M. repr. glands for male reproductive glands; Malp. tubule for Malpighian tubule; prob. max. palp for proboscis and maxillary palp.

FCA Figure S25

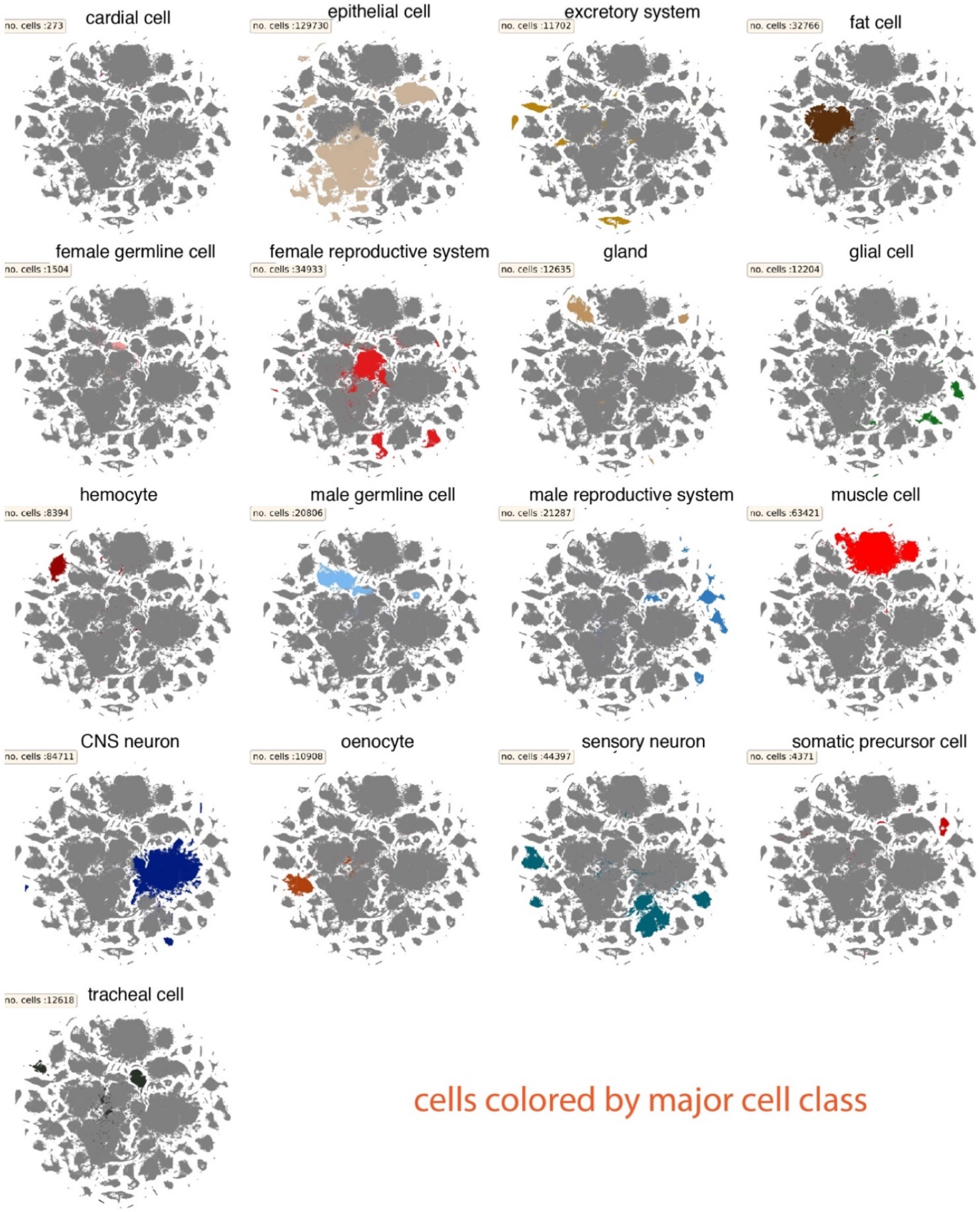

cells colored by major cell class

Figure S25. tSNE plots of all cells from the *Stringent* 10x dataset. Cell types from broad categories are highlighted and cell numbers are indicated.

FCA Figure S26

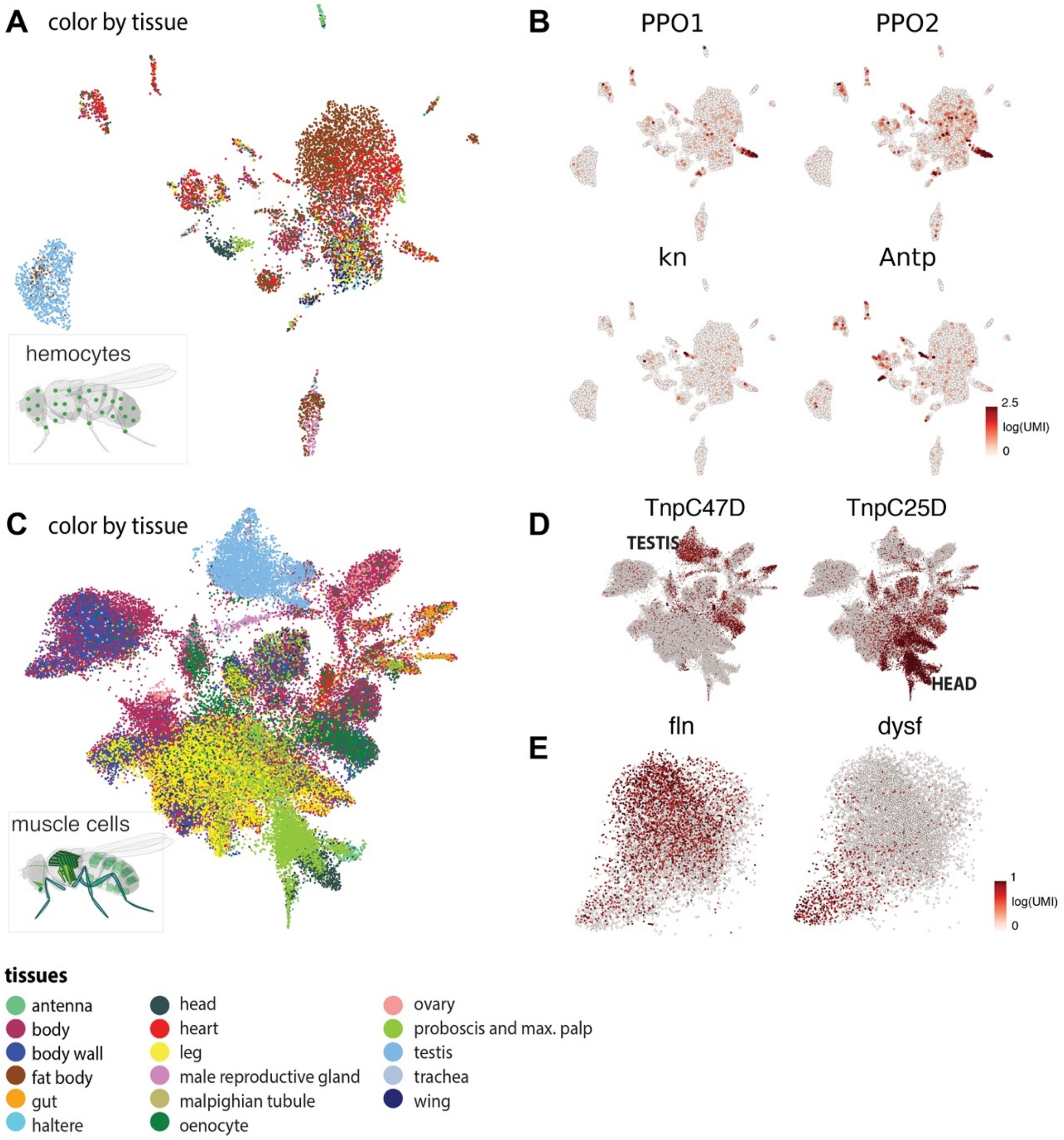

Figure S26. Cross-tissue analysis of hemocytes and muscle cells.
(A) tSNE plot of all annotated hemocytes colored by tissue types.
(B) Expression of *PPO1* and *PPO2* labeling crystal cells. Expression of *Antp* and *kn labeling* the presumptive lymph gland posterior signaling center.
(C) tSNE plot of all annotated muscle cells colored by tissue types.
(D) Expression of *TnpC47D* and and *TnpC25D* in all annotated muscle cells.
(E) Expression of *fln* and *dysf* showing gradients in the indirect flight muscle cluster.

FCA Figure S27

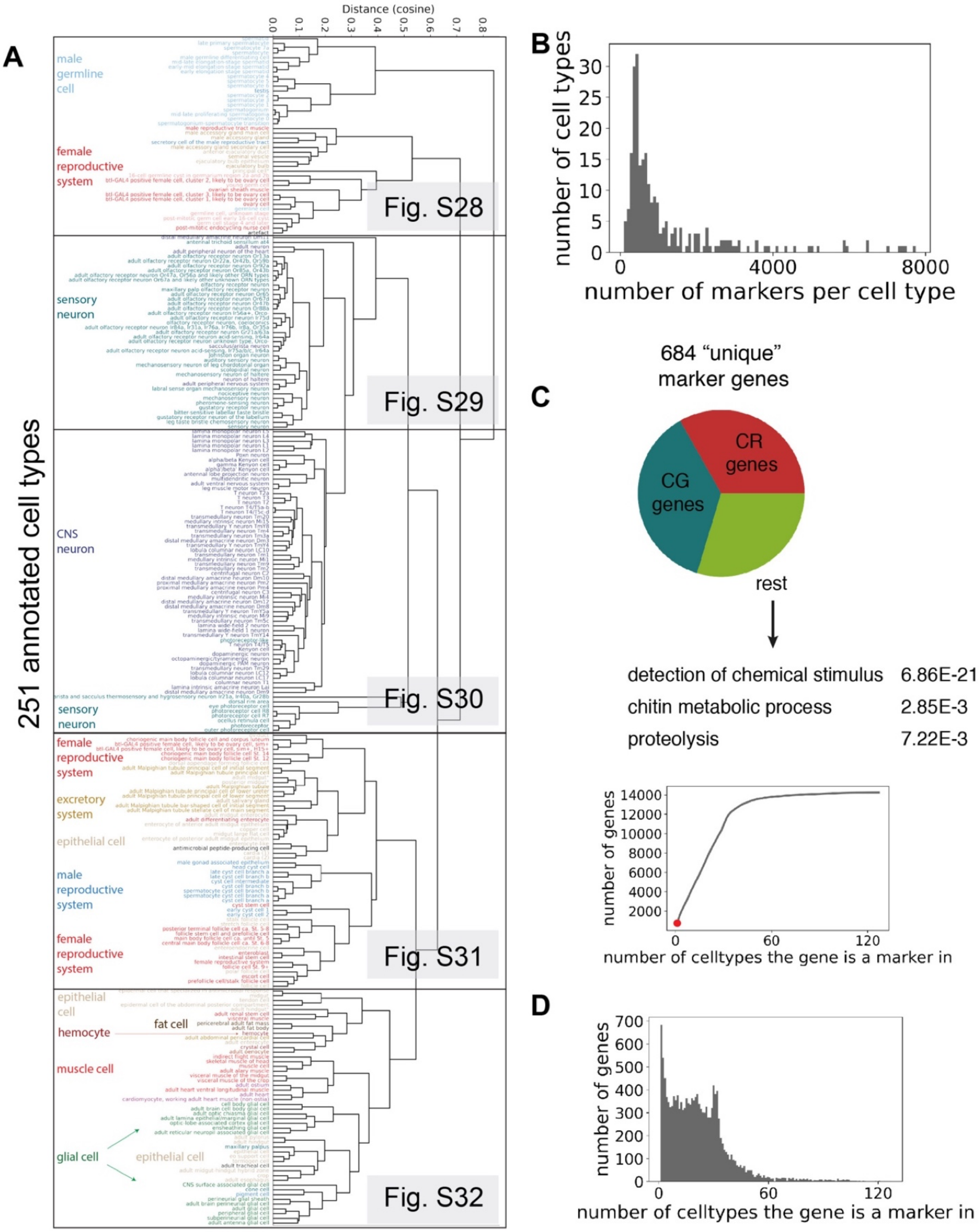

Figure S27. Organism-wide gene expression comparison

(A) Dendrogram showing the cosine similarity of the transcriptomes of the different annotated cell types. Cell types are colored based on broad classes. Enlarged details shown in fig. S28-S32.

(B) Histogram showing the number of markers calculated per cell type (avg. logfc>1, pval adj<0.05).

(C) Pieplot showing the 684 marker genes detected in only one cell type. Majority of unique marker genes are unknown CG and CR numbers, while the known marker genes are mostly linked to receptors. (pval adj shown as calculated by FlyMine). Insert shows a cumulative plot of the uniqueness of marker genes: 684 genes are markers in only one cell type, while almost all genes (~14k) can be found as markers in multiple cell types.

(D) Histogram showing the number of cell types a gene is expressed in on x-axis and number of genes on y-axis.

FCA Figure S28

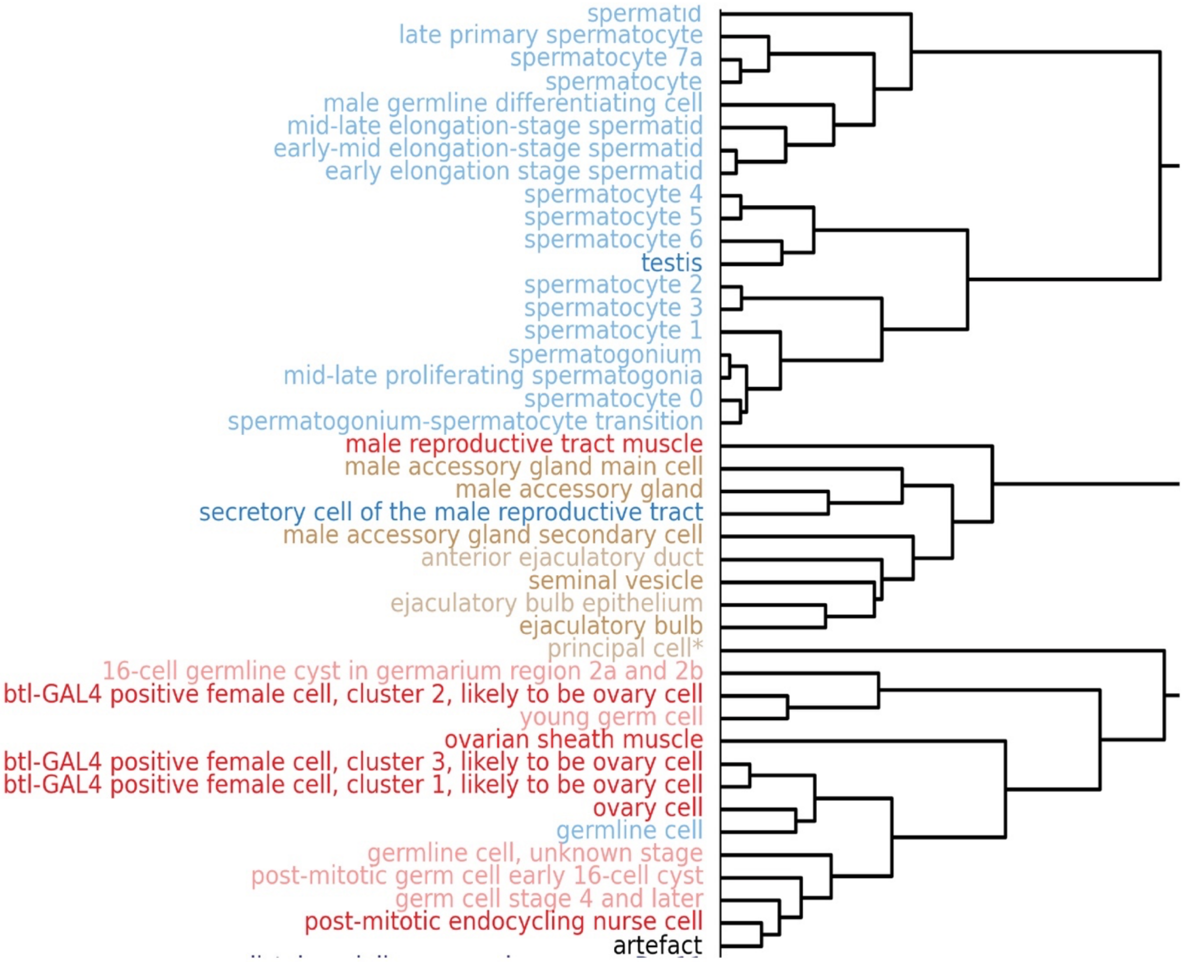
spermatid
late primary spermatocyte
spermatocyte 7a
spermatocyte
male germline differentiating cell
mid-late elongation-stage spermatid
early-mid elongation-stage spermatid
early elongation stage spermatid
spermatocyte 4
spermatocyte 5
spermatocyte 6
testis
spermatocyte 2
spermatocyte 3
spermatocyte 1
spermatogonium
mid-late proliferating spermatogonia
spermatocyte 0
spermatogonium-spermatocyte transition
male reproductive tract muscle
male accessory gland main cell
male accessory gland
secretory cell of the male reproductive tract
male accessory gland secondary cell
anterior ejaculatory duct
seminal vesicle
ejaculatory bulb epithelium
ejaculatory bulb
principal cell*
16-cell germline cyst in germarium region 2a and 2b
btl-GAL4 positive female cell, cluster 2, likely to be ovary cell
young germ cell
ovarian sheath muscle
btl-GAL4 positive female cell, cluster 3, likely to be ovary cell
btl-GAL4 positive female cell, cluster 1, likely to be ovary cell
ovary cell
germline cell
germline cell, unknown stage
post-mitotic germ cell early 16-cell cyst
germ cell stage 4 and later
post-mitotic endocycling nurse cell
artefact

Figure S28. Dendrogram showing the cosine similarity of the transcriptomes of the different annotated cell types. Cell types are colored based on broad classes. Part 1 from fig. S27A.

FCA Figure S29

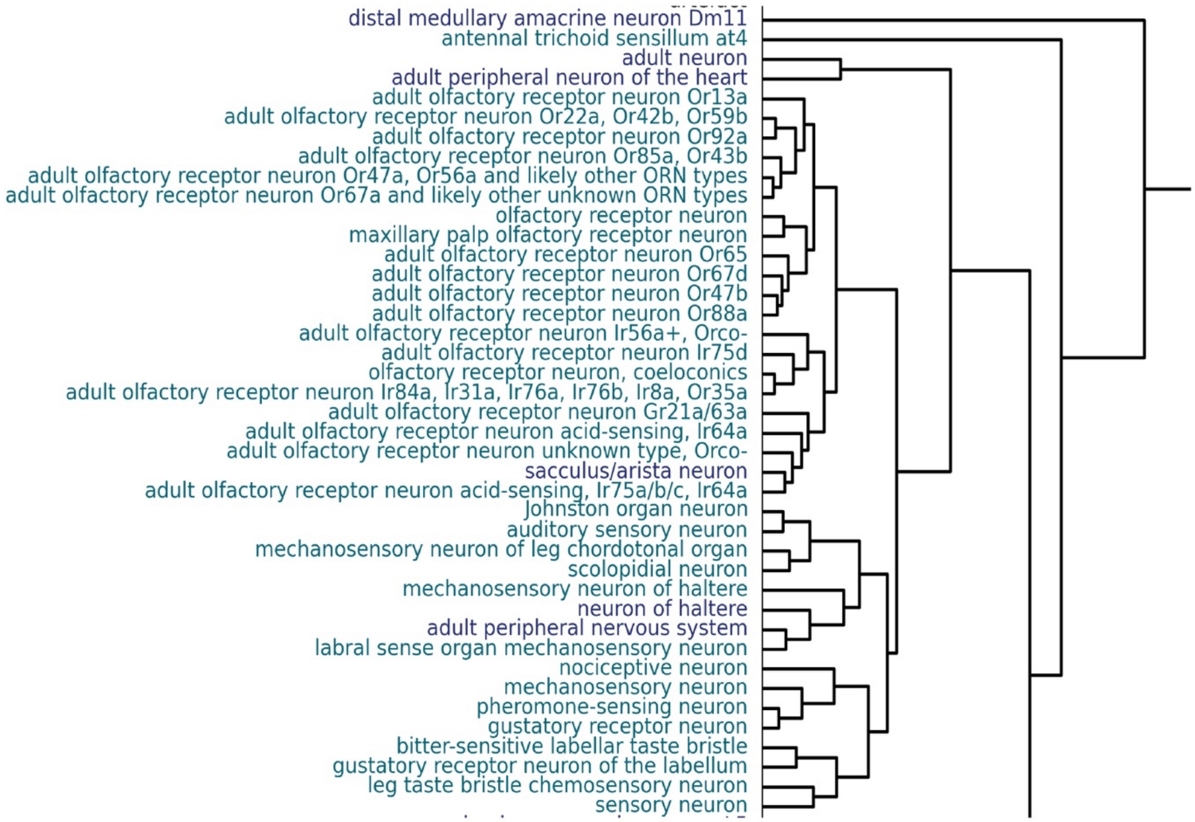
distal medullary amacrine neuron Dm11
antennal trichoid sensillum at4
adult neuron
adult peripheral neuron of the heart
adult olfactory receptor neuron Or13a
adult olfactory receptor neuron Or22a, Or42b, Or59b
adult olfactory receptor neuron Or92a
adult olfactory receptor neuron Or85a, Or43b
adult olfactory receptor neuron Or47a, Or56a and likely other ORN types
adult olfactory receptor neuron Or67a and likely other unknown ORN types
olfactory receptor neuron
maxillary palp olfactory receptor neuron
adult olfactory receptor neuron Or65
adult olfactory receptor neuron Or67d
adult olfactory receptor neuron Or47b
adult olfactory receptor neuron Or88a
adult olfactory receptor neuron Ir56a+, Orco-
adult olfactory receptor neuron Ir75d
olfactory receptor neuron, coeloconics
adult olfactory receptor neuron Ir84a, Ir31a, Ir76a, Ir76b, Ir8a, Or35a
adult olfactory receptor neuron Gr21a/63a
adult olfactory receptor neuron acid-sensing, Ir64a
adult olfactory receptor neuron unknown type, Orco-
sacculus/arista neuron
adult olfactory receptor neuron acid-sensing, Ir75a/b/c, Ir64a
Johnston organ neuron
auditory sensory neuron
mechanosensory neuron of leg chordotonal organ
scolopidial neuron
mechanosensory neuron of haltere
neuron of haltere
adult peripheral nervous system
labral sense organ mechanosensory neuron
nociceptive neuron
mechanosensory neuron
pheromone-sensing neuron
gustatory receptor neuron
bitter-sensitive labellar taste bristle
gustatory receptor neuron of the labellum
leg taste bristle chemosensory neuron
sensory neuron

Figure S29. Dendrogram showing the cosine similarity of the transcriptomes of the different annotated cell types. Cell types are colored based on broad classes. Part 2 from fig. S27A.

FCA Figure S30

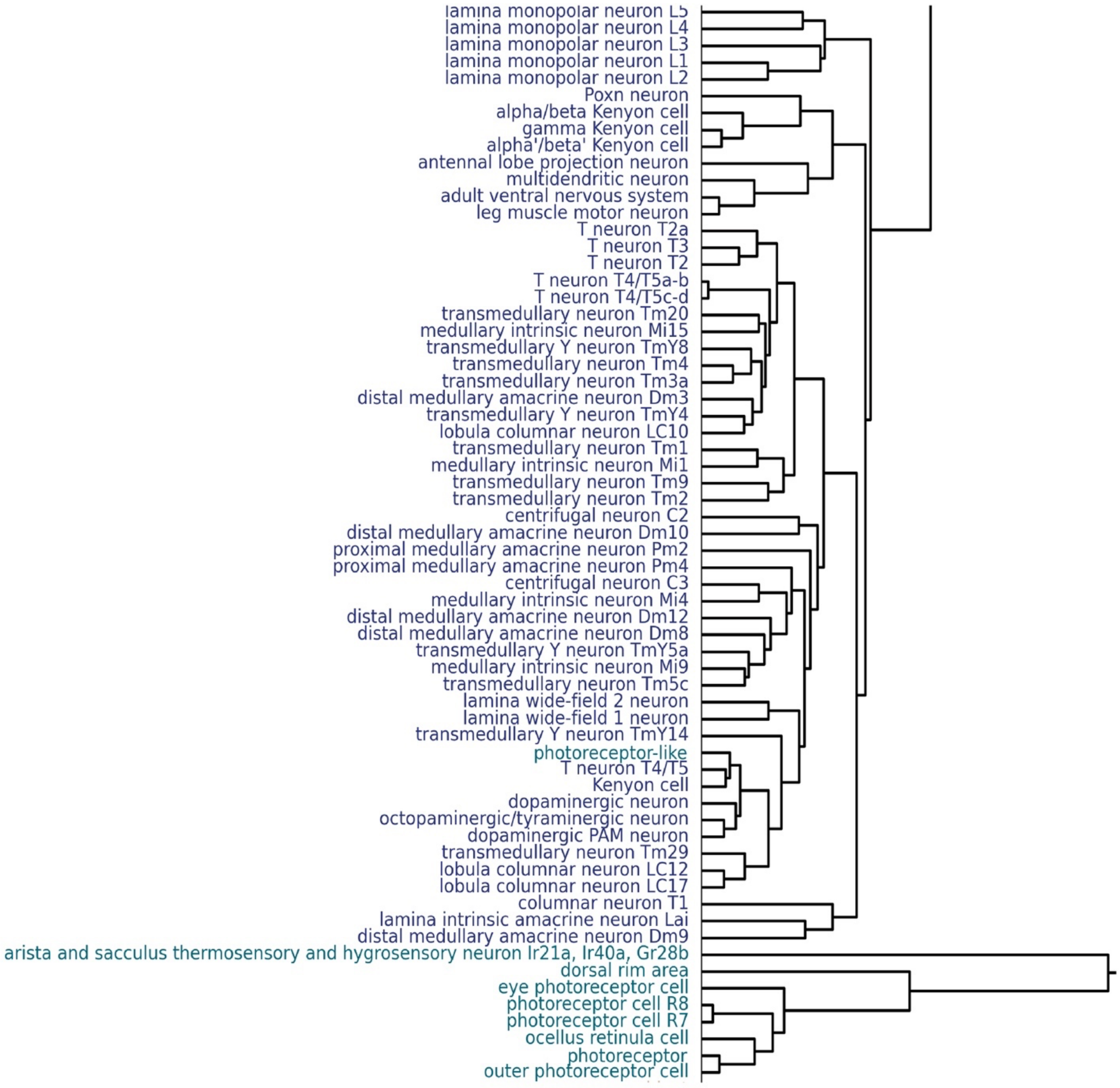
lamina monopolar neuron L5
lamina monopolar neuron L4
lamina monopolar neuron L3
lamina monopolar neuron L1
lamina monopolar neuron L2
Poxn neuron
alpha/beta Kenyon cell
gamma Kenyon cell
alpha'/beta' Kenyon cell
antennal lobe projection neuron
multidendritic neuron
adult ventral nervous system
leg muscle motor neuron
T neuron T2a
T neuron T3
T neuron T2
T neuron T4/T5a-b
T neuron T4/T5c-d
transmedullary neuron Tm20
medullary intrinsic neuron Mi15
transmedullary Y neuron TmY8
transmedullary neuron Tm4
transmedullary neuron Tm3a
distal medullary amacrine neuron Dm3
transmedullary Y neuron TmY4
lobula columnar neuron LC10
transmedullary neuron Tm1
medullary intrinsic neuron Mi1
transmedullary neuron Tm9
transmedullary neuron Tm2
centrifugal neuron C2
distal medullary amacrine neuron Dm10
proximal medullary amacrine neuron Pm2
proximal medullary amacrine neuron Pm4
centrifugal neuron C3
medullary intrinsic neuron Mi4
distal medullary amacrine neuron Dm12
distal medullary amacrine neuron Dm8
transmedullary Y neuron TmY5a
medullary intrinsic neuron Mi9
transmedullary neuron Tm5c
lamina wide-field 2 neuron
lamina wide-field 1 neuron
transmedullary Y neuron TmY14
photoreceptor-like
T neuron T4/T5
Kenyon cell
dopaminergic neuron
octopaminergic/tyraminergic neuron
dopaminergic PAM neuron
transmedullary neuron Tm29
lobula columnar neuron LC12
lobula columnar neuron LC17
columnar neuron T1
lamina intrinsic amacrine neuron Lai
distal medullary amacrine neuron Dm9
arista and sacculus thermosensory and hygrosensory neuron Ir21a, Ir40a, Gr28b
dorsal rim area
eye photoreceptor cell
photoreceptor cell R8
photoreceptor cell R7
ocellus retinula cell
photoreceptor
outer photoreceptor cell

Figure S30. Dendrogram showing the cosine similarity of the transcriptomes of the different annotated cell types. Cell types are colored based on broad classes. Part 3 from fig. S27A.

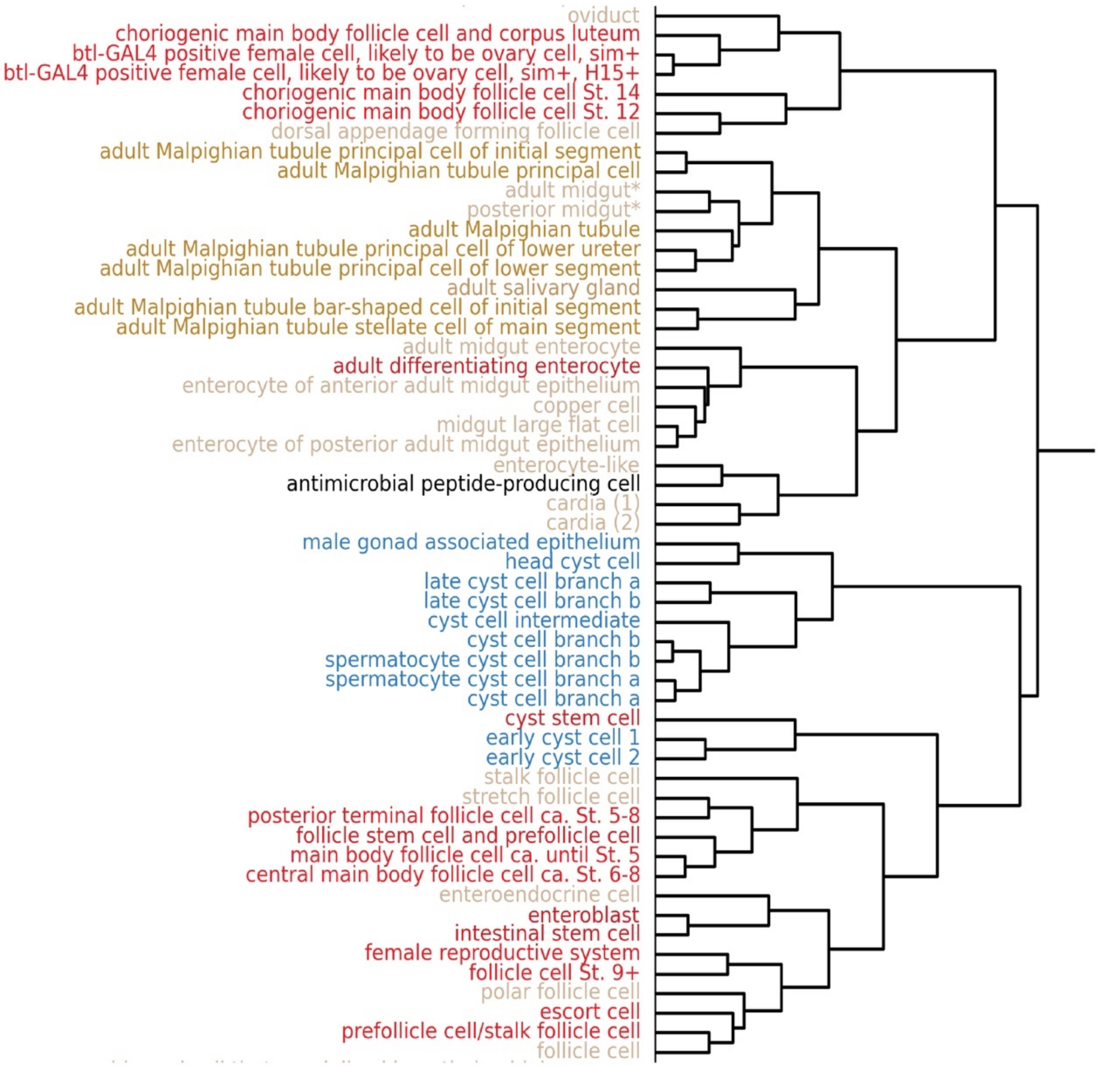
oviduct
choriogenic main body follicle cell and corpus luteum
btl-GAL4 positive female cell, likely to be ovary cell, sim+
btl-GAL4 positive female cell, likely to be ovary cell, sim+, H15+
choriogenic main body follicle cell St. 14
choriogenic main body follicle cell St. 12
dorsal appendage forming follicle cell
adult Malpighian tubule principal cell of initial segment
adult Malpighian tubule principal cell
adult midgut*
posterior midgut*
adult Malpighian tubule
adult Malpighian tubule principal cell of lower ureter
adult Malpighian tubule principal cell of lower segment
adult salivary gland
adult Malpighian tubule bar-shaped cell of initial segment
adult Malpighian tubule stellate cell of main segment
adult midgut enterocyte
adult differentiating enterocyte
enterocyte of anterior adult midgut epithelium
copper cell
midgut large flat cell
enterocyte of posterior adult midgut epithelium
enterocyte-like
antimicrobial peptide-producing cell
cardia (1)
cardia (2)
male gonad associated epithelium
head cyst cell
late cyst cell branch a
late cyst cell branch b
cyst cell intermediate
cyst cell branch b
spermatocyte cyst cell branch b
spermatocyte cyst cell branch a
cyst cell branch a
cyst stem cell
early cyst cell 1
early cyst cell 2
stalk follicle cell
stretch follicle cell
posterior terminal follicle cell ca. St. 5-8
follicle stem cell and prefollicle cell
main body follicle cell ca. until St. 5
central main body follicle cell ca. St. 6-8
enteroendocrine cell
enteroblast
intestinal stem cell
female reproductive system
follicle cell St. 9+
polar follicle cell
escort cell
prefollicle cell/stalk follicle cell
follicle cell

Figure S31. Dendrogram showing the cosine similarity of the transcriptomes of the different annotated cell types. Cell types are colored based on broad classes. Part 4 from fig. S27A.

FCA Figure S32

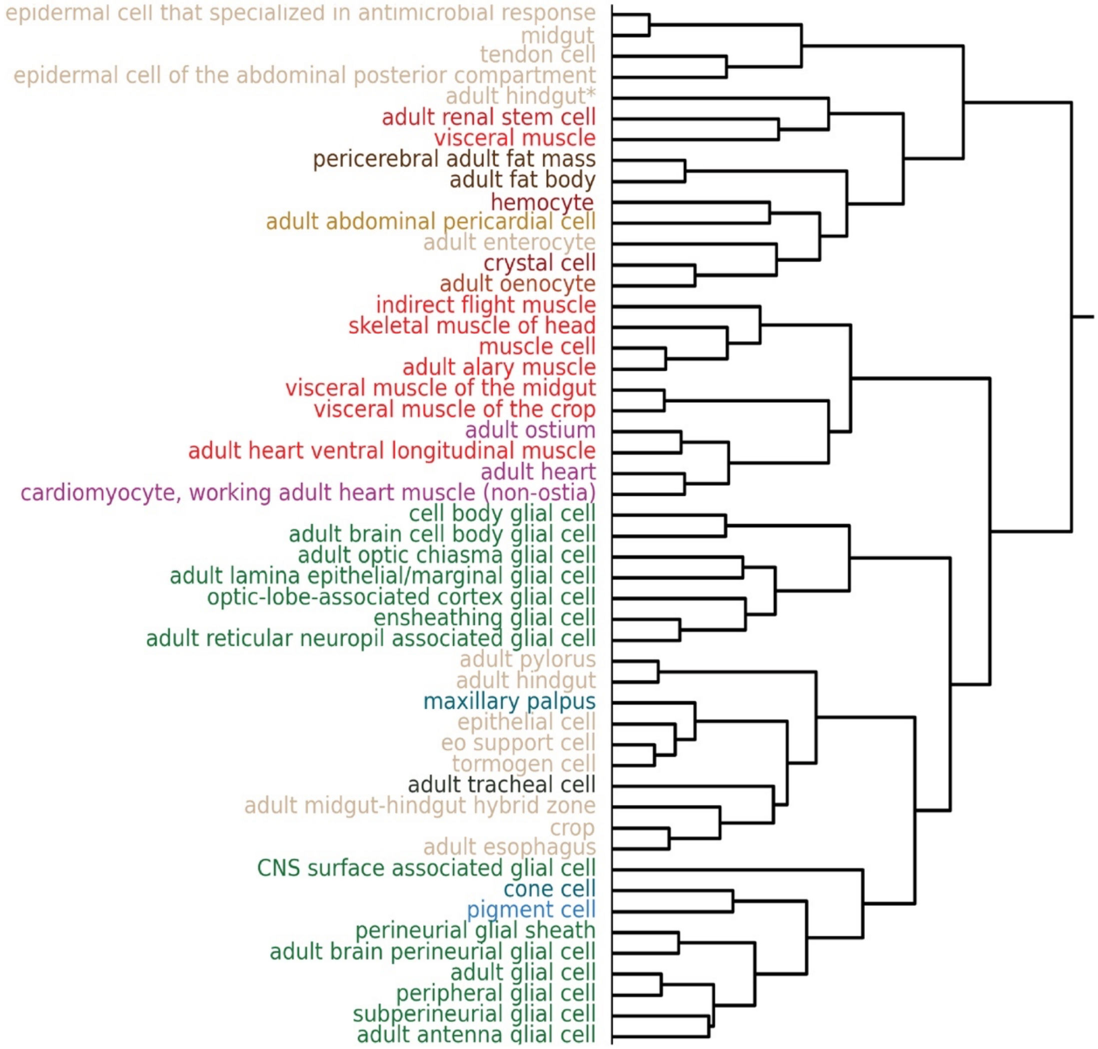
epidermal cell that specialized in antimicrobial response
midgut
tendon cell
epidermal cell of the abdominal posterior compartment
adult hindgut*
adult renal stem cell
visceral muscle
pericerebral adult fat mass
adult fat body
hemocyte
adult abdominal pericardial cell
adult enterocyte
crystal cell
adult oenocyte
indirect flight muscle
skeletal muscle of head
muscle cell
adult alary muscle
visceral muscle of the midgut
visceral muscle of the crop
adult ostium
adult heart ventral longitudinal muscle
adult heart
cardiomyocyte, working adult heart muscle (non-ostia)
cell body glial cell
adult brain cell body glial cell
adult optic chiasma glial cell
adult lamina epithelial/marginal glial cell
optic-lobe-associated cortex glial cell
ensheathing glial cell
adult reticular neuropil associated glial cell
adult pylorus
adult hindgut
maxillary palpus
epithelial cell
eo support cell
tormogen cell
adult tracheal cell
adult midgut-hindgut hybrid zone
crop
adult esophagus
CNS surface associated glial cell
cone cell
pigment cell
perineurial glial sheath
adult brain perineurial glial cell
adult glial cell
peripheral glial cell
subperineurial glial cell
adult antenna glial cell

Figure S32. Dendrogram showing the cosine similarity of the transcriptomes of the different annotated cell types. Cell types are colored based on broad classes. Part 5 from fig. S27A.

FCA Figure S33

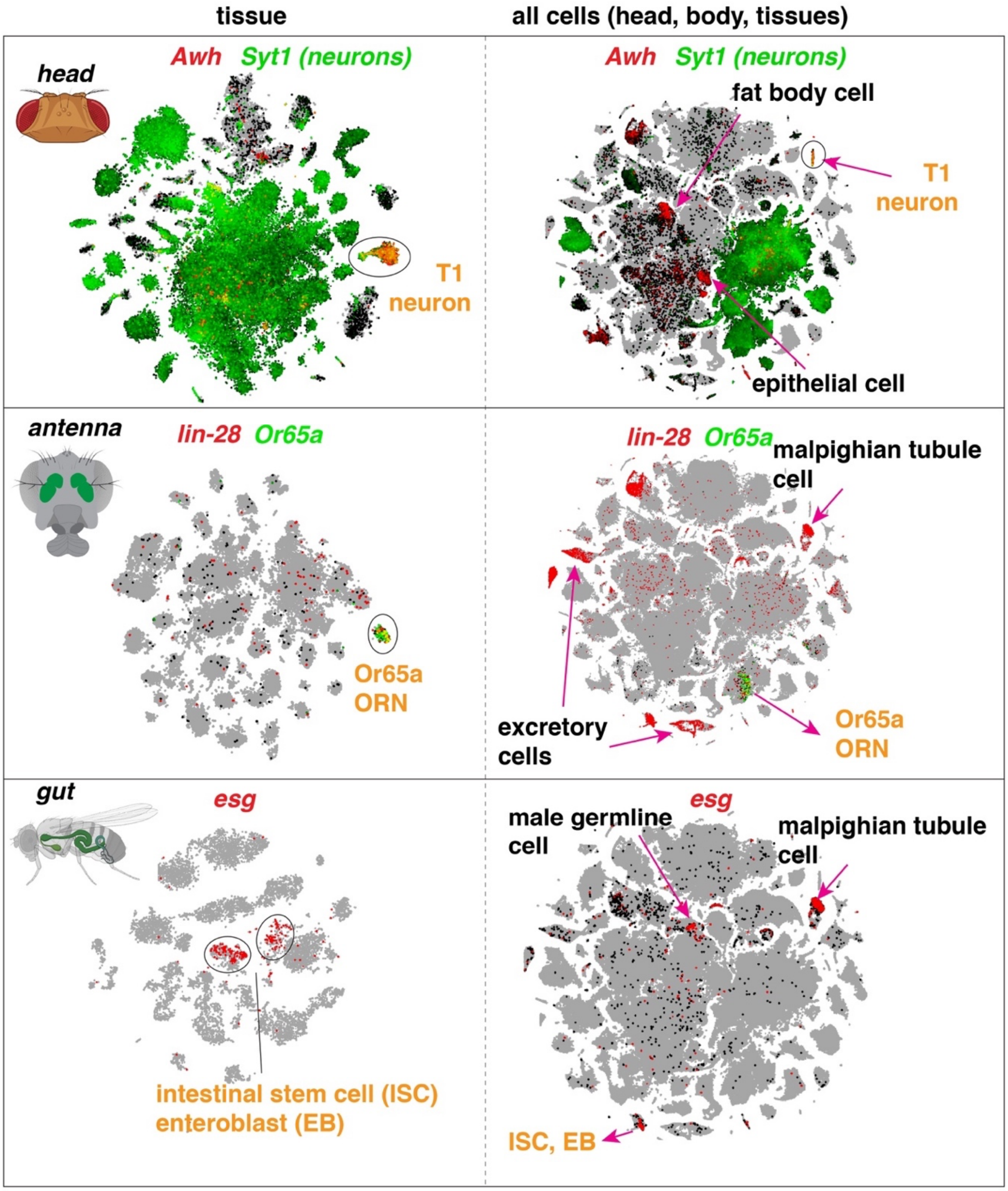

Figure S33. Cell-type specific markers in individual tissues and in all cells. Some cell type-specific markers identified in a specific tissue may have broader expression outside that tissue. *Awh* is specifically expressed in T1 neurons within the head, but also shows expression in fat body cells and epithelial cells. *lin-28* is specifically expressed in *Or65a* olfactory receptor neurons (ORNs) within the antenna, but also shows expression in malpighian tubule cells. *esg* is specifically expressed in intestinal stem cells (ISCs) and enteroblasts (EBs) within the gut, but also shows expression in Malpighian tubule stem cells and in the testis.

FCA Figure S34

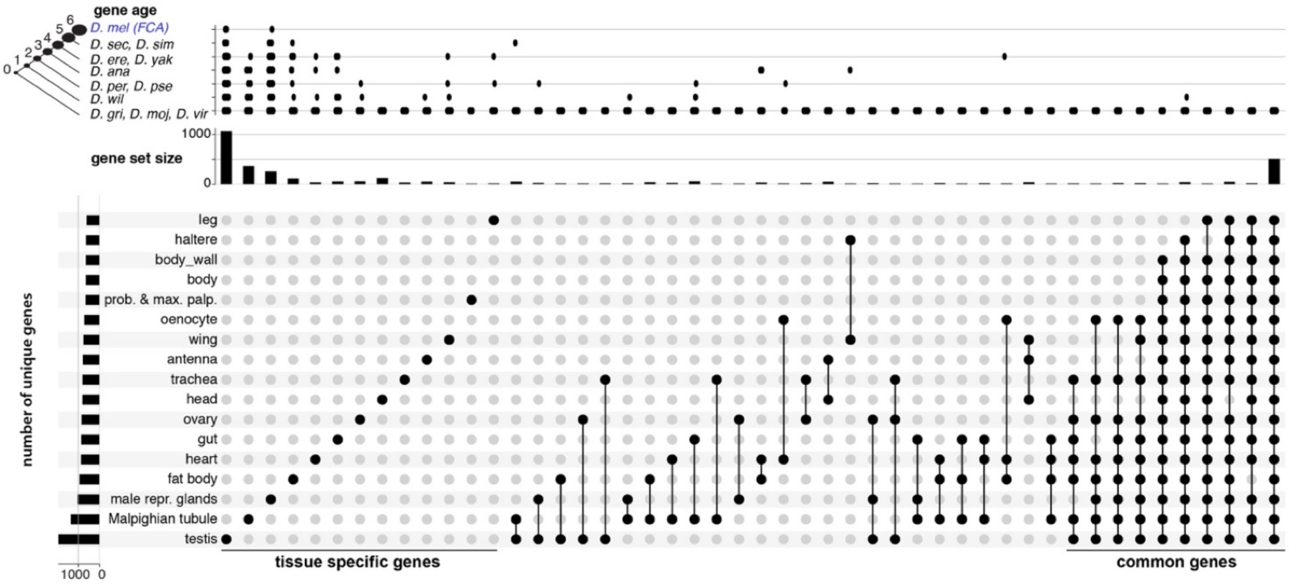

Figure S34. Common genes and tissue-specific genes shown by the UpSetPlot. Comparison of genes expressed per tissue (mean log2CPM>1) shows highly unique gene expression in the testis, Malpighian tubule, and male reproductive glands, while also highlighting a common module of conserved, ubiquitously expressed genes. Only sets with more than 10 genes are shown. The left bar graph shows the number of uniquely expressed genes for each tissue. The top bar graph shows the gene age in branches, ranging from the common ancestor to *Drosophila melanogaster*-specific genes (http://gentree.ioz.ac.cn).

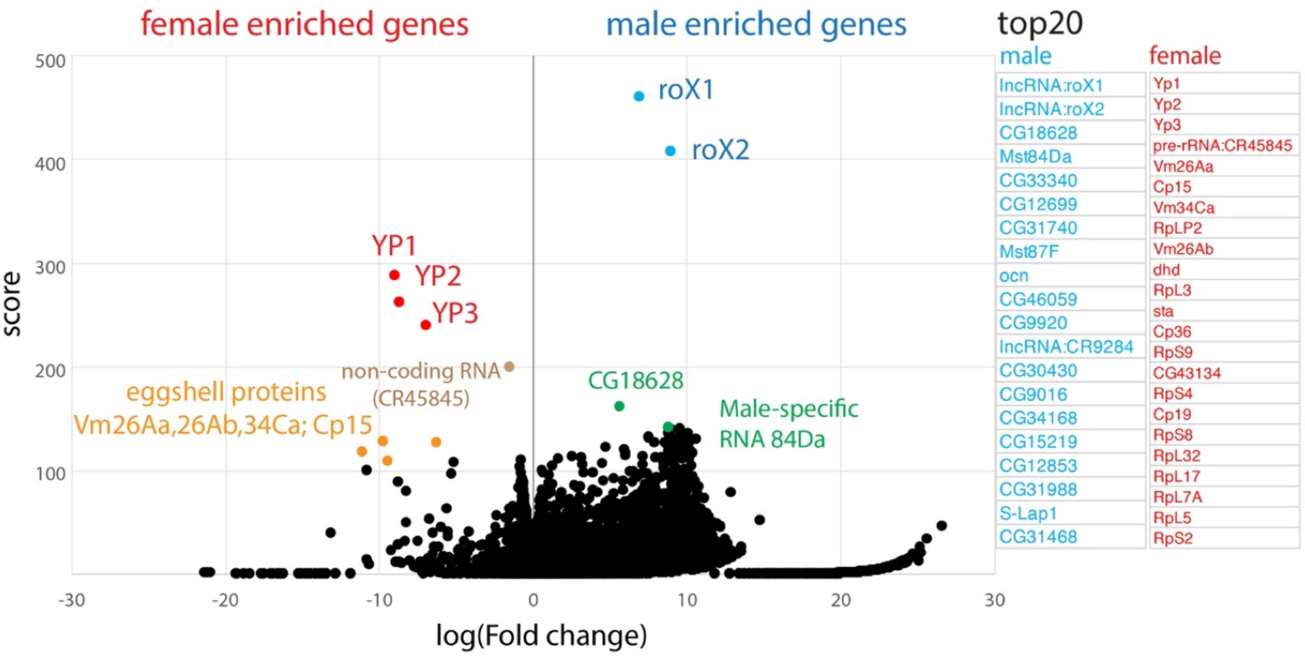

top20

male	female
lncRNA:roX1	Yp1
lncRNA:roX2	Yp2
CG18628	Yp3
Mst84Da	pre-rRNA:CR45845
CG33340	Vm26Aa
CG12699	Cp15
CG31740	Vm34Ca
Mst87F	RpLP2
ocn	Vm26Ab
CG46059	dhd
CG9920	RpL3
lncRNA:CR9284	sta
CG30430	Cp36
CG9016	RpS9
CG34168	CG43134
CG15219	RpS4
CG12853	Cp19
CG31988	RpS8
S-Lap1	RpL32
CG31468	RpL17
	RpL7A
	RpL5
	RpS2

Figure S35. Volcano plot showing male and female enriched genes. Differential expression was performed between all male against all female cells in the dataset, using the Wilcoxon test in Scanpy. Score is the underlying z-value used to calculate the p-value. Fold change is in Log$_2$ scale. Male and female enriched genes with top scores (20) are shown on the right. Known male specific makers (*roX1, roX2*) and female specific genes (*Yp1, Yp2, Yp3*) have the highest scores as previously seen (*39*, *57*), validating the quality of the data. A large number of CG genes (poorly studied or uncharacterized genes) are on the male enriched list (*58*), suggesting their potential sex-related functions.

FCA Figure S36

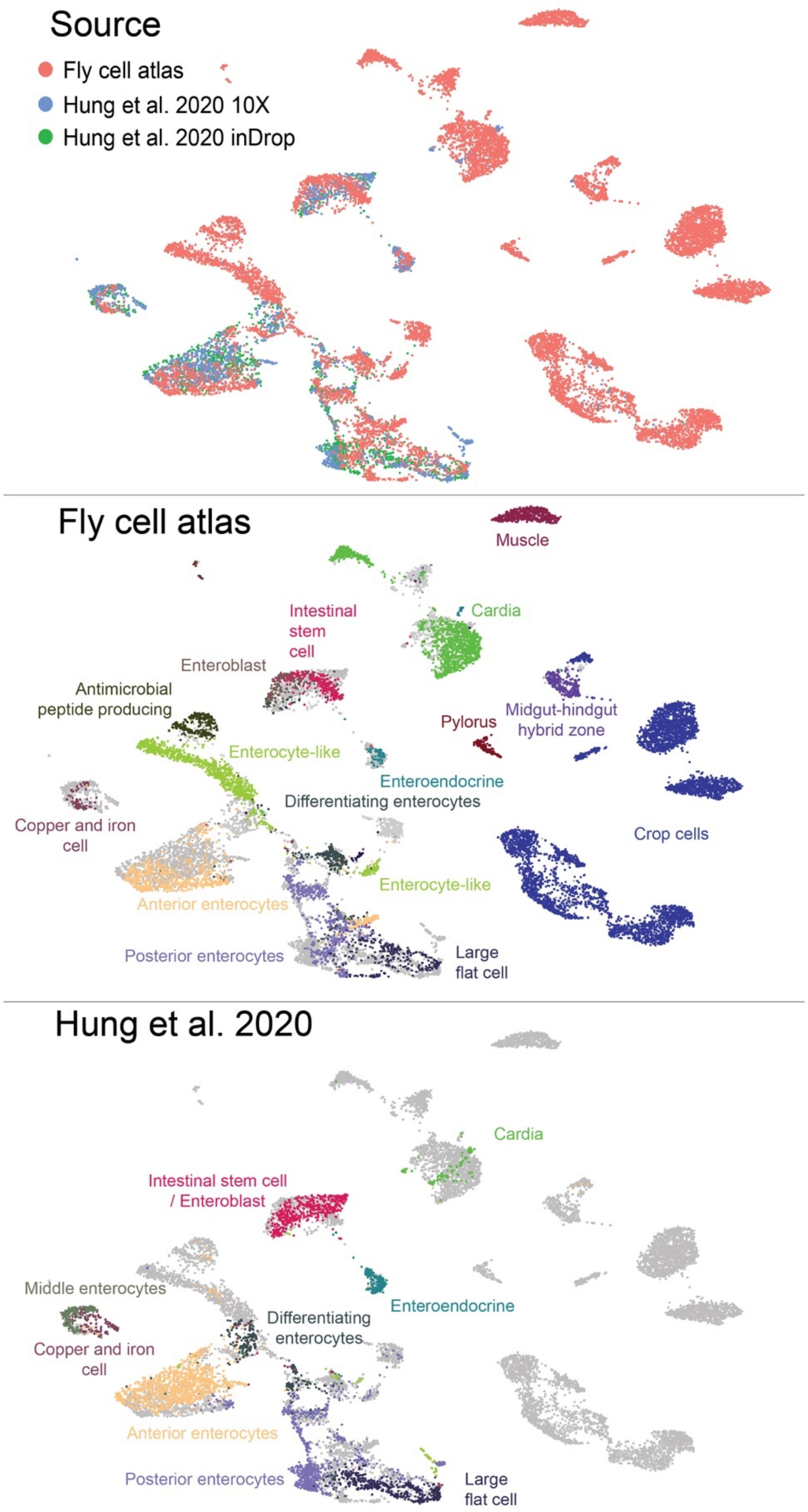
Source

Fly cell atlas

Hung et al. 2020

Figure S36. Integration of FCA snRNA-seq data and published scRNA-seq data of the gut. The published data are from two scRNA-seq platforms, 10x and inDrop (*40*). Data integration was performed using Harmony (*16*) using the first 30 PCA dimensions. From this analysis, we were able to identify all previously known cell types in the gut. In addition, we were able to characterize more cell types, including visceral muscle cells and 5 subtypes of crop cells.

Note that for Hung et al gut sample, the crop and midgut/hindgut junction (where the Malpighian tubules branch out of the gut) and Malpighian tubules were removed. For the FCA gut sample, we included the midgut/hindgut junction and the crop.

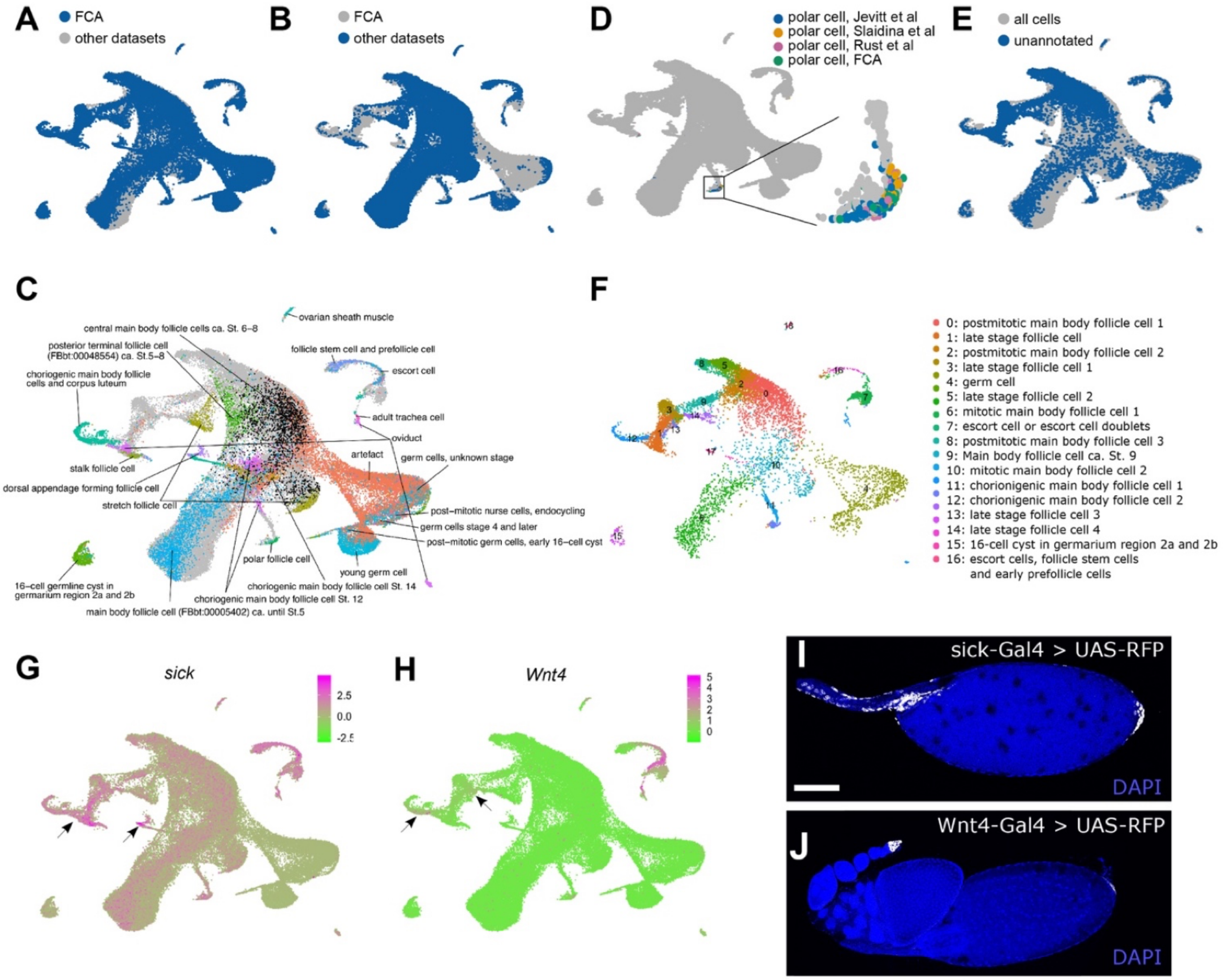

Figure S37. Integration of FCA snRNA-seq data and published scRNA-seq data of the ovary

(A) FCA cells are highlighted in blue, and other cells are colored in gray.
(B) Cells from the other three datasets are shown in blue, and FCA cells are displayed in gray.
(C) Annotated FCA clusters as noted. Unannotated cells and cells from other datasets are in gray.
(D) Polar cells identified in all datasets are highlighted and a magnified region of the UMAP plot containing polar cell clusters.
(E) Unannotated FCA cells are labeled blue, all other cells are shown in gray.
(F) Unannotated cells clustered independently. Presumptive cluster identities were determined by expression of marker genes as well as co-clustering with previously determined cell types.
(G, H) Expression of *sickie (sick)* and *Wnt4* labeling late stage terminal follicle cells indicated by arrows.
(I, J) Confocal images of *sick-GAL4* driving UAS-RFP showing expression in all late stage terminal follicle cells and of *Wnt4-GAL4* driving UAS-RFP showing expression in low levels in posterior terminal follicle cells and in high levels in escort cells. Confocal images are maximum intensity projections.

Confocal images are maximum intensity projections. Primary antibody, rat anti-RFP (ChromoTek 5F8, 1:1000); secondary antibody, goat anti-rat 555 (Thermo Fisher Scientific A-21434, 1:1000).
All plots are from UMAP. Three published adult ovarian scRNA-seq datasets are from (*41*, *42*, *55*). Datasets were integrated and batch corrected using Seurat v4.0.1. Scale bars in G and H depict average expression levels in log(((UMI + 1)/total UMI)×10^4). Scale bar in I and J, 100 µm.

References and Notes

1. T. H. Morgan, SEX LIMITED INHERITANCE IN DROSOPHILA. *Science*. **32**, 120–122 (1910).
2. M. D. Adams, S. E. Celniker, R. A. Holt, C. A. Evans, J. D. Gocayne, P. G. Amanatides, S. E. Scherer, P. W. Li, R. A. Hoskins, R. F. Galle, R. A. George, S. E. Lewis, S. Richards, M. Ashburner, S. N. Henderson, G. G. Sutton, J. R. Wortman, M. D. Yandell, Q. Zhang, L. X. Chen, J. C. Venter, The genome sequence of Drosophila melanogaster. *Science*. **287**, 2185–2195 (2000).
3. A. Larkin, S. J. Marygold, G. Antonazzo, H. Attrill, G. Dos Santos, P. V. Garapati, J. L. Goodman, L. S. Gramates, G. Millburn, V. B. Strelets, C. J. Tabone, J. Thurmond, FlyBase Consortium, FlyBase: updates to the Drosophila melanogaster knowledge base. *Nucleic Acids Res.* **49**, D899–D907 (2021).
4. R. Lyne, R. Smith, K. Rutherford, M. Wakeling, A. Varley, F. Guillier, H. Janssens, W. Ji, P. Mclaren, P. North, D. Rana, T. Riley, J. Sullivan, X. Watkins, M. Woodbridge, K. Lilley, S. Russell, M. Ashburner, K. Mizuguchi, G. Micklem, FlyMine: an integrated database for Drosophila and Anopheles genomics. *Genome Biol.* **8**, R129 (2007).
5. A. Jenett, G. M. Rubin, T.-T. B. Ngo, D. Shepherd, C. Murphy, H. Dionne, B. D. Pfeiffer, A. Cavallaro, D. Hall, J. Jeter, N. Iyer, D. Fetter, J. H. Hausenfluck, H. Peng, E. T. Trautman, R. R. Svirskas, E. W. Myers, Z. R. Iwinski, Y. Aso, G. M. DePasquale, C. T. Zugates, A GAL4-driver line resource for Drosophila neurobiology. *Cell Rep.* **2**, 991–1001 (2012).
6. N. Milyaev, D. Osumi-Sutherland, S. Reeve, N. Burton, R. A. Baldock, J. D. Armstrong, The Virtual Fly Brain browser and query interface. *Bioinformatics*. **28**, 411–415 (2012).
7. M. M. Kudron, A. Victorsen, L. Gevirtzman, L. W. Hillier, W. W. Fisher, D. Vafeados, M. Kirkey, A. S. Hammonds, J. Gersch, H. Ammouri, M. L. Wall, J. Moran, D. Steffen, M. Szynkarek, S. Seabrook-Sturgis, N. Jameel, M. Kadaba, J. Patton, R. Terrell, M. Corson, R. H. Waterston, The ModERN Resource: Genome-Wide Binding Profiles for Hundreds of Drosophila and Caenorhabditis elegans Transcription Factors. *Genetics*. **208**, 937–949 (2018).
8. modENCODE Consortium, S. Roy, J. Ernst, P. V. Kharchenko, P. Kheradpour, N. Negre, M. L. Eaton, J. M. Landolin, C. A. Bristow, L. Ma, M. F. Lin, S. Washietl, B. I. Arshinoff, F. Ay, P. E. Meyer, N. Robine, N. L. Washington, L. Di Stefano, E. Berezikov, C. D. Brown, M. Kellis, Identification of functional elements and regulatory circuits by Drosophila modENCODE. *Science*. **330**, 1787–1797 (2010).
9. V. R. Chintapalli, J. Wang, J. A. T. Dow, Using FlyAtlas to identify better Drosophila melanogaster models of human disease. *Nat. Genet.* **39**, 715–720 (2007).
10. H. Li, Single-cell RNA sequencing in Drosophila: Technologies and applications. *Wiley Interdiscip. Rev. Dev. Biol.* **10**, e396 (2021).
11. C. N. McLaughlin, M. Brbić, Q. Xie, T. Li, F. Horns, S. S. Kolluru, J. M. Kebschull, D. Vacek, A. Xie, J. Li, R. C. Jones, J. Leskovec, S. R. Quake, L. Luo, H. Li, Single-cell transcriptomes of developing and adult olfactory receptor neurons in Drosophila. *eLife*. **10** (2021), doi:10.7554/eLife.63856.
12. G. X. Y. Zheng, J. M. Terry, P. Belgrader, P. Ryvkin, Z. W. Bent, R. Wilson, S. B. Ziraldo, T. D.

Wheeler, G. P. McDermott, J. Zhu, M. T. Gregory, J. Shuga, L. Montesclaros, J. G. Underwood, D. A. Masquelier, S. Y. Nishimura, M. Schnall-Levin, P. W. Wyatt, C. M. Hindson, R. Bharadwaj, J. H. Bielas, Massively parallel digital transcriptional profiling of single cells. *Nat. Commun.* **8**, 14049 (2017).

13. S. Picelli, Å. K. Björklund, O. R. Faridani, S. Sagasser, G. Winberg, R. Sandberg, Smart-seq2 for sensitive full-length transcriptome profiling in single cells. *Nat. Methods*. **10**, 1096–1098 (2013).
14. M. De Waegeneer, C. C. Flerin, K. Davie, G. Hulselmans, vib-singlecell-nf/vsn-pipelines: v0.26.0 (v0.26.0). Zenodo. https://doi.org/10.5281/zenodo.5055627. *Zenodo* (2021).
15. S. Yang, S. E. Corbett, Y. Koga, Z. Wang, W. E. Johnson, M. Yajima, J. D. Campbell, Decontamination of ambient RNA in single-cell RNA-seq with DecontX. *Genome Biol.* **21**, 57 (2020).
16. I. Korsunsky, N. Millard, J. Fan, K. Slowikowski, F. Zhang, K. Wei, Y. Baglaenko, M. Brenner, P.-R. Loh, S. Raychaudhuri, Fast, sensitive and accurate integration of single-cell data with Harmony. *Nat. Methods*. **16**, 1289–1296 (2019).
17. K. Davie, J. Janssens, D. Koldere, M. De Waegeneer, U. Pech, Ł. Kreft, S. Aibar, S. Makhzami, V. Christiaens, C. Bravo González-Blas, S. Poovathingal, G. Hulselmans, K. I. Spanier, T. Moerman, B. Vanspauwen, S. Geurs, T. Voet, J. Lammertyn, B. Thienpont, S. Liu, S. Aerts, A Single-Cell Transcriptome Atlas of the Aging *Drosophila* Brain. *Cell*. **174**, 982-998.e20 (2018).
18. F. P. A. David, M. Litovchenko, B. Deplancke, V. Gardeux, ASAP 2020 update: an open, scalable and interactive web-based portal for (single-cell) omics analyses. *Nucleic Acids Res.* **48**, W403–W414 (2020).
19. M. Costa, S. Reeve, G. Grumbling, D. Osumi-Sutherland, The Drosophila anatomy ontology. *J. Biomed. Semantics*. **4**, 32 (2013).
20. S. Levy, A. Elek, X. Grau-Bové, S. Menéndez-Bravo, M. Iglesias, A. Tanay, T. Mass, A. Sebé-Pedrós, A stony coral cell atlas illuminates the molecular and cellular basis of coral symbiosis, calcification, and immunity. *Cell*. **184**, 2973-2987.e18 (2021).
21. J. Cao, J. S. Packer, V. Ramani, D. A. Cusanovich, C. Huynh, R. Daza, X. Qiu, C. Lee, S. N. Furlan, F. J. Steemers, A. Adey, R. H. Waterston, C. Trapnell, J. Shendure, Comprehensive single-cell transcriptional profiling of a multicellular organism. *Science*. **357**, 661–667 (2017).
22. M. N. Özel, F. Simon, S. Jafari, I. Holguera, Y.-C. Chen, N. Benhra, R. N. El-Danaf, K. Kapuralin, J. A. Malin, N. Konstantinides, C. Desplan, Neuronal diversity and convergence in a visual system developmental atlas. *Nature*. **589**, 88–95 (2021).
23. H. Li, F. Horns, B. Wu, Q. Xie, J. Li, T. Li, D. J. Luginbuhl, S. R. Quake, L. Luo, Classifying Drosophila Olfactory Projection Neuron Subtypes by Single-Cell RNA Sequencing. *Cell*. **171**, 1206-1220.e22 (2017).
24. Y. Z. Kurmangaliyev, J. Yoo, J. Valdes-Aleman, P. Sanfilippo, S. L. Zipursky, Transcriptional programs of circuit assembly in the drosophila visual system. *Neuron*. **108**, 1045-1057.e6 (2020).
25. B. Cho, S.-H. Yoon, D. Lee, F. Koranteng, S. G. Tattikota, N. Cha, M. Shin, H. Do, Y. Hu, S. Y. Oh, D. Lee, A. Vipin Menon, S. J. Moon, N. Perrimon, J.-W. Nam, J. Shim, Single-cell transcriptome maps of myeloid blood cell lineages in Drosophila. *Nat. Commun.* **11**, 4483 (2020).
26. V. A. Pavlov, K. J. Tracey, The cholinergic anti-inflammatory pathway. *Brain Behav. Immun.* **19**, 493–499 (2005).
27. P. Sanchez Bosch, K. Makhijani, L. Herboso, K. S. Gold, R. Baginsky, K. J. Woodcock, B. Alexander, K. Kukar, S. Corcoran, T. Jacobs, D. Ouyang, C. Wong, E. J. V. Ramond, C. Rhiner, E. Moreno, B. Lemaitre, F. Geissmann, K. Brückner, Adult drosophila lack hematopoiesis but rely on a blood cell reservoir at the respiratory epithelia to relay infection signals to surrounding tissues.

Dev. Cell. **51**, 787-803.e5 (2019).

28. J. Krzemień, L. Dubois, R. Makki, M. Meister, A. Vincent, M. Crozatier, Control of blood cell homeostasis in Drosophila larvae by the posterior signalling centre. *Nature*. **446**, 325–328 (2007).
29. L. Mandal, J. A. Martinez-Agosto, C. J. Evans, V. Hartenstein, U. Banerjee, A Hedgehog- and Antennapedia-dependent niche maintains Drosophila haematopoietic precursors. *Nature*. **446**, 320–324 (2007).
30. R. J. Siviter, G. M. Coast, A. M. Winther, R. J. Nachman, C. A. Taylor, A. D. Shirras, D. Coates, R. E. Isaac, D. R. Nässel, Expression and functional characterization of a Drosophila neuropeptide precursor with homology to mammalian preprotachykinin A. *J. Biol. Chem.* **275**, 23273–23280 (2000).
31. S. Aibar, C. B. González-Blas, T. Moerman, V. A. Huynh-Thu, H. Imrichova, G. Hulselmans, F. Rambow, J.-C. Marine, P. Geurts, J. Aerts, J. van den Oord, Z. K. Atak, J. Wouters, S. Aerts, SCENIC: single-cell regulatory network inference and clustering. *Nat. Methods*. **14**, 1083–1086 (2017).
32. J. Mattila, V. Hietakangas, Regulation of Carbohydrate Energy Metabolism in Drosophila melanogaster. *Genetics*. **207**, 1231–1253 (2017).
33. K. Moses, M. C. Ellis, G. M. Rubin, The glass gene encodes a zinc-finger protein required by Drosophila photoreceptor cells. *Nature*. **340**, 531–536 (1989).
34. H. Kaessmann, Origins, evolution, and phenotypic impact of new genes. *Genome Res.* **20**, 1313–1326 (2010).
35. Y. Shao, C. Chen, H. Shen, B. Z. He, D. Yu, S. Jiang, S. Zhao, Z. Gao, Z. Zhu, X. Chen, Y. Fu, H. Chen, G. Gao, M. Long, Y. E. Zhang, GenTree, an integrated resource for analyzing the evolution and function of primate-specific coding genes. *Genome Res.* **29**, 682–696 (2019).
36. E. B. Lewis, A gene complex controlling segmentation in Drosophila. *Nature*. **276**, 565–570 (1978).
37. J. Andrews, G. G. Bouffard, C. Cheadle, J. Lü, K. G. Becker, B. Oliver, Gene Discovery Using Computational and Microarray Analysis of Transcription in the *Drosophila melanogaster* Testis. *Genome Res.* **10**, 2030–2043 (2000).
38. H. K. Salz, J. W. Erickson, Sex determination in Drosophila: The view from the top. *Fly (Austin)*. **4**, 60–70 (2010).
39. E. Clough, E. Jimenez, Y.-A. Kim, C. Whitworth, M. C. Neville, L. U. Hempel, H. J. Pavlou, Z.-X. Chen, D. Sturgill, R. K. Dale, H. E. Smith, T. M. Przytycka, S. F. Goodwin, M. Van Doren, B. Oliver, Sex- and tissue-specific functions of Drosophila doublesex transcription factor target genes. *Dev. Cell*. **31**, 761–773 (2014).
40. R.-J. Hung, Y. Hu, R. Kirchner, Y. Liu, C. Xu, A. Comjean, S. G. Tattikota, F. Li, W. Song, S. Ho Sui, N. Perrimon, A cell atlas of the adult Drosophila midgut. *Proc Natl Acad Sci USA*. **117**, 1514–1523 (2020).
41. K. Rust, L. E. Byrnes, K. S. Yu, J. S. Park, J. B. Sneddon, A. D. Tward, T. G. Nystul, A single-cell atlas and lineage analysis of the adult Drosophila ovary. *Nat. Commun.* **11**, 5628 (2020).
42. A. Jevitt, D. Chatterjee, G. Xie, X.-F. Wang, T. Otwell, Y.-C. Huang, W.-M. Deng, A single-cell atlas of adult Drosophila ovary identifies transcriptional programs and somatic cell lineage regulating oogenesis. *PLoS Biol.* **18**, e3000538 (2020).
43. Tabula Muris Consortium, Overall coordination, Logistical coordination, Organ collection and processing, Library preparation and sequencing, Computational data analysis, Cell type annotation, Writing group, Supplemental text writing group, Principal investigators, Single-cell transcriptomics of 20 mouse organs creates a Tabula Muris. *Nature*. **562**, 367–372 (2018).

44. X. Han, R. Wang, Y. Zhou, L. Fei, H. Sun, S. Lai, A. Saadatpour, Z. Zhou, H. Chen, F. Ye, D. Huang, Y. Xu, W. Huang, M. Jiang, X. Jiang, J. Mao, Y. Chen, C. Lu, J. Xie, Q. Fang, G. Guo, Mapping the Mouse Cell Atlas by Microwell-Seq. *Cell*. **173**, 1307 (2018).

45. J. Cao, D. R. O'Day, H. A. Pliner, P. D. Kingsley, M. Deng, R. M. Daza, M. A. Zager, K. A. Aldinger, R. Blecher-Gonen, F. Zhang, M. Spielmann, J. Palis, D. Doherty, F. J. Steemers, I. A. Glass, C. Trapnell, J. Shendure, A human cell atlas of fetal gene expression. *Science*. **370** (2020), doi:10.1126/science.aba7721.

46. X. Han, Z. Zhou, L. Fei, H. Sun, R. Wang, Y. Chen, H. Chen, J. Wang, H. Tang, W. Ge, Y. Zhou, F. Ye, M. Jiang, J. Wu, Y. Xiao, X. Jia, T. Zhang, X. Ma, Q. Zhang, X. Bai, G. Guo, Construction of a human cell landscape at single-cell level. *Nature*. **581**, 303–309 (2020).

47. J. Janssens, S. Aibar, I. I. Taskiran, J. N. Ismail, A. E. Gomez, G. Aughey, K. I. Spanier, F. V. De Rop, C. B. González-Blas, M. Dionne, K. Grimes, X. J. Quan, D. Papasokrati, G. Hulselmans, S. Makhzami, M. De Waegeneer, V. Christiaens, T. Southall, S. Aerts, Decoding gene regulation in the fly brain. *Nature* (2022), doi:10.1038/s41586-021-04262-z.

48. G. L. Henry, F. P. Davis, S. Picard, S. R. Eddy, Cell type-specific genomics of Drosophila neurons. *Nucleic Acids Res*. **40**, 9691–9704 (2012).

49. M. Brbić, M. Zitnik, S. Wang, A. O. Pisco, R. B. Altman, S. Darmanis, J. Leskovec, MARS: discovering novel cell types across heterogeneous single-cell experiments. *Nat. Methods*. **17**, 1200–1206 (2020).

50. C. Hafemeister, R. Satija, Normalization and variance stabilization of single-cell RNA-seq data using regularized negative binomial regression. *Genome Biol.* **20**, 296 (2019).

51. T. Stuart, A. Butler, P. Hoffman, C. Hafemeister, E. Papalexi, W. M. Mauck, Y. Hao, M. Stoeckius, P. Smibert, R. Satija, Comprehensive Integration of Single-Cell Data. *Cell*. **177**, 1888-1902.e21 (2019).

52. M. Sarov, C. Barz, H. Jambor, M. Y. Hein, C. Schmied, D. Suchold, B. Stender, S. Janosch, V. V. K J, R. T. Krishnan, A. Krishnamoorthy, I. R. S. Ferreira, R. K. Ejsmont, K. Finkl, S. Hasse, P. Kämpfer, N. Plewka, E. Vinis, S. Schloissnig, E. Knust, F. Schnorrer, A genome-wide resource for the analysis of protein localisation in Drosophila. *eLife*. **5**, e12068 (2016).

53. C. Schönbauer, J. Distler, N. Jährling, M. Radolf, H.-U. Dodt, M. Frasch, F. Schnorrer, Spalt mediates an evolutionarily conserved switch to fibrillar muscle fate in insects. *Nature*. **479**, 406–409 (2011).

54. M. B. Chechenova, S. Maes, S. T. Oas, C. Nelson, K. G. Kiani, A. L. Bryantsev, R. M. Cripps, Functional redundancy and nonredundancy between two Troponin C isoforms in Drosophila adult muscles. *Mol. Biol. Cell*. **28**, 760–770 (2017).

55. M. Slaidina, T. U. Banisch, S. Gupta, R. Lehmann, A single-cell atlas of the developing Drosophila ovary identifies follicle stem cell progenitors. *Genes Dev.* **34**, 239–249 (2020).

56. L. Bai, A. L. Goldman, J. R. Carlson, Positive and negative regulation of odor receptor gene choice in Drosophila by acj6. *J. Neurosci.* **29**, 12940–12947 (2009).

57. J. C. Lucchesi, M. I. Kuroda, Dosage compensation in Drosophila. *Cold Spring Harb. Perspect. Biol.* **7** (2015), doi:10.1101/cshperspect.a019398.

58. B. R. Graveley, A. N. Brooks, J. W. Carlson, M. O. Duff, J. M. Landolin, L. Yang, C. G. Artieri, M. J. van Baren, N. Boley, B. W. Booth, J. B. Brown, L. Cherbas, C. A. Davis, A. Dobin, R. Li, W. Lin, J. H. Malone, N. R. Mattiuzzo, D. Miller, D. Sturgill, S. E. Celniker, The developmental transcriptome of Drosophila melanogaster. *Nature*. **471**, 473–479 (2011).